NTNU – Trondheim
Norwegian University of
Science and Technology

High-resolution Meso- and Microstructural Study of polyphase Deformation in the Orkanger Region, Sør-Trøndelag, Central Norway

Eero Matti Bekkedal

Geology
Submission date: May 2015
Supervisor: Giulio Viola, IGB

Norwegian University of Science and Technology
Department of Geology and Mineral Resources Engineering

Abstract

The Orkanger Road Cut (ORC) is a 300 m long section of exposed country rock that has preserved an important record of structures linked to the tectonic history of the Mid-Western Gneiss Region. High-resolution field mapping conducted on all structures, combined with microscopical analysis of thin sections is presented in a systematic meso- and micro-scale evaluation. A highly detailed cross section of the ORC has been produced as a key guide to the position and orientation of the structures and to ease the work of combining and separating complex structures from heavy overprinting. The structures of the ORC show cutting relationships yielding a relative age for each type of structure. The described structures of the ORC display very consistent trends for pegmatites, folds, high strain zones, ductile shear zones and brittle faults. A ductile thrust may be a part of the roof-contact of an extrusion wedge in the Jämtland-Västerbotten area of Sweden. Crosscutting relationships have yielded a relative age to the structures of the ORC listed from the oldest to the youngest: high strain zones, generation 1 pegmatites , F1 folding, generation 2 pegmatites, F2 folding, generation 3 pegmatites, ductile shear zones, brittle-ductile faults and finally brittle faulting.

Three types of relict structures are especially prone to reactivation within the ORC. These include pegmatites, ductile shear zones and folds, which show reactivation along different types of contacts. A model based on these observations was made to explain the evolution of these brittle reactivations. A paleostress analysis of the brittle faults in the ORC produced three different stress fields, which of two can be regarded as paleostress fields based on the orientation of the fault planes and their mineral coating. These stress fields include: 1. a fault group yielding NE-SW dip-slip extension with quartz coating, interpreted to be a paleo-stress field 2. a fault group showing NW-SE oblique slip extension with epidote, which also is regarded as a paleo stress field, 3. NE-SW compression related to neo-tectonics. Structures at the ORC show a close connection between structures found within the ORC and the complex tectonic history of the region, dominated by the MTFC. The structures observed at the ORC can be linked to both the compressional and extensional phase of the orogenic evolution of the Caledonides.

Sammendrag

Veiskjæringa i Orkanger (ViO) er en 300 meter lang eksponert skjæring som har konservert viktige strukturer tilhørende den tektoniske historien vedrørende den Midt-Vestre Gneisregionen. Feltarbeidet, kombinert med høydetaljerte beskrivelser av alle strukturer gjennom meso- og mikroskopiske analyser, har ligget til grunn for presentasjonen av studiet. Ei høydetaljert skisse av hele veiskjæringa i Orkanger, som inkluderer alle strukturer, har blitt produsert for å lette arbeidet med å kombinere og separere de komplekse strukturene fra den sterke sprø deformasjonen. Strukturene i ViO viser flere kuttende forhold som gir en relativ alder for hver struktur. Strukturene som er beskrevet i ViO viser sterke trender for strukturer som pegmatitter, folder, høy-skjærdeformasjonssoner, duktile skjærsoner og sprø forkastninger. En duktil skyveskjærsone i ViO kan ha vært en del av en duktil skjærsone i den øvre kontakten av en ekstrusjons-kile i Jämtland-Västerbotten området i Sverige.

Tre typer remanente strukturer er spesielt utsatt for reaktivering av sprø forkastninger i ViO. Disse inkluderer pegmatitter, duktile skjærsoner, og folder, som viser reaktivering langs forskjellige typer kontakter. En modell basert på disse observasjonene har blitt laget for å forklare evolusjonen av disse sprø reaktiverende forskastningene. En paleostress-analyse av sprø forkastninger i ViO resulterte i tre forskjellige stressfelt. Av disse tre stressfeltene kan to regnes som paleostress-felt basert på mineraliseringene som ble observert på forkastningsplanene. Disse stressfeltene inkluderer: 1. Paleostressfelt som viser NØ-SV fallrettet ekstensjon med kvarts-mineraliserte forskastningsplan. 2. Paleostressfelt som viser NV-SØ skråretted ekstensjon med epidot-mineraliserte forkastningsplan. 3. NØ-SV kompresjon relatert til et nylig aktivt stressfelt. Strukturene i ViO viser en sterk korrelasjon med regionens tektonisk komplekse historie, som er dominert av Møre Trøndelag Forkastningskompleks. Strukturene som er observert i ViO kan knyttes til både kompresjonsfasen og ekstensjonsfasen i utviklingen av Kaledonidene.

Acknowledgements

This work is a co-operation by NGU and NTNU. I am grateful for all the guidance my two supervisors, Iain Henderson and Giulio Viola, have given me inspiration through years of field work during the summers and intriguing lectures on structural geology at NTNU.

I would also like to thank my field assistants, my father, Hans Jørgen Kjøll and Ivar Hole for handling the harsh weather during long days at the outcrop.

Table of contents

1. Introduction

The Scandinavian Caledonides are the remnants of a mountain chain that runs from Greenland and Svalbard in the North, to Scandinavia and Scotland in the South. The Caledonides formed to accommodate the closure of the Iapetus Ocean during Mid-Late Silurian times (Torsvik, 1998; Corfu et al., 2014). The corresponding part of the Caledonides on the Laurentian plate forms the Appalachian mountain chain running from eastern Canada in the North and as far south as Florida, USA (Bird and Dewey, 1970; Williams, 1979; Torsvik et al., 1996; Mckerrow et al., 2000); (Figure 1.1) The evolution of the Caledonides has been the focus of many tectonic and metamorphic studies (Strand, 1961; Andersen et al., 1991; Torsvik et al., 1996; Krabbendam and Dewey, 1998; Roberts, 2003; Osmundsen et al., 2005b; Hacker et al., 2010). The majority of these studies has focussed on the allochthonous units that were emplaced eastward onto the Baltic Shield in Silurian time (Dewey, 1969; Gee, 1978; Roberts, 2003).

1.1 Evolution of the Caledonides

The Scandian phase is a term used to refer to the product of the late Silurian orogenic collisional event between the Baltica and Laurentia plates, culminating approximately 425 Ma ago (Dewey, 1969; Torsvik et al., 1996). The collision was a result of subduction of the Baltic plate beneath the Laurentian plate, with convergence rates of up to 8-10 cm/year (Torsvik, 1998).

On the Baltic Craton, the precursor to this translational event was the erosion of Precambrian rocks that formed a peneplain, which was subsequently covered by Mesozoic sediments that later acted as a dècollement zone upon which the Caledonian nappe stacks were emplaced with an overall eastward emplacement (Roberts and Wolff, 1981; Tucker et al., 2004). During this coeval subduction and thrust event, the western edge of the Baltic Craton was severely deformed and produced the ultra-high metamorphic rocks of the region (Hurich et al., 1989; Andersen and Jamtveit, 1990). These well preserved ultra-high metamorphic rocks, exhumed to shallow depths by significant transtensional shearing and faulting within Western Norway, are regarded as somewhat unique due to their close connection to mountain roots (Gee, 1975; Krabbendam and Dewey, 1998; Hacker et al., 2010).

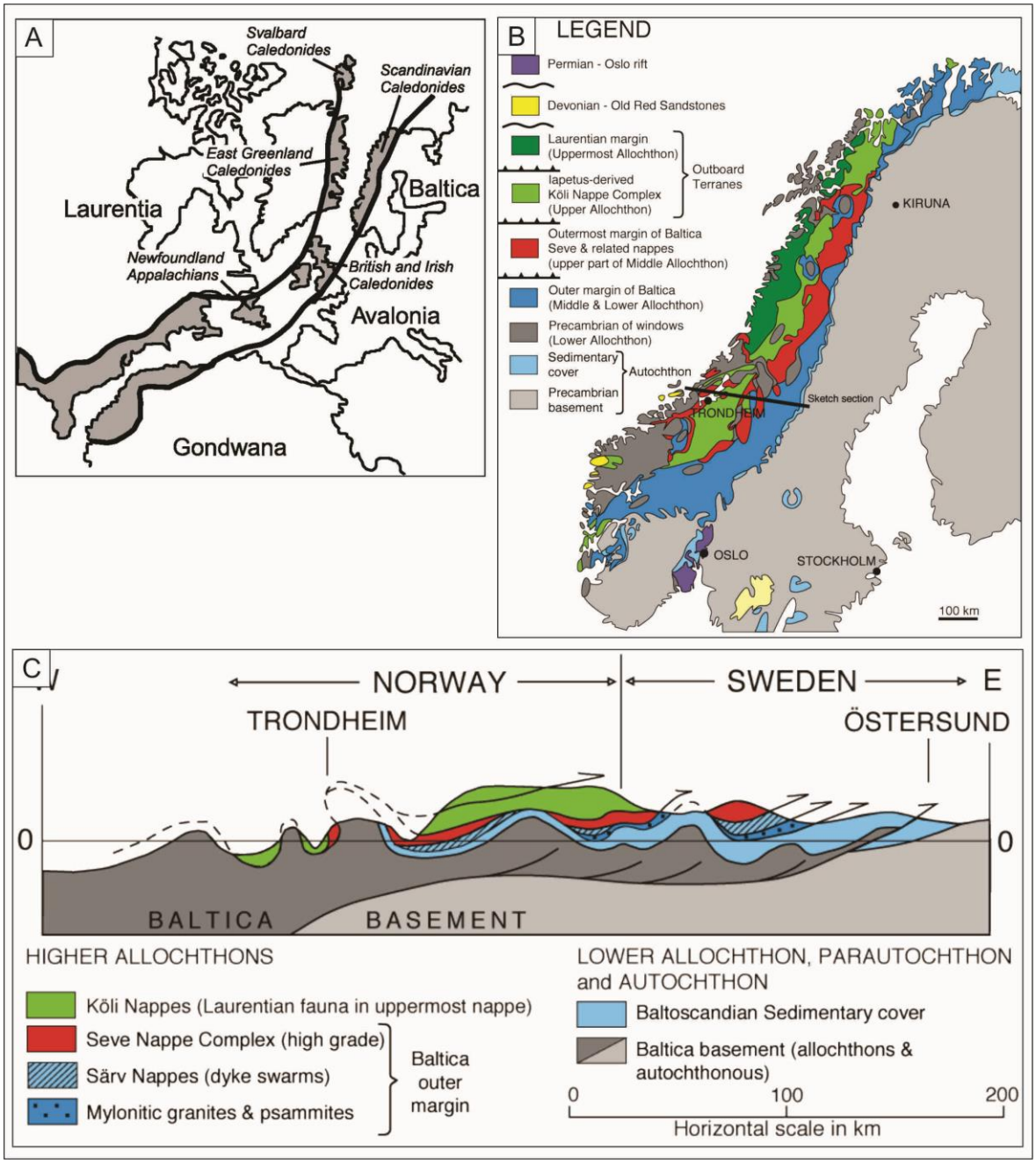

Figure 1.1: A) Map showing the length of what is regarded as the Caledonides today. B) Figure showing the different nappes and sedimentary covers. C) Profile taken from figure B showing folding and thrusting towards the south. Note the Seve Nappe segment left in the Trondheim region to the left. From Gee et al. (2013).

The creation of high mountain belts results in a much thicker continental crust. Gravitational instability of these orogens can result in subsequent orogenic collapse and extreme lithospheric extension (Platt, 1986). Orogenic relaxation is evident through structural inhomogeneities, subduction rollback, advective thinning of lithosphere and the isostatically compensated elevation of mountains and their steep elevation gradients. (Dewey, 1988; Andersen and Jamtveit, 1990; Platt et al., 2003) Extensive extensional orogenic collapse may lead to exhumation and block extrusion of high grade metamorphic rocks such as amphibolites,

granulites and ultra-high grade rocks such as coesites and eclogites, which can induce potential partial melting (Dewey et al., 1993; Platt et al., 2003; Osmundsen et al., 2005b). Different parts of the Mid-Western Gneiss Region (MWGR) show varying metamorphic grade. The regional metamorphic pattern has been examined extensively to determine the amount of exhumation and metamorphic grade (Osmundsen et al., 2005b; Hacker et al., 2010). Folds, measured from the southern part of the WGR up to the MWGR in the Trøndelag area, show an evolution where the fold axes trend from E-W to a more NE trend through time (Chauvet and Séranne, 1994; Hacker et al., 2010) (Figure 1.2).

The Western Gneiss Region (WGR) represents the area between Bergen in the south and Mo i Rana in the north, where Precambrian crystalline basement rocks are exposed due to tectonic exhumation (Seranne, 1992; Ramberg I., 2006; Hacker et al., 2010). In the northernmost part of the WGR the extensional structures, that accommodated most exhumation during the late orogenic evolution of the Norwegian Caledonides, are considered to be the result of mega-scale, gravity-induced collapse of the collision-related thrust-thickened continental crust (Fossen, 1992; Andersen, 1998; Braathen et al., 2002; Osmundsen et al., 2006; Chauvet and Dallmeyer, 1992). Indeed, the termination of subduction of the Baltic plate gave way to major extensional ductile shearing and subsequent brittle faulting seen all along the present Norwegian coast, with a suite of generally E-W striking extensional structures (Andersen, 1998). This allowed exhumation of high-grade metamorphic rocks during early Devonian times. In the late Devonian, mostly top-to-the-west ductile extensional detachment faults developed much of the present-day first-order structural grain.

The tectonic setting of the Mid-Western Gneiss Region (MWGR), the geological domain where the field area of this study is located, is also directly linked to the accommodation of the Caledonian compressional phase and post-orogenic relaxation. The tectonic structures known from the MWGR juxtapose different component parts of the WGR and belong to large, prominent fault complexes such as the MTFC. The MTFC is indeed regarded as one of Norway's largest and most significant fault complexes, shaped by long periods of deformation, with an onshore strike-parallel extension from the county of Trøndelag to Møre.

1.2. The Møre Trøndelag Fault Complex

The MTFC is an intricate array of lineaments trending ENE-WSW in the Trøndelag region, and is characterized by a complex faulting history (Grønlie and Roberts, 1989; Seranne, 1992). The MTFC is up to 20-30 km in width and more than 300 km long. A very pervasive ENE-WSW structural grain is observed in the field, on remote imagery of the region and on the regional potential-field geophysical signatures of aeromagnetic data (Figure 1.2B) (Nasuti et al., 2012) Due to its long and tectonically complex history, it is regarded as especially important in understanding the tectonic evolution of the region. (Seranne, 1992; Mosar, 2003; Osmundsen et al., 2006). The MTFC is interpreted to be the product of the post-orogenic E-W relaxation during Late-Silurian to Early Devonian times, when it initiated as a sinistral strike-slip fault, although evidence of multiple reactivations are evident (Grønlie and Roberts, 1989; Redfield et al., 2005a). Kinematic analysis of structures that can be positively associated with its Palaeozoic evolution suggests that the fault complex has undergone at least three different modes of faulting: 1. Dextral strike-slip in Late Silurian time, 2. Sinistral transtension in Devonian times, 3. Sinistral strike-slip in the Carboniferous and 4. dip-slip extension in Mid-Jurassic time (Bøe and Bjerkli, 1989; Grønlie and Roberts, 1989; Seranne, 1992; Gabrielsen et al., 1999; Braathen et al., 2002; Nasuti et al., 2011). Interpretation of geophysical data indicates that the MTFC extends offshore and played an important role influencing the development of the Møre and Vøring sedimentary basins of mid-Devonian age (Osmundsen et al., 2005b).

The importance of the fundamental mid-Norwegian structure has caught the attention of many geologists and has led to a vast amount of studies focussing on its tectonic evolution and the impact thereof on the Trøndelag region as a whole (e.g (Seranne, 1992; Braathen et al., 2002; Osmundsen et al., 2003; Osmundsen et al., 2006). Understanding the tectonic evolution of the MTFC has therefore been a key issue in interpreting and developing models for late Devonian sedimentary basins and their offshore continuation (Gabrielsen et al., 1999). Onshore, the MTFC has been central in reconstructing the tectonic history of the orogenic relaxation and its later evolution. The influence on the processes of landscape development along the present-day Norwegian coastal range is also closely related to the evolution of the MTFC (Seranne, 1992; Osmundsen et al., 2006; Nasuti et al., 2012; Redfield et al., 2005b). The seismic activity recorded along the MTFC is gathered offshore (Figure 1.2B) and studies of the fault complex is therefore regarded as of societal importance (Roberts and Myrvang, 2004).

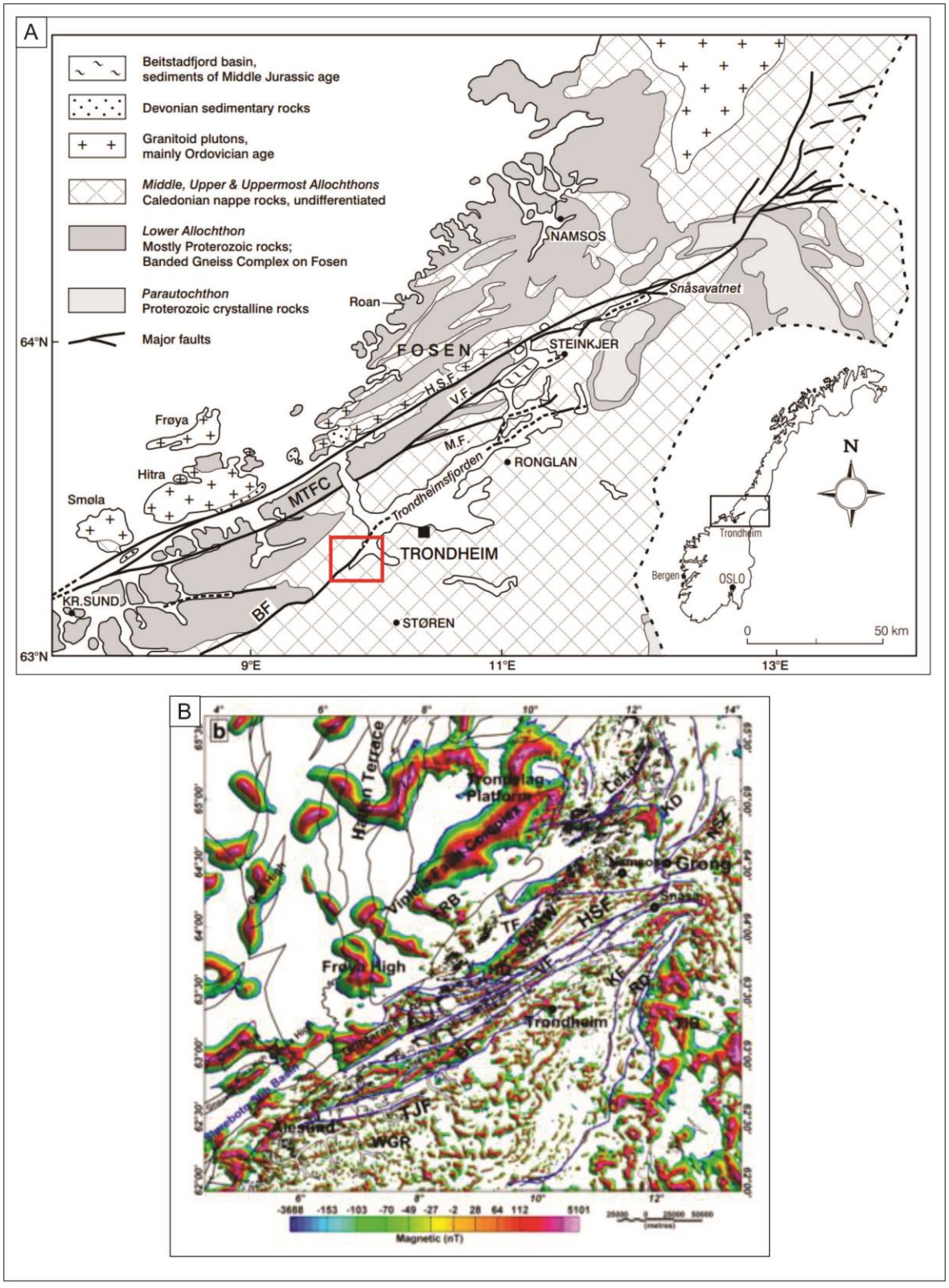

Figure 1.2: A) Geological map of the main constituents of the MWGR with the main lineaments marked in black trending NE-SE (after Roberts and Myrvang (2004)). B) Magnetic map of the MWGR with large lineaments marked in purple. From Nasuti et al. (2011).

1.3 Detachment zones

The Nordfjord-Sogn Detachment Zone (NSDZ), where eclogites are found juxtaposed against Devonian basin sediments, was the first structure recognized to have accommodated the late-Caledonian major extensional event (Norton, 1987). Subsequently, many large scale extensional shear zones have later been identified and characterized, such as the Hardangerfjord Shear Zone (HSZ) (Norton, 1987; Osmundsen and Andersen, 2001; Fossen and Hurich, 2005; Osmundsen et al., 2006) (Figure 1.3). These deformation zones commonly consist of several kilometres thick carapaces of mylonites to ultramylonites formed mainly during simple shearing and record very large amounts of shear strain and significant exhumation of the footwall rocks (Norton, 1986; Andersen et al., 1991; Chauvet and Séranne, 1994; Andersen, 1998; Braathen et al., 2002; Tucker et al., 2004).

There are several other major shear zones in the immediate surroundings of the MTFC, such as the Nesna Shear Zone Detachment (NSZD), The Høybakken Detachment Fault (HDF) the Kollstraumen Detachment Fault (KDF), the Hitra-Snåsa Fault, the Verran Fault and the Bæverdalen Lineament (Figure 1.2A). The detachments are believed to be reactivations of remnant thrust shear zones underlying each nappe sheet that die out in transpressional and transtensional faults (Grønlie and Roberts, 1989). The HDF, which yielded NE-SW extension, is situated within the MTFC (Fosen area) and juxtaposes rocks of the Upper- and Uppermost Allochthons and sedimentary rocks in sedimentary basins, such as the Asenøy-Tristeinen basin (Nordgulen et al., 2002). The footwall of the HDF experienced exhumation for more than 30 Ma, from Early Devonian to Early Carboniferous (Osmundsen et al., 2006).

The complex tectonic evolution of the MWGR and the regional work is all based on studies of individual structures such as folds and shear zones, detachments or late brittle faulting. The high-resolution structural study of a road cut close to Orkanger, presented in this thesis compiles all the regional deformation events recorded through their respective structures within the road cut. In addition to observe most of the tectonic evolution of the region the compilation yields the possibility to study structures that may have affected each other, with emphasis on the concentration of late brittle reactivation. A paleostress analysis of the brittle faults will aid in constraining the heavy brittle faulting found within the road cut. The examined road cut lies within the Seve Nappe of the Upper Allochthon and a thorough introduction of the tectonostratigraphy is therefore presented below.

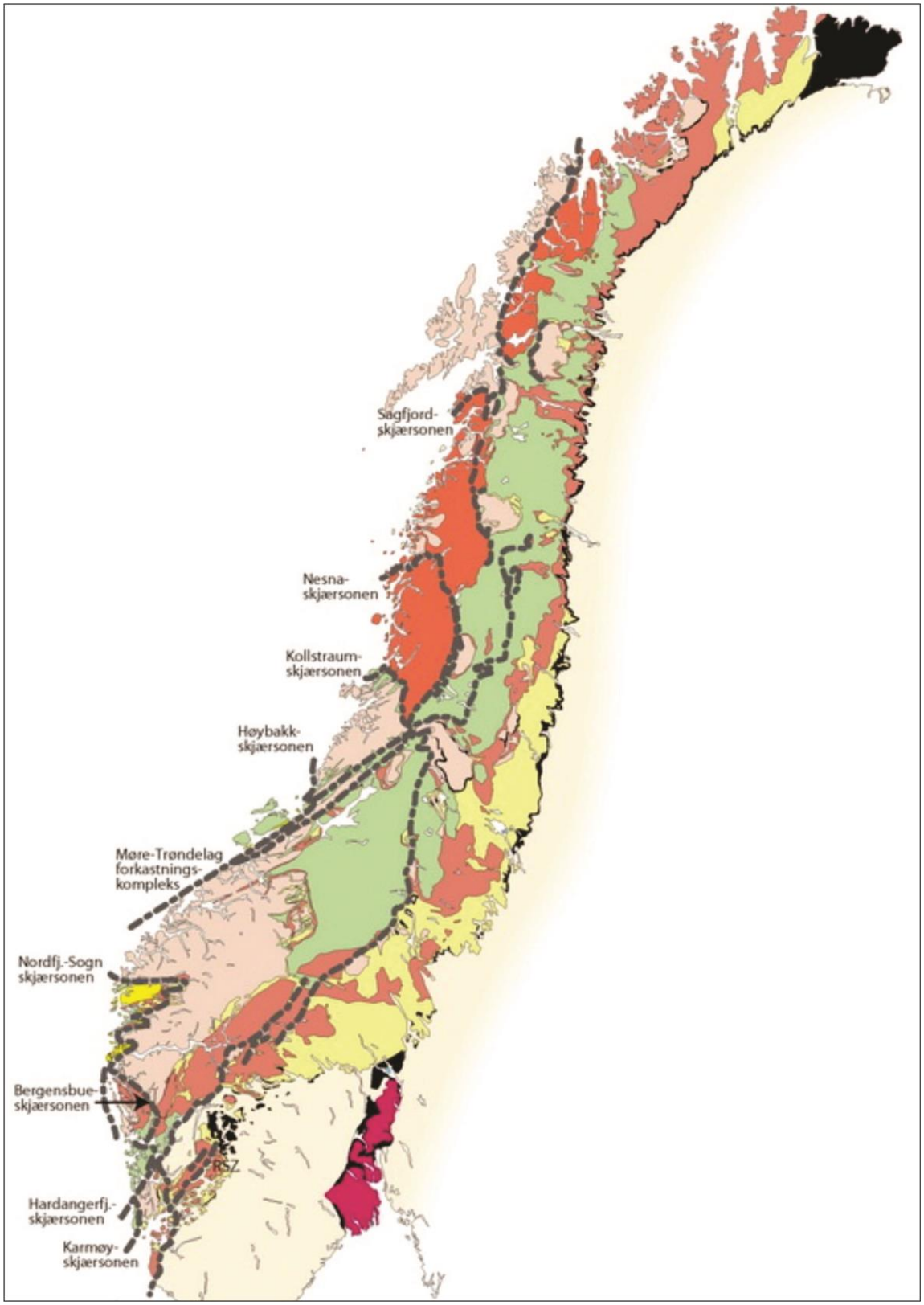

Figure 1.3: Map showing extensional shear zones in Norway. The MTFC is oriented NE-SW north of Trondheim, after Ramberg I. (2006).

2. Geological background of the study area

2.1. Tectonostratigraphy

The tectonostratigraphic stack of nappes emplaced onto the Baltic continental shield has commonly been divided into the Lower, Middle, Upper and Uppermost allochthon (Andersen et al., 1991). The nappes differ in thickness and composition from Finnmark in the north to Kristiansand in the south. (Gayer and Roberts, 1973). They are interpreted to form sheets or wedges that moved in relation to each other. In addition, some extensive parts of the nappes have been removed during especially deep erosion of the Caledonian Orogen (Gee, 1975). Possible suitable mechanisms for transporting these allochthons have been widely debated in the literature (Roberts and Sturt, 1980). It is believed that the Precambrian basement, which was highly eroded in the late Proterozoic, was covered by deposition of thick sedimentary sequences in the early Palaeozoic. These sediments were then wedged between the overriding Laurentian plate and the subducting Baltica plate (Hurich et al., 1989). The sediments consisting of, amongst others, shallow marine shales, were deformed into phyllitic and quartzitic rocks of Neoproterozoic and early Palaeozoic age and acted as low-friction preferential glide planes bounding the nappe complexes. (Milnes et al., 1997) This greatly reduced the friction allowing the nappe complexes to be transported in excess of at least 500 km eastwards (Strand, 1961; Gee, 1975). The orogenic development ceased at approximately 400 Ma, followed by a subsequent period of tectonic relaxation (Gee, 1978; Braathen et al., 2002).

The Lower and Middle Allochthons are believed to represent fragments of the Baltic Shield significantly translated by thrusting (Stephens and Gee, 1985; Roberts, 2003). The Lower Allochthon consists of late Precambrian to early Palaeozoic sediments and is characterised by relatively short transport distance and minor deformation under low metamorphic conditions. The Middle Allochthon consists of highly deformed crystalline basement rocks. The different allochthons have different names for their respective nappes based on their geographical position (Figure 1.3) (Roberts and Gee, 1985; Ramberg I., 2006).

REGIONS / Main tectonostrati-divisions	NORTHERN NORWAY (Ramsay *et al.*)	NORTH-CENTRAL NORWAY/SWEDEN (Stephens *et al.*)	SOUTH-CENTRAL NORWAY/SWEDEN (Gee *et al.*)	SOUTHEASTERN NORWAY/SWEDEN (Bockeilie and Nystuen)	SOUTHWESTERN NORWAY (Bryhni and Sturt)
UPPERMOST ALLOCHTHON	Tromsø Nappe	Helgeland Nappe Cpx and Beiarn Nappe Rödingsfjäll Nappe Cpx	Helgeland Nappe Complex		
UPPER ALLOCHTHON	Lyngen, Dyrøy, Magerøy, Kåfkord, Senja and Vaddas Nappes	K Storfjället, Gasak, ö Stikke, Gjersvik l and Bjørkvattnet i Nappes Seve Nappes	Støren Nappe, Gula Nappe, Meråker and other nappe units } Trondheim Nappe Cpx. Seve Nappes (incl. Essandsjø, Skjøtingen and Blåhø Nappes)	Köli Nappes Seve Nappes	Sunnhordland Nappe Complex Eugeosynclinal rocks of western Sogn and Sunnfjord
MIDDLE ALLOCHTHON	Kalak Nappe Cpx. Laksefjord Nappe	? Särv Nappes Offerdal, Stalon and Abisko Nappes	Särv, Sætra and Leksdal Nappes Offerdal, Tännäs, Risberget and Hærvola Nappes	Särv Nappes Tännäs and Veman Ns. Rondane Nappe Kvitvola Nappe Valdres Nappe	Hardangervidda-Ryfylke and Jotun Nappe Cpxs. Bergen Anorthosite Cpx. (Lindås Nappe) Dalsfjord Nappe Valdres Nappe
LOWER ALLOCHTHON	Gaissa and Jerta Nappes	Jämtlandian, Blaik, Ström and Rautas Nappes	Jämtlandian Nappes Osen-Røa Nappe Cpx.	Synnfjell Nappe Osen-Røa, Hede and Vemdalen Nappes	Unnamed Nappes ('Phyllite Division') Synnfjell Nappe Aurdal Nappe (Osen-Røa Nappe Cpx.)
PARAUTOCHTHON	Minor thrust sheets	Minor thrust sheets	Various minor thrust sheets	Various minor thrust sheets	Autochthon and/or various minor thrust sheets
AUTOCHTHON	Precambrian crystalline basement	Precambrian crystalline basement	Precambrian crystalline basement	Precambrian crystalline basement	Precambrian crystalline basement

Figure 2.1: A) Table offering a review of the main tectonic units of the Scandinavian Caledonides and correlating them and their respective names in different parts of Norway and Sweden (from Roberts and Gee, 1985).

In the Trøndelag region, the Upper Allochthon within the Trøndelag region consists of the Seve and Köli nappes and is interpreted to represent the remaining parts of the subducted passive margin of Baltica. The nappes contain ophiolitic sequences and rocks from magmatic arc settings, which are believed to represent vestiges of the Iapetus Ocean and associated micro-continents (Gale and Roberts, 1974; Grenne et al., 1999). During subduction, the Seve Nappe complex underwent amphibolite- and, to some extent, granulite facies metamorphism (Andréasson and Gee, 1989). The Seve Nappe Complex is overlain by the Köli- and Helgeland Nappe Complex, representing the Uppermost Allochton, which contains rocks that underwent greenschist facies. The roof of the Seve Nappe Complex marks the boundary between the continental-derived Seve Nappes of Baltica and the oceanic fragments representing the Iapetus Ocean in the Upper Allochthon (Grimmer et al., 2015).

There overall thrust transport direction in the Norwegian Caledonides, including MWGR and its respective allochthons, is top-to-the ESE. (Gee, 1978; Roberts and Sturt, 1980; Milnes et al., 1997).

Folding of the Caledonian sequences in the study area is characterized by fold axes broadly oriented NE-SW. Regional scale folding in south-western Norway can be divided into two groups: Group 1 consists of orogen-parallel synforms and antiforms striking more or less N-S. Group 2 consists of antiforms and synforms with E-W to NE-SW striking fold axes in the southern parts of the WGR (Ramberg, 1980). Folding in the Trøndelag region can be largely explained by the extensional phase of the Caledonian orogenic history. Folds representing the compressional phase of the Caledonides are oriented NE-SW, perpendicular to the general top-NE thrust direction. Fold axes from Sunnfjord in Sogn og Fjordane in the southern part show E-W orientation, while the northern parts of the WGR show NE-SW orientation and are genetically assigned to the extensional phase in late Devonian (Seranne, 1992; Chauvet and Séranne, 1994). It is believed that pre-existing fold axes and axial planes were reoriented into a NE-SW trend due to the ductile extensional phases of the MTFC when reaching the northern parts of the WGR (Escher and Watterson, 1974; Seranne, 1992).

In the Orkanger area, west of Trondheim, exhumed high grade metamorphic rocks are generally represented by amphibolite or amphibolite garnet schist (Tucker et al., 2004). As a response to

the exhumation and denudation, magmatic intrusions were concentrated in the MWGR. This is in contrast to the southern parts of the WGR where intrusions are scarce (Braathen et al., 2000).

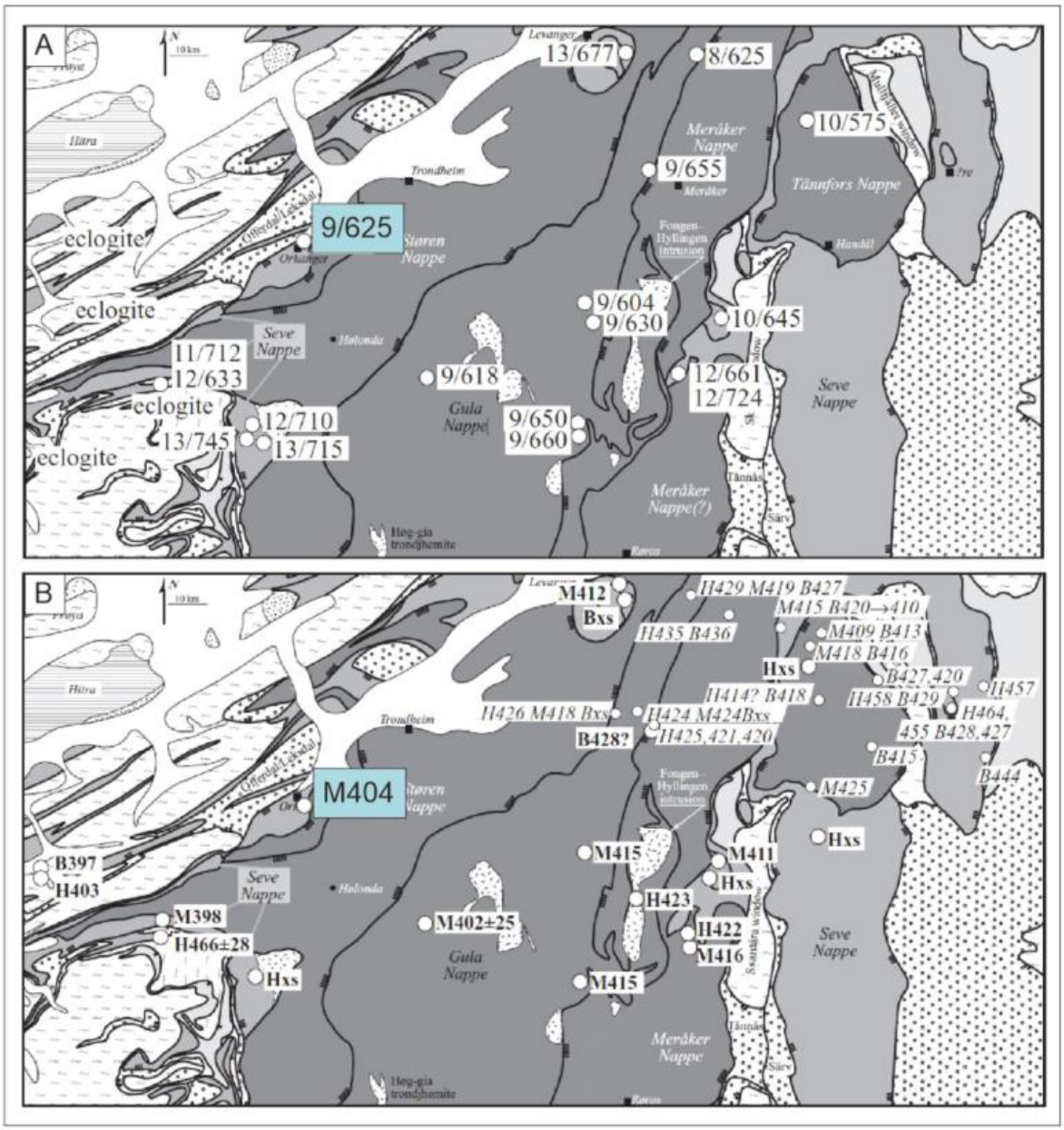

Figure 2.2: A) Samples taken from different locations within the Mid-Norwegian region showing pressure and temperature conditions. First number represents the pressure in kbar and second number represents maximum temperature. B) Map of Mid-Norwegian region with ages in millions of years given for each sample location. Both figures are from Hacker and Gans (2005).

2.2. The Orkanger Road Cut

Intrusions in the west-Trøndelag occur mostly as boudinaged pegmatites. In Tråsåvika and Fanrem, west-Trøndelag, two pegmatites have been dated by Tucker et al. (2004) yielding ages of ca. 431 Ma and 422 Ma and which Robinson (2008) believed to belong to the same group of

pegmatites found within the Orkanger region (Tucker et al., 2004).

Previous studies of the Mid-Western part of the Caledonian orogeny have focused on syn-orogenic processes with most emphasis on the South-Western Gneiss Region (Andersen, 1998; Fossen and Dunlap, 1998; Krabbendam and Dewey, 1998). Late orogenic processes including exhumation of gneiss-complexes, activity along large-scale detachments such as the Høybakken detachment and development of Devonian basins are especially well studied. Progress has been made towards a better knowledge of the details of the late- to post-orogenic extensional phase in this region by e.g (Chauvet and Séranne, 1994; Braathen et al., 2002; Roberts, 2003; Osmundsen et al., 2006).

Interestingly, a significant component of the late to post-orogenic deformation phase in the area was accommodated by brittle deformation, resulting in a broad spectrum of still poorly investigated and understood deformation features. These brittle structures have commonly reactivated ductile features inherited from the evolution of the large detachments. The variety and complexity of brittle reactivation seen in the Trøndelag area is impressive and deserves careful investigations. More attention has so far been paid to the structural brittle template of the South-Western Gneiss Region (Eide et al., 1997; Redfield et al., 2005b; Redfield et al., 2005a).

The outcrop studied in this thesis is a part of the Seve-Nappe, with Blåhø being its Norwegian equivalent, of the Upper Allochthon (Figure 1.2). The Orkanger Road Cut (ORC) is a several hundred meters long and up to 5 m high exposure along the E39 road just northeast of the city of Orkanger (Figure 2.3). The mapped road cut trends NW-SE. Structures including folds, several foliation types, thrust and extensional ductile shear zones and brittle faults are observed obliquely because the outcrop face is not perpendicular to foliation. Exposed lithologies consist mainly of intermediate to mafic metamorphic rocks such as amphibolites. Abundant pegmatites are also found at the outcrop and in the greater Orkanger region.

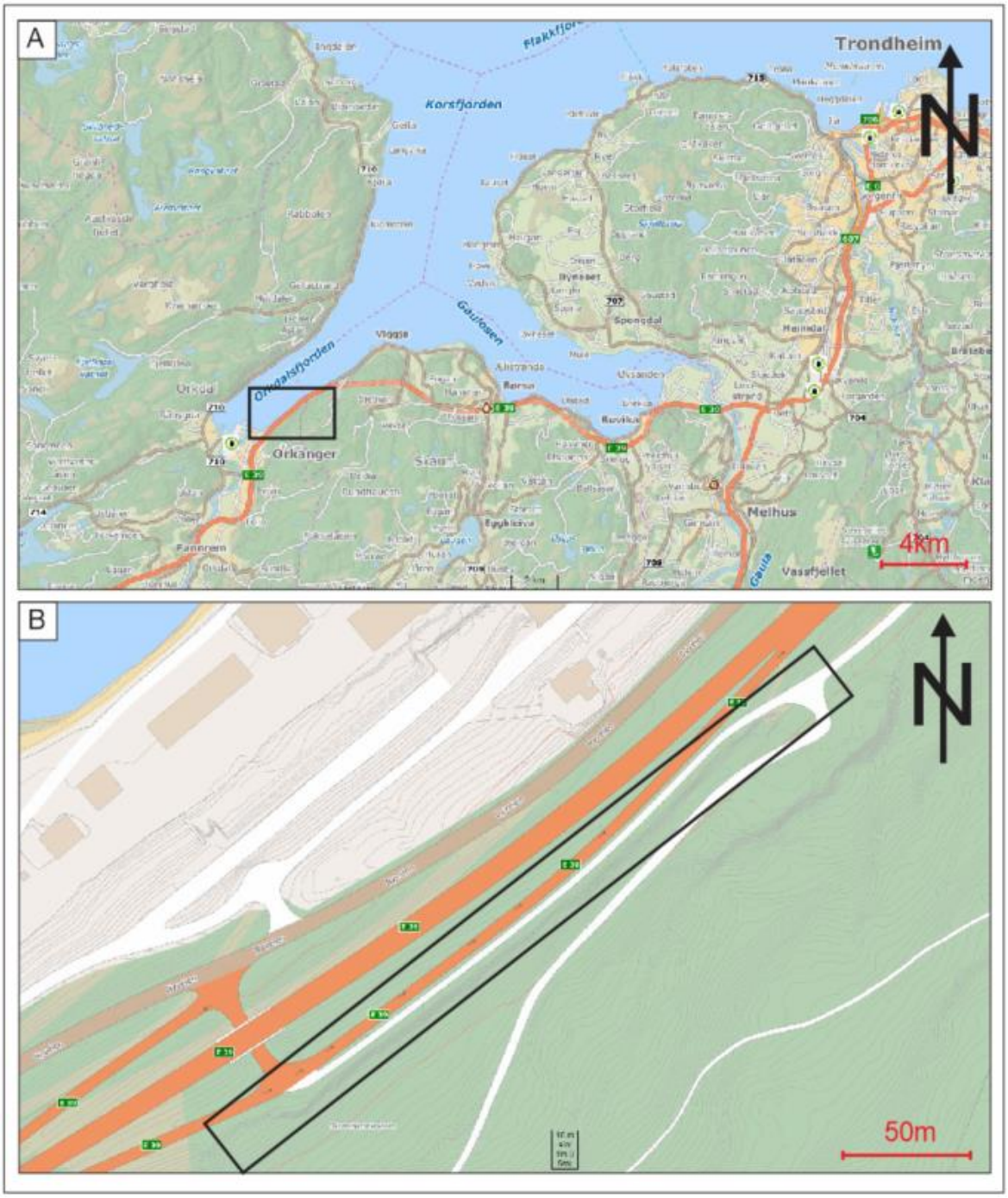

Figure 2.3: A) Location of the field area along the E39, ca. 1 km northeast of the city of Orkanger. B) Close up of the outcrop measuring 300 m in length. The Elkem Thamshavn plant is situated just across the road.

Two aspects deserve particular attention when trying to improve our current knowledge of the geometrical and kinematic evolution of transtensional deformation associated with gravitational collapse of the Caledonian orogen: This thesis will, by careful selection of key outcrops, (1) document the exhumation in the MWGR in terms of the temporal sequence of developed structures that made it possible, before (2) investigating the role played by pre-existing structures on the localization of both ductile and brittle strain within the extensional structures.

This study consisted of a high-resolution structural analysis of the ORC, which led to the creation of a unique structural database of all structures including faults, folds, foliations, lineations, fault core, damage zones, thrust zones, extensional ductile shear zones and brittle extensional structures. Mapping, characterization and sorting in terms of geometric characteristics, kinematics, metamorphic grade and overall deformational style were used to reconstruct the structural chronological evolution of the final assembly, collapse and exhumation of the Caledonian orogen in the study area. This unique data set also allows the detailed analysis of fundamental processes that steer brittle fault reactivation, with emphasis paid to the study of how brittle fault cores and damage zones exploit pre-existing ductile precursors and lithological anisotropies such as pegmatites and folds. Existing meso-scale structural studies in the region will therefore be supported by a more detailed data set and structural analysis on both mesoscopic and microscopic level with emphasis on different types of brittle reactivation. The obtained results have been used to further our knowledge of the regional tectonic evolution in the MWGR.

3. Theory

3.1. Faults

A fault can be defined as a discontinuous undulatory plane with a surrounding fault zone where slip occurs both parallel and sub-parallel to the fault plane. (Fossen, 2010) The principal way for faults to slip gave way for the Anderson model. In 1951 Anderson published the article on principal tectonic stress regimes. He was the first to categorize faults into normal, thrust and strike-slip faults by perpendicular stress axes. The principle is that there is always one vertical stress axis (σ_V), which also defines each regime:

$\sigma_V = \sigma_1$; normal fault regime
$\sigma_V = \sigma_2$; strike slip fault regime
$\sigma_V = \sigma_3$; thrust fault regime

Andersons tectonic stress regime is only valid when observing isotropic rocks with horizontal and vertical stress axes. The classification is no longer valid during stress axis rotation, which can be caused by anisotropic rocks, folding or reactivation of relict faults. Stress axis rotation may therefore lead to the development of oblique-slip faults (Bott, 1959).

3.2. Shear zones

The development of a ductile shear zone is the product of continuous plastic deformation. Based on the orientation of the biggest compressive stress tensor, the rock will shear and develop one of the three fault regimes described by Anderson (1951) (Figure 3.1A, B and D).

Ductile shear zones develop through shearing of rock where shear describes the deformation of a rock and the subsequent development of deformation textures (Simpson and De Paor, 1993). Ductile shear zones are most easily observed in homogeneous magmatic bodies, allowing for easy kinematic and geometric interpretation of the shear zone (Selverstone et al., 1991). Shear zones evolve through continuous deformation, which leads to dynamic recrystallization and grain size reduction on the microscopic level. This will lead to strain softening over a wider

area with a central zone of increased deformation and subsequent displacement (Poirier, 1980). Shear can be divided into pure shear and simple shear. Pure shear is a co-axial form of deformation where the principal axes have not been rotated from their initial position and there is no change in volume. Simple shear represent deformation where the principal axes rotate from their original position and allows for asymmetric structures to develop yielding clues to the transport direction (Passchier and Simpson, 1986; Gapais, 1989; Simpson and De Paor, 1993; Fossen, 2010). Ductile shear zones often show unique structures and textures such as asymmetric clasts, shear bands and quartz recrystallization that may be used to infer the transport direction of the hanging wall (Hanmer, 1986; Passchier and Simpson, 1986; Gerald and Stünitz, 1993). Lineations as well as foliation represent the finite state of strain in a plastically deformed rock and are considered good strain markers (Ramsay, 1980).

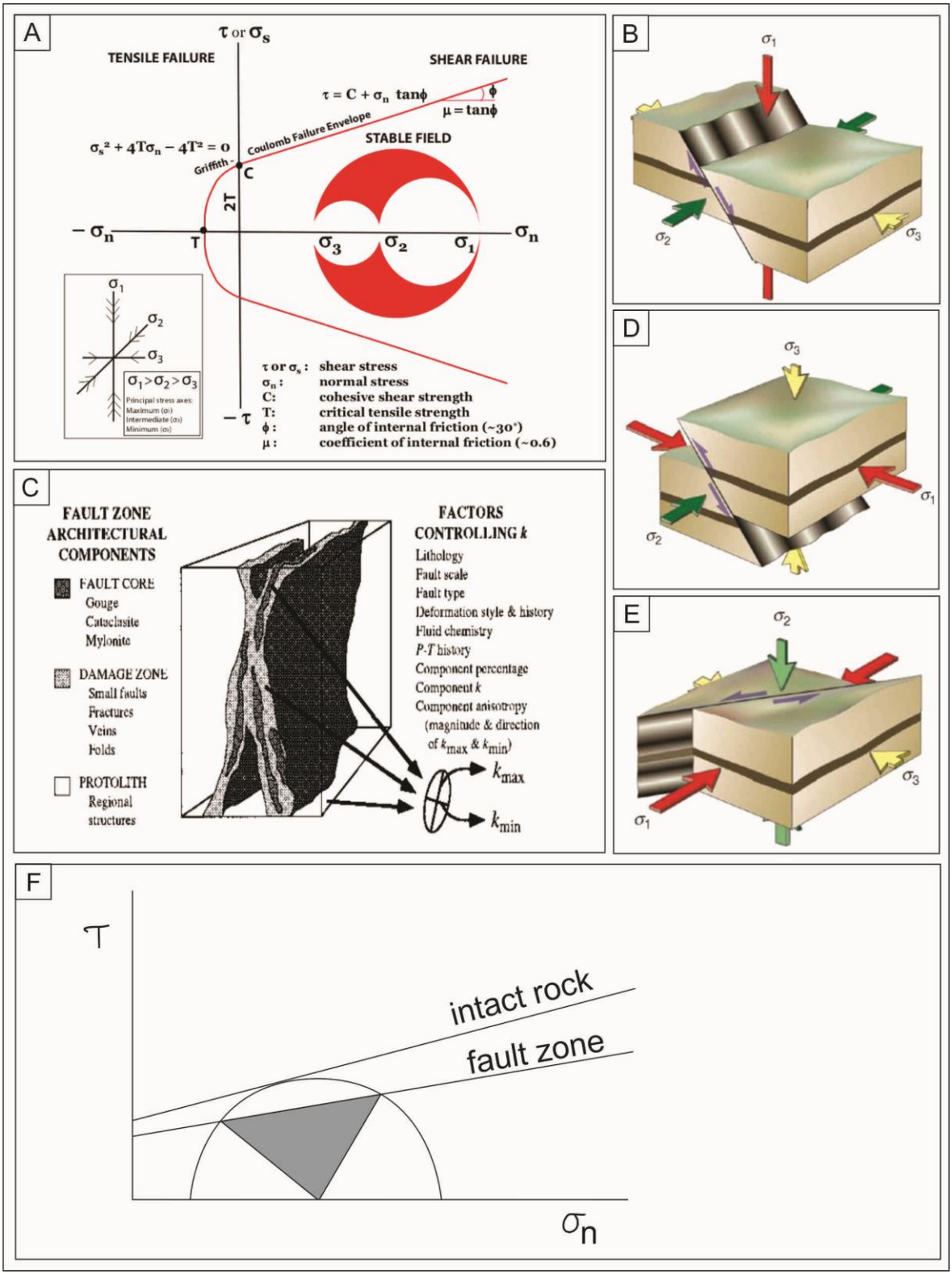

Figure 3.1: A) Mohr diagram with explanation of the different parameters used to calculate shear strength, after Fossen (2010). B) Normal faulting described by Anderson, 1951. C) Fault zone characterization after Chester and Logan (1986) D) Reverse faulting described by Anderson in his article from 1951. E) Strike-slip faulting also described by Anderson, 1951. F) Brittle reactivation of faults shown in the Mohr diagram, after Etheridge (1986).

3.3. Brittle-ductile faults

Brittle-ductile faults are developed in the crust at the brittle-ductile transition, which represents upper greenschist facies and is therefore dependent on both temperature and pressure conditions. Rocks deform under different conditions as minerals behave differently at various temperatures. Studies on brittle-ductile faults have mostly been done on fault rocks containing feldspar and quartz (Kjøll et al., 2015). Feldspar, quartz and olivine are the three most abundant minerals in the earth. Feldspars undergo brittle deformation at the same pressure and temperature conditions whereas quartz will deform plastically (Sibson, 1977; Simpson, 1985). This is due to the fact that quartz needs a lower resolved shear stress than feldspar to enable dislocation glide along its slip planes (Tullis and Yund, 1977; Marshall and Mclaren, 1977; Fossen, 2010). A mylonite is an example where granites were deformed at brittle-ductile conditions show an overall grain size reduction of feldspars. Microscopical analysis of rocks deformed under these conditions show both brittle and ductile deformation features, where the main indicator is an overall grain size reduction of both feldspar and quartz (Mitra, 1984). Microscopical studies show evidence of fracturing and cataclastic flow controlled by diffusion or dislocation movement. (Mitra, 1984). Both Mitra (1984) and Hirth and Tullis (1994) observed that rocks belonging to the brittle part of the transition often show fractures cutting through randomly oriented faults, while other parts of a fault showed evidence of ductile deformation. This included grain size reduction and oriented clasts with fractures that terminated at the boundary between clast and matrix in thin section.

3.4. Brittle faults

Brittle faults develop within the upper 10 km of the crust where temperatures reach up to 300°C and slip discontinuously contrary to ductile faults. It is widely acknowledged that faults can develop in at least three different ways: through linkage of relict brittle structures, through linkage of precursory structures and reactivation of relict shear planes (Peacock and Sanderson, 1991; Dawers and Anders, 1995; Fossen, 2010). A three stage model for brittle fault generation was made by Crider and Peacock (2004) where stage 1 is represented by shearing along relict structures such as extension fractures, stage 2 show the linkage of relict structures in the fault zone due to stress perturbation and fault propagation. Stage 3 represent completion of the fault

and slip along one continuous fault.

A brittle fault often consists of a fault core and a damage zone where the fault core consists of mylonite, cataclasite or gouge. The damage zone show structures such as small faults, joints and veins (Caine et al., 1996). Strain in brittle faults is concentrated into the fault core whereas the damage zone undergo far less deformation. The damage zone will consist of shattered rock where strain has been localized often yielding lens-shaped rocks (Kim et al., 2004). This differentiates the brittle fault from the ductile shear zone which show a continuous strain gradient throughout the shear zone with ductile kinematic indicators (Segall and Pollard, 1980; Crider and Peacock, 2004). Brittle faults are also regarded as important fluid conduits, where permeability is controlled by the fault core composition. A granular fault core will act as a fluid barrier while a fault core with fault parallel fractures will act as a conduit (Wibberley et al., 2008).

Microscopic examination of brittle faults reveal several different structures that develop during slip. These include cataclasis and extensional micro-fractures. Cataclasis is a form of fracturing of grains through rigid body rotation whereas extensional micro-fracturing is a tensional fracture developed in the σ_1-σ_2 plane (Ramsay, 1980; Chester and Logan, 1986). These structures are products of syn-tectonic deformation within the fault core and damage zone (Sibson, 1977; Fossen, 2010). If a fault core has undergone extensive cataclasis the fault core material will evolve into gouge, a mix of clay sized fault material that is produced in response to the grinding of fault material (Scholz, 1987; Haggert et al., 1992).

3.5. Brittle reactivation

Reactivation of faults is a response to the reorientation of the stress field within the crust and is mechanically favoured in contrast to generation of new faults (White et al., 1986; Etheridge, 1986). Fault slip is expected when the maximum resolved shear stress exceeds the frictional coefficient F. The frictional coefficient, a number describing the rocks ability to resist slip, is equal to the normal stress acting perpendicular to the fault plane (Jaeger et al., 2009). In addition to the strength of the fault, host rock strength and fault orientation in relation to the regional stress field will determine the mode of faulting (Etheridge, 1986). The maximum resolved shear stress needed for slip initiation is reduced when slip occurs in a relict shear zone, which contains

a shear plane oriented foliation (White et al., 1986). The frictional failure envelope indicates that reactivation of faults will need less differential stress in contrast to a fault free country rock to reach failure (Figure 3.1). If the size of all the principal stress tensors are known, the shear strength, normal stress and maximum resolved shear stress can be found.

Relict faults often experience fault reactivation as the principal stress field rotates in their presence. Old ductile shear zones and brittle-ductile faults often experience reactivation of the shear plane/fault plane (Sibson et al., 1988). Through denudation ductile shear zones and brittle-ductile faults are exposed to lower temperatures and pressures, which allows for the presence of brittle faulting (Crider and Peacock, 2004). Microstructures can reveal how fault-oriented minerals show coaxial brittle faulting. The pre-existing plane of weakness developed by either ductile or brittle-ductile faulting, with a differently oriented foliation, will therefore be the preferred slip plane for late brittle faults (Sykes, 1978; Crider and Peacock, 2004). Normal, thrust and strike-slip faults may all be reactivated by younger faults if the maximum principal stress tensor is large enough. Most earthquakes nucleate repeatedly at the same location as a result of fault reactivation (Wiens and Snider, 2001; Collettini et al., 2005).

3.6. Mohr diagram

The Mohr diagram is based on the work of Christian Otto Mohr and is a graphical presentation of a rock's mechanical strength (Fossen, 2010). The diagram consists of a rotated coordinate system where the vertical axis represents the shear strength (T) and the horizontal axis represents the differential stress (σ_n). The difference between the largest (σ_1) and smallest stress tensor (σ_3) is the diameter of the Mohr circle and represents the amount of differential stress. The Mohr circle is enveloped by what is known as a failure envelope, and when intersected by the Mohr circle, will yield the shear strength of the rock. The failure envelope (line) is a best-fit line calculated for each rock type based on several triaxial experiments where the differential stress (σ_1- σ_3) is varied, yielding Mohr circles of varying sizes (Fossen, 2010).

The failure envelope consists of different sections with different fracture criteria (Fossen, 2010). Where differential stresses are negative (tensile regime), the criterion is named the Griffith criterion. The Coulomb criterion defines the area where the envelope line is linear and rocks fails through shearing. Von Mises criterion is the area where the envelope line is horizontal,

indicating ductile deformation conditions with constant shear strength. The shear strength of a rock is therefore based on the differential stress through the Mohr circle. This diagram thus allows the analyst to calculate any possible shear stress and normal stress of a homogeneous body of rock at failure, which is critical to structural engineers and geo-technicians (Fossen, 2010).

The Mohr circle operates in reference state stress fields. Deviations from a reference state are often addressed to tectonic stress, both local and regional. Regional stress fields represent deformation patterns seen over large areas while local stress fields may deviate from regional stress fields. A local stress field can be rotated by transposed layers, fault and fold interference within a regional stress field (Fossen, 2010). It is also important to address the constraints of the Mohr diagram. Shear strength calculated through the Mohr diagram is based on rocks that are homogeneous and undeformed. Any presence of old faults, fracture zones, heterogenic rocks or poly-phase deformation will greatly affect the values calculated by the Mohr diagram (Fossen, 2010).

3.7. Folds

A fold is a geometrically bent layer that is a response to ductile deformation of multi-layered rocks and their interpretation may yield significant information concerning the local stress field (Ramsay, 1974). Folds can be classified based on different parameters such as the thickness of hinges and limbs and their spatial orientation. Their geometry is acknowledged as a specifically important parameter in fold classification (Hudleston, 1973).

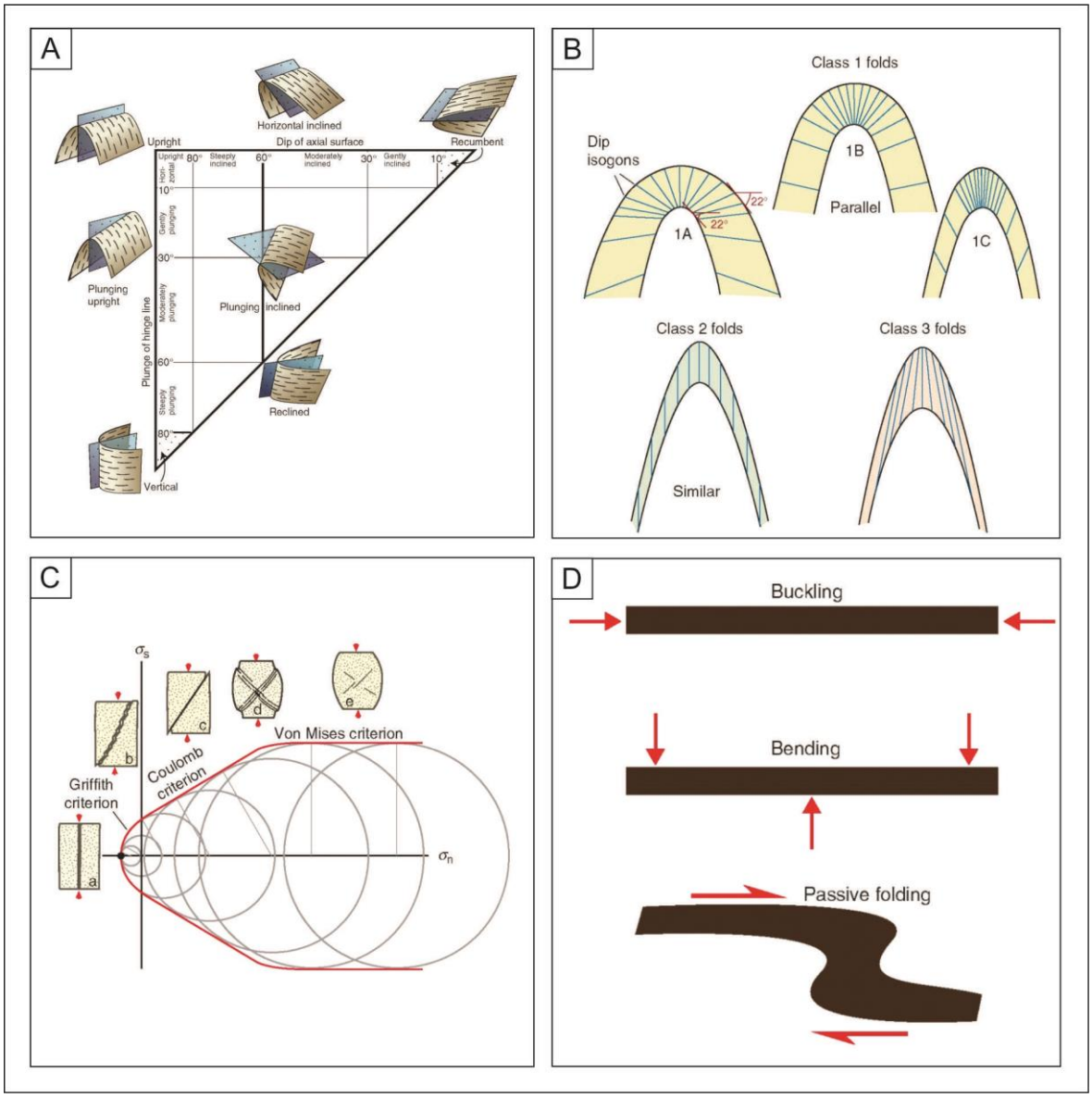

Figure 3.2: All figures are after Fossen (2010). A) Fold classification based on axial plane orientation. B) Fold classification based on dip isogons developed by Fleuty, 1959. C) Mohr diagram with its respective fracture criterions developed by Christian Otto Mohr in 1882. D) Different types of folding, after Fossen (2010).

A widely used classification system is that of Ramsay (1974) who classified folds based on dip isogons. Dip isogons are lines that can be drawn between the inner part of a limb or hinge and the outer part of a limb or hinge, which have the same dip. This produces different sets of isogons for different fold geometries and allows the categorization of folds. Ramsay divided folds into three distinct groups based on their dip isogons. Class 1 show dip isogons converging inwards. Class 2 has dip isogons, which run parallel to the axial trace. Class 3 show dip isogons converging towards the outer arc of the fold (Fossen, 2010).

Fold geometry may give indications of the amount of deformation that the rock has undergone and allow for categorisation of their shape. A characterization of the fold geometry is presented

in Fleuty (1964). He developed a system that named folds based on the spatial orientation of the axial plane. Together with fold geometry, the orientation of folds may aid the reconstruction of a paleostress-fields with an indication of induced strain (Hudleston, 1973; Fossen, 2010).

3.8. Win Tensor

Win tensor is a structural geology programme, which allows the plotting of fault planes, axial planes, fold axes and fault plane mineral coating. It is made specifically for brittle faults and paleostress reconstruction. This comprehensive tool allows the user to generate local stress fields based on input data that will produce stereonets. These stereonets can also be processed further by choosing the processing tab. This allows the user to optimize the principal stress axes by running a set of iterations yielding the ideal position based on input data. This will yield the stress field orientation present during fault generation.

3.9. Fault slip data inversion

The paleostress inversion method is used to reconstruct stress fields and their evolution through time. The analysis starts out with collecting data on brittle faults in the field. This data includes the orientation of the fault plane, slip direction and the sense of slip on the plane. The most basic versions of paleostress analysis yields the orientation of the stress field, consisting of the principal stresses σ_1, σ_2 and σ_3 oriented perpendicular to each other. To predict the relative size of the principal stresses, more advanced paleostress inversion methods are used.

Paleostress inversion that is concordant with Andersonian theory can be regarded as one of the most basic types of paleostress inversion. One of the three principal stress tensors (σ_1, σ_2 or σ_3) is oriented vertically and depending on the faulting regime will show dip slip (Figure 3.3). The problem arises when oblique slip faults are evaluated, which do not follow the theory of Anderson (Reches, 1978). Different paleostress methods make several assumptions and simplifications: no stress field perturbations during fault generation, no block faulting, and the host rock must be homogeneous and isotropic. A stress field will therefore represent the volume of host rock that contains the faults measured and the time interval when the faults were formed or reactivated (Lacombe, 2012).

The direct inversion method is a method based on an algorithm that finds the best stress tensor that is compatible with all the fault data and at the same time keeps the misfit angle below 30° (Delvaux and Sperner, 2003). The misfit angle is the angle between the optimally oriented slip along each of the fault planes (dip-slip) and the actual slip directions (Angelier, 1979; Pollard et al., 1993). Direct inversion methods are only concerned with fault plane orientation and slip direction and can therefore not infer any stress tensor magnitudes. This means that the direct inversion methods describes the reduced stress tensor of a stress field, which consist of four variables: the principal stresses σ_1, σ_2 and σ_3 and their ratio. Four variables need a minimum of four fault planes with slip directions to be able to solve the reduced stress tensor. If more fault data is added the statistical strength of the produced stress field will increase (Lisle et al., 2006).

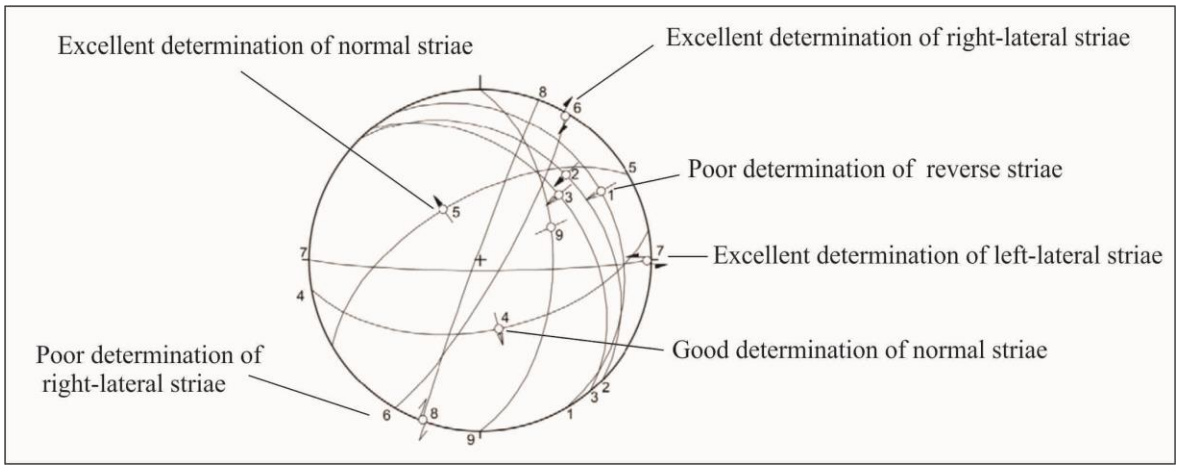

Figure 3.3: Stereonet displaying faults (great circles) and the consideration of different types of striae. Redrawn after Viola and Ganerød (2007).

In addition to the fault data described above, the type and presence of minerals coating fault planes are of great importance. Typical mineral coatings include epidote, quartz and chlorite, which often make up the slickenlines used to measure the slip directions. The type of coating may infer what crustal level the fault set developed at. The separation and treatment of fault data gathered from the field is an iterative process involving both separating and regrouping data into more homogeneous groups until they display a plausible natural set of stress fields. The operator controls this separation fully (Nemcok, 1995). Some heterogeneity, e.g. oblique slip faults, must be a part of the data set to allow for the calculation of the stress field (Hippolyte et al., 2012).

4. Methods

The methods used in this master thesis includes field work, sampling, thin sections microscopy, fold and fault measurements with a compass, photos, photo stitching, CorelDraw and Win_Tensor.

Field work

Four weeks of field work was done between November 2013 and November 2014. All measurements were done with a Silva Expedition S compass using the dip and dip direction system.

Photos

Photos taken during sampling, of faults and folds, were all given geographical orientations.

Photo stitching

The whole road cut was methodically photographed with a Canon EOS 500D with an 18-55mm lens. Both Hugin Panorama Stitcher and Adobe Photoshop were used to stitch a total of 80 pictures into one picture representing the whole section.

CorelDraw X7

The photo stitch was interpreted in CorelDraw X7, which allowed for accurate and detailed sketching and re-iterational interpretation as the amount of data increased.

Samples

Samples collected in the field consisted of gouge and oriented country rock samples. Dip and dip direction as well as trend and plunge were noted for each oriented sample. Samples were marked with the stratigraphic correct way up by an arrow as well as an arrow indicating the plunge of the lineation. Faults and folds were also measured with the Silva compass.

Thin section preparation

Thin sections were cut by the thin section preparation laboratory at the Institute of Geology and Rock Mechanics (NTNU). Samples were cut vertically along the lineation to get the correct section for shear sense analysis. Small 4x2x0,7 cm sections were then glued on to glass plates for further preparation. The sections were then grinded down to 30 µm and overlain by a glass

plate.

Optical microscopy

Two optical microscopes have been used to do thin section analysis. A ZEISS axioskop 40 with a ZEISS Axiocam MRc5 digital video imaging sensor were used for taking photomicrographs.

Win_Tensor

Data measured in the field consists of fault planes, axial planes, fold axis, fold limbs and mineral lineations. The data was plotted in Schmidt diagrams.

5. Results

Here, results are presented that allow the unravelling of the complex structural evolution recorded along the ORC before examining the modes of brittle reactivation of inherited ductile structures. Relevant data gathered through detailed mesoscopic field observations and thin section analysis provides a contribution to the analysis of these questions.

Every meter of the ORC has been meticulously studied and photographed. A photo-stitch of the entire length of the road cut has been generated to facilitate detailed interpretations. The labelled section is provided as an attachment in the appendix (coined the "cross section" in Appendix 4) based on the photo-stitch (Appendix 3). The cross section is measured in meters starting at 0 in the NE termination of the outcrop and ending at 300m in the SW. Every comment and observation is referred exactly to the precise observation spot at the outcrop by a meter marker that allows the reader to pinpoint the accurate location of the structure on the cross section.

The cross section (Appendix 4) is a high-resolution sketch map where the main lithological contacts, pegmatites, faults, folds, shear zones, high strain zones, foliation and samples are drawn and marked at their exact spot along the road cut. The cross section also contains stereoplots of the orientation of the main fabric elements such as foliation, lineation and fold axis.

5.1. The structural evolution of the Orkanger Road cut

5.1.1. The outcrop

Mesoscale observations

The host rock of the ORC is represented by a grey to black coloured garnet-bearing amphibolite (Figure 5.3A and B). The rock is compositionally heterogeneous and layered, with irregularly alternating thick mafic domains and thinner felsic intervals. The felsic parts are formed by coarse-grained feldspar and quartz. Parts of the ORC also show a green, red and orange rust-coloured section that is constrained by pegmatites and shear zones 16A, 16B and 18B (cross section and Figure 5.1). These rust coloured zones is most likely a product of late fluid interaction. Pegmatites have intruded into the amphibolite schist parallel to foliation as well as

being part of old high strained zones. These three pegmatite generations are for convenience now called generation 1, 2 and 3. Generation 1 consists of the earliest pegmatites, which are incorporated into high strain zones (HSZ). Generation 2 represents a large foliation-parallel intrusion. Generation 3 represents the latest intrusional event, cutting through the former generations. Sulphides, anhedral calcite, epidote, chlorite and quartz are displayed on brittle and brittle ductile faults, as well as in segments of the country rock. Deep red garnets averaging 0,5 cm in diameter are common and occur in tight clusters in random segments of the ORC (Figure 5.3A).

Microscale observations

The host rock of the ORC show large amounts of feldspar and fractured garnets. Feldspar crystals occur as sheared and fractured grains with intergrowths. Feldspar neo-crystallisation is also present. The host rock is an amphibolite, which consists of an average of 43% percent hornblende, 29% plagioclase, 15% and additional minor minerals such as garnet, biotite, calcite, sphene, epidote and sulphides such as pyrite. The texture of the amphibolite varies from bands with phase mixing between plagioclase and hornblende to levels of segregated sections hornblende and feldspar with quartz. Biotite wraps around feldspar clasts and occurs as stable phase along discrete shear bands. Sphene occur as inclusions within hornblende grains. Evidence of strain partitioning is seen throughout the ORC, e.g in Figure 5.23. Other thin sections display less strain through the lack of compositional banding and grain size reduction.

In summary, garnet amphibolites of the ORC equilibrated under amphibolite facies metamorphic conditions and are probably derived from a gabbro. Evidence of this is the large quantity of hornblende. This observation is also consistent with work done in the region (Hacker et al., 2010). Biotite in shear bands can reveal the age of deformation, but has not been dated in this study.

Figure 5.1: Rust-coloured sections of the ORC which are constrained by ductile shear zones to the left and right in the in picture A and by pegmatites in B. These sections show evidence of significant fluid interaction, displayed through high amounts of sulphides within the amphibolite host rock.

5.1.2. High Strain Zones (HSZ)

Mesoscopic observations

The outcrop contains several high strain ductile zones (HSZ) shown in brown in the cross section (Figure 5.2). These zones are visible throughout the ORC, but vary somewhat in thickness. The HSZ are folded making them a part of the oldest structures within the ORC and important in structuring the crosscutting relationships. High strain caused dynamic recrystallization of the protolith resulting in bands of mylonite to ultramylonite with thicknesses ranging 40-70 cm in width. The HSZ display mylonitic textures characterized by a compositional banding consisting of the alternation of thin (< 0,5 cm) felsic bands containing clasts of feldspar that, in total, make up highly thinned boudin-structures (Figure 5.2). Hornblende crystals occur as sigmoidal grains that envelope plagioclase clasts. The HSZ can be observed from distance 60 m to 220 m. They are cut by all other identified structures along the ORC, which gives it a relative age predating all other structures (see Figure 5.3).

Mapping indicate that the small segments of HSZ found within the ORC can be related to one single specific high strain zone. They can be used to assess the displacement across later faults and shear zones. The HSZ are characterised by thin bands with feldspar clasts (d=0,2 - 1cm) originating from the severe transposition of generation 1 pegmatites, running parallel to what is referred to as the general foliation. From distance 210 m to 220 m, in Figure 5.2C the thin feldspar bands are extremely attenuated from an undeformed thickness of 10 cm to a deformed thickness of 0,7 cm. Grain size differs from 0,5 cm within the clasts to 0,1 cm within the thin bands connecting the clasts. These thin bands show symmetric kinematic indicators of clasts with tails that are oriented parallel to the general foliation, which suggests a component of pure shear. Thin section analysis show a high amphibolite content in the HSZ (cross section: 205-220 m).

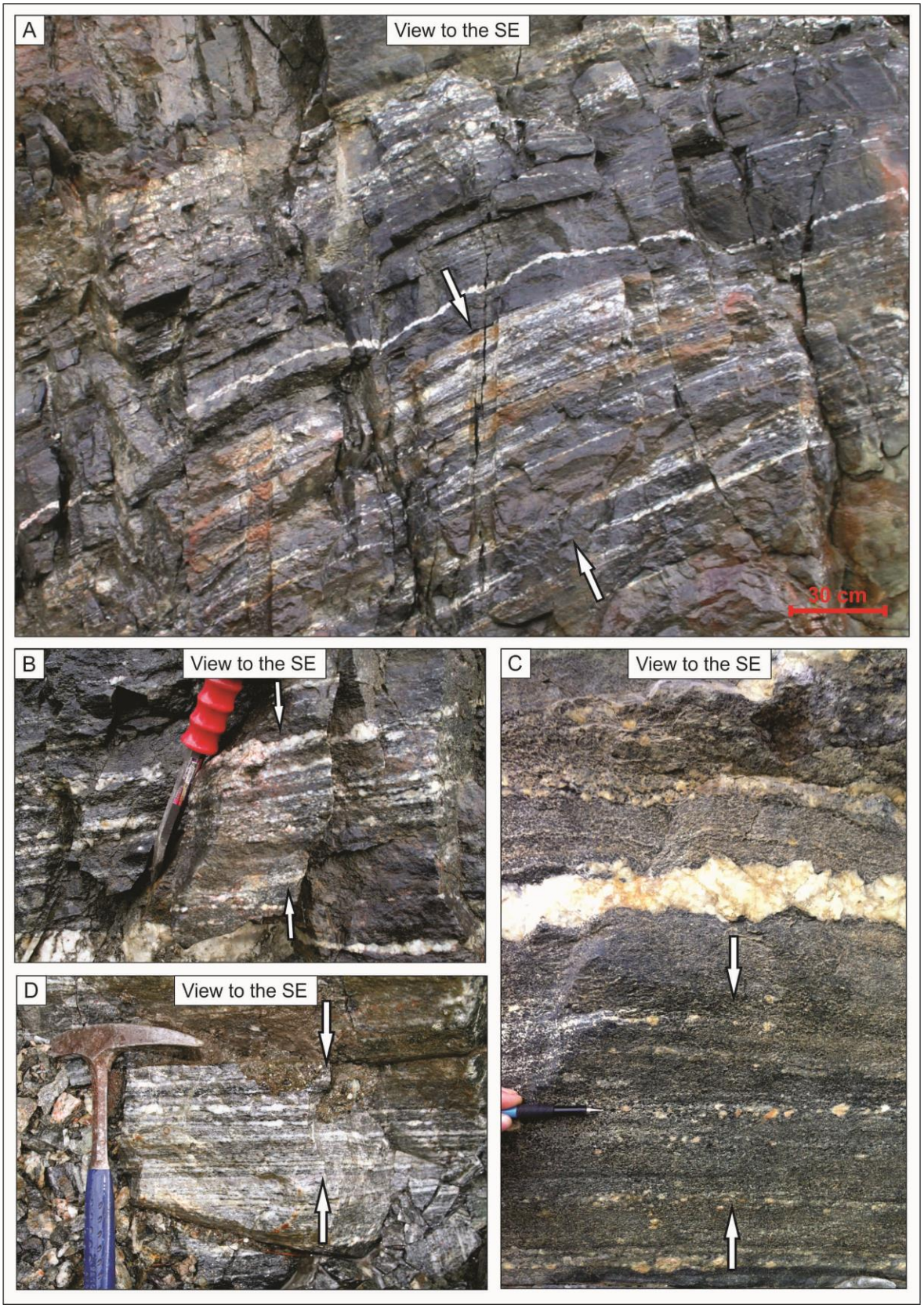

Figure 5.2: A) HSZ (cross section: 169 m) showing mylonitic fabric with overall augen texture characterized by mm-size clasts of plagioclase dispersed within a finer matrix of amphibolite. B) Picture of similar mylonitic fabric found within the amphibolite (cross section: 229 m). C) Mylonitic fabric found above ductile thrust 23 is consistent with other mylonitic fabrics within the ORC. D) Picture of similar texture (cross section: 194 m) as displayed in the latter pictures.

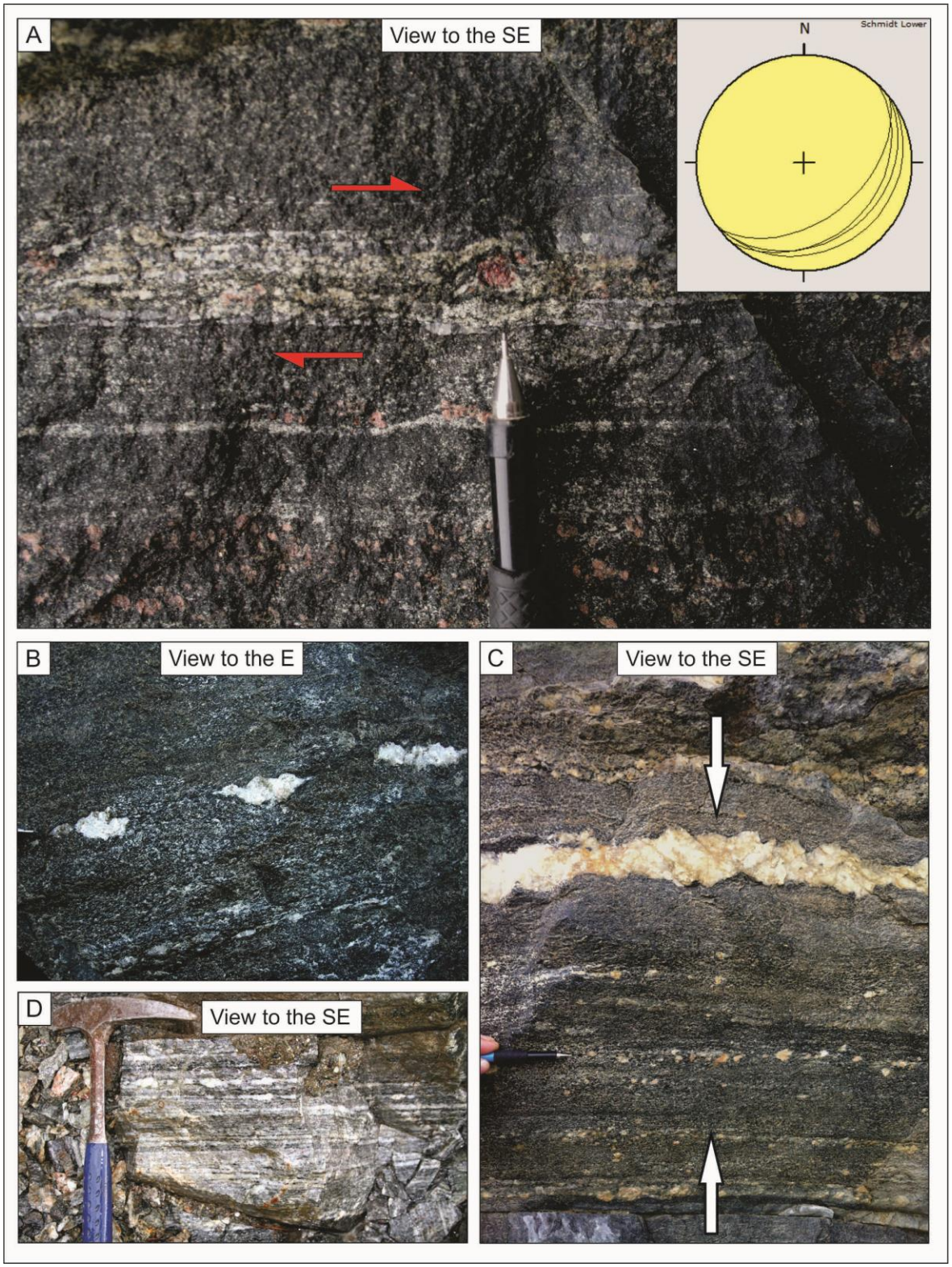

Figure 5.3: A) Thinned and transposed pegmatite with rotated garnets enveloped by felsic bands (cross section: 35 m) with its orientation displayed in the stereonet. B) Asymmetric feldspar clasts detached from each other along a highly transposed thin pegmatitic level (cross section: 63 m) C) Top of picture showing slightly deformed pegmatites oriented parallel to foliation. In the lower section (marked by the pen), only thin bands of feldspar clasts are seen oriented parallel to the foliation, indicating high strain (cross section: 217 m). D) Thinned white feldspar bands indicating high strain and transposition of pegmatite (cross section: 194 m).

The HSZ run parallel to regional foliation and separates less deformed domains. The high strain zones themselves are folded by large-scale road cut sub-parallel folding (ENE-WSW), which folds the foliation and the HSZ. The fold orientation is displayed in the summary stereonet in Figure 5.8B.

The described HSZ are cut by all other identified structures and must therefore be a part of an early strain accommodation history that nonetheless postdates generation 1 pegmatites, as there are boudinaged plagioclase bands within the shear zones that are interpreted as highly transposed pegmatites. Highly thinned and boudinaged pegmatites indicate that the HSZ predate generation 2 pegmatites as thinned pegmatite-bands from generation 1 are included within the HSZ. The thin feldspar bands of the HSZ, with symmetric feldspar clasts and overall lack of monoclinic asymmetries, are indicative of pure shear strain.

Microscopic observations

Feldspars show a clear grain size reduction in thin section (Figure 5.30) of this mylonitic horizon. The feldspars are thinned into discontinuous microscopic boudin-structures wrapped by hornblende grains, showing sigmoidal geometry and making up segments rich in hornblende. These hornblende layers are separated by feldspar-rich bands mimicking the texture observed at the scale of the outcrop. Thin section 194_1 consists of large amounts of plagioclase and some hornblende (see Appendix 1 for more details).

5.1.3. Pegmatites

Mesoscopic observations

The ORC contains three distinct sets of white pegmatites (generation 1, 2 and 3), which are mineralogically and lithologically alike. Generation 1 is incorporated within the HSZ and are therefore described in section 5.1.2. Generation 2 is oriented parallel to the general foliation within the ORC, and dip towards the NE at about 40°. Generation 2 pegmatites are commonly deformed and transposed into boudins and are folded by small drag folds and large scale folds in the ORC. Generation 3 is oriented sub-vertically, dipping both to the east and the west where they cut generation 1 and 2.

Both pegmatite generations contain feldspar, quartz and calcite. There are, however, several intriguing observations that require mentioning. Pegmatites belonging to generation 1 are invariably bigger and thicker (up to 70 cm) than pegmatites of generation 2, which measure instead no more than 1-2 cm in width. Crosscutting relationships can be viewed in several places (Figure 5.4) within the ORC where generation 2 cuts through generation 1 and the general foliation. This yields a relative age where generation 1 predates generation 2. All pegmatites, however, are transposed by almost all extensional and compressional ductile shear zones (see coss section). As mentioned in the geological background of the study area, the pegmatites found within the ORC are believed to be of the same age as those found at Tråsåvika and Fanrem, dated to 431 Ma and 422 Ma (Tucker et al., 2004; Robinson, 2008).

In terms of pegmatite abundance, the ORC can be divided into pegmatite-rich and pegmatite poor sections (Figure 5.5). Pegmatite-poor sections are delimited by the 0-40 m markers and from the 240-300 m markers in the cross section. These segments are also generally poorly faulted and fractured, though lithologically similar to the remaining parts of the outcrop.

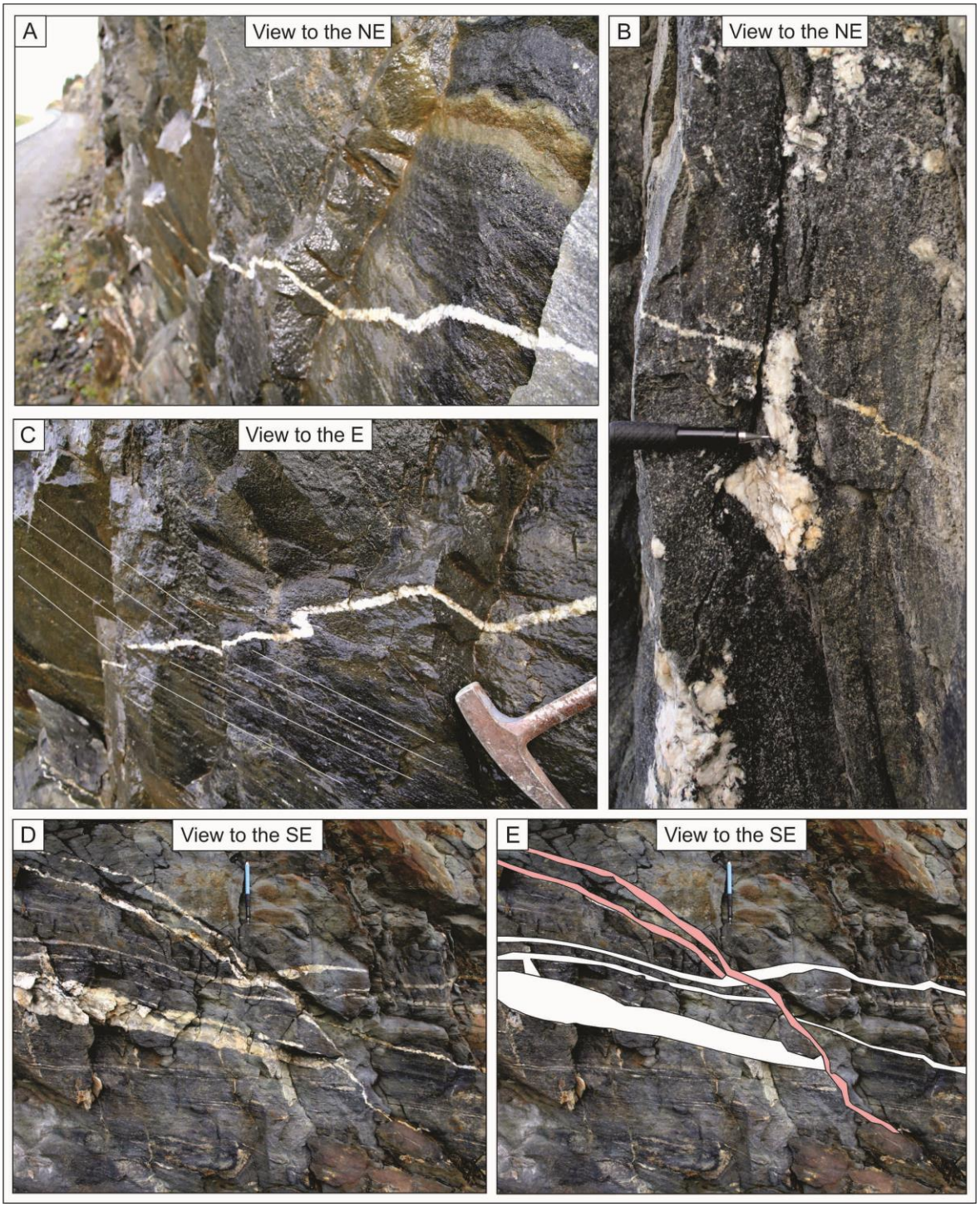

Figure 5.4: A) Pegmatite generation 3 cutting through foliation (cross section: 214m). B) Pegmatite generation 3 cutting diagonally through the foliation and coaxially oriented generation 2 (cross section: 225m). C) Pegmatite 3 is slightly folded as it cuts foliation sub-vertically (cross section: 214m). D) Pegmatite 1 is oriented sub-horizontally through the picture (parallel to foliation) and is cut diagonally by a pegmatite of generation 3, which is oriented sub-vertically and cuts through the foliation discordantly. E) Sketch of picture D showing the crosscutting relations of the two pegmatite generations. The white pegmatite represents generation 2, which is cut by generation 3 in pink.

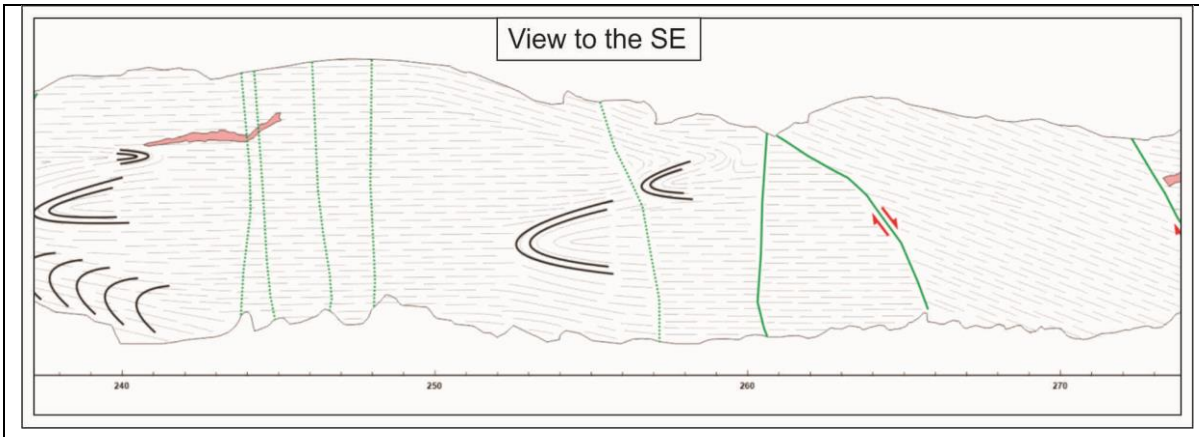

Figure 5.5: Pegmatite poor section from 240-270 meters within the ORC cross section. This section also contain the only rootless folds of the ORC.

Generation 2 intruded into an already strongly foliated country rock, which explains why it is oriented parallel to the general foliation. Generation 2 has undergone extensive transposition and folding, whereas generation 3 cut through the folded generation 2 and must therefore represent the latest intrusion.

Microscopic observations

Thin section 30_1 made of a sample of generation 2, taken at the 30 m marker, shows large subhedral feldspar crystals with a small amount of quartz and calcite with grain size of plagioclase ranging from 0,5-7 mm. The porphyroclasts of plagioclase show evidence of both plastic and brittle deformation through the presence of deformation twins tapering into the centre of plagioclase phenocrysts as well as consistent fracturing. Two sets of fractures are filled with both quartz and calcite that crosscut each other. Surrounding the large feldspar clasts is a matrix of fine-grained plagioclase and quartz. Quartz shows evidence of dynamic recrystallization by grain boundary migration (GBM). Activity of GBM is evidence of deformation temperatures in excess of at least 400 °C (Hirth and Tullis, 1992). At the same time, anhedral grains with 1. order grey interference colours showing deformation twins, polysynthetic twins, heavy sausseritization, undulatory extinction and deformation kinking attest to accommodation of low-grade viscous deformation, thus before the system entered the brittle regime during exhumation en route to the surface.

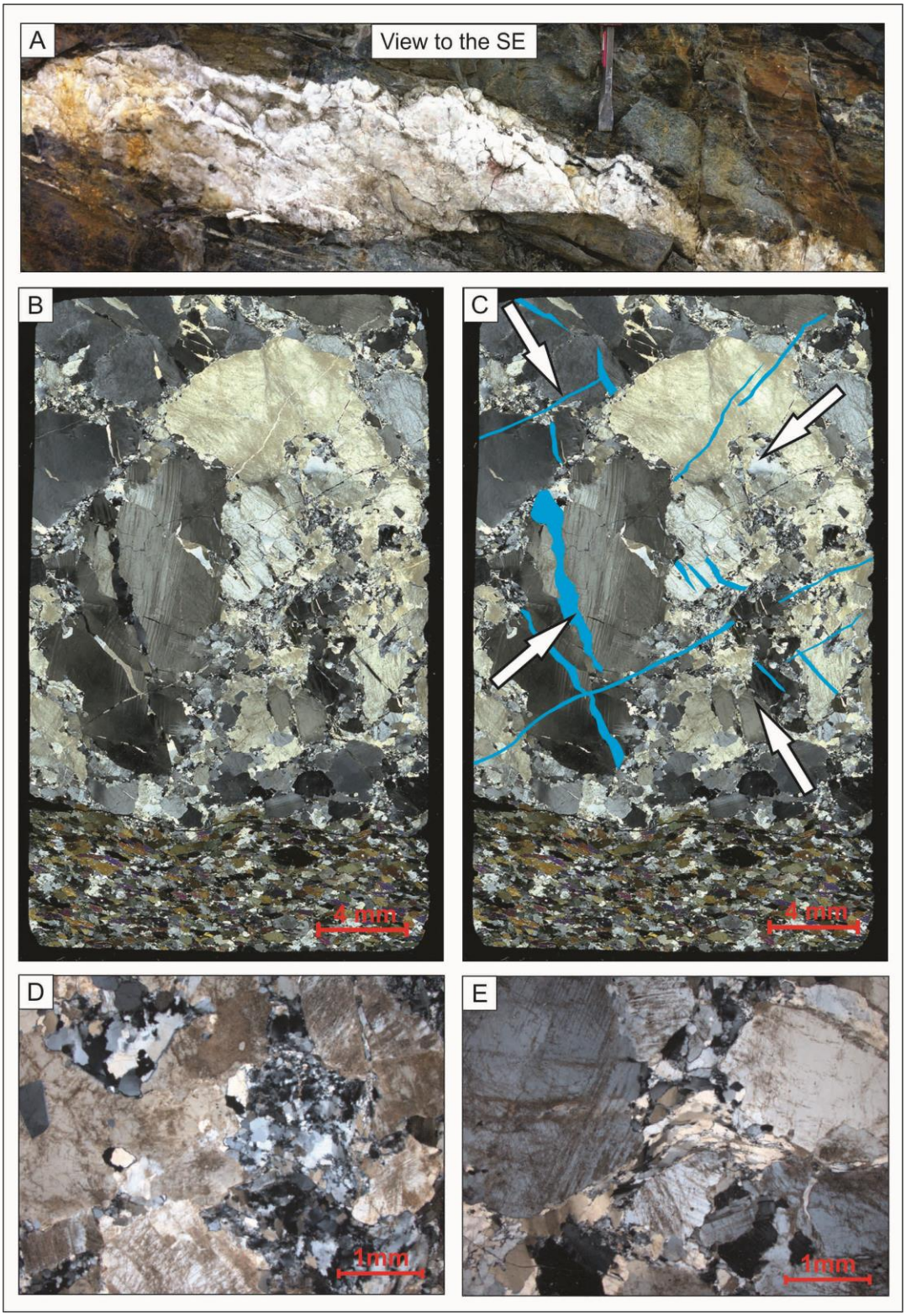

Figure 5.6: A) Slightly boudinaged pegmatite with chisel marking the sample spot of thin section 20_1, which is described in B. B) Thin section from sample 20_1 showing the pegmatite minerals and the contact between the pegmatite and the highly deformed amphibolite country rock. C) Sketch of photomicrograph in B with fractures filled with late quartz and calcite. These veins show two distinct sets of fractures marked in blue. Two sets of σ_1 orientations have been marked with white arrows. D) Small grained plagioclase among larger feldspar grains seen in brighter grey are indicative of high strains and temperature. E) Centre of photomicrograph showing elongated and dynamically recrystallized quartz grains bent by large plagioclase grains.

5.1.4. Folds

The ORC is folded in a complex manner. Detailed analyses of the folding style shows a clear folding trend of mostly tight folds oriented parallel to the strike of the road cut. There exists two generations of folding (F1 and F2). F1 represent a few old rootless and transposed folds, while F2 represent a major folding phase that folded the whole road cut with fold axes oriented NE-SW, with shallowly dipping axial planes towards SE (Figure 5.7 and Figure 5.8). This trend does not include intrafolial folds from within ductile shear zones, which are mostly isoclinal. Fold axes of F1 generation are most probably reoriented during the F2 folding phase, which show similarly oriented fold axes and axial planes.

Four different geometric types are identified within the F2 folds of the ORC (Appendix 2: Folds). A simple categorization of folds can produce the following fold subsets:

- Gentle (180-120°)

- Open (120-70°)

-Tight (70-30°)

- Isoclinal (30-0°)

Pegmatites found within shear zones are often folded isoclinal in contrast to folds outside the shear zones, showing tight geometries (cross section: fold 20 and 21) and are confined to ductile shear zones where they provide excellent kinematic indications.

Pegmatite-generation 1 and 2 are folded by the F2 whereas generation 3 pegmatites cut F2 folding (Figure 5.4B, cross section: fold 16 and 180-200 m). The F2 folds are only observed between the 240-300 m marker of the cross section and are interpreted as foliation parallel rootless folds, because the limbs die out in the surrounding foliation.

The axial plane of fold 19,5 (Figure 5.9) is parallel to the shear plane of ductile shear zone 23. This fact may indicate that folds 19,5 and 20 were developed during the thrusting-phase of the shear zone.

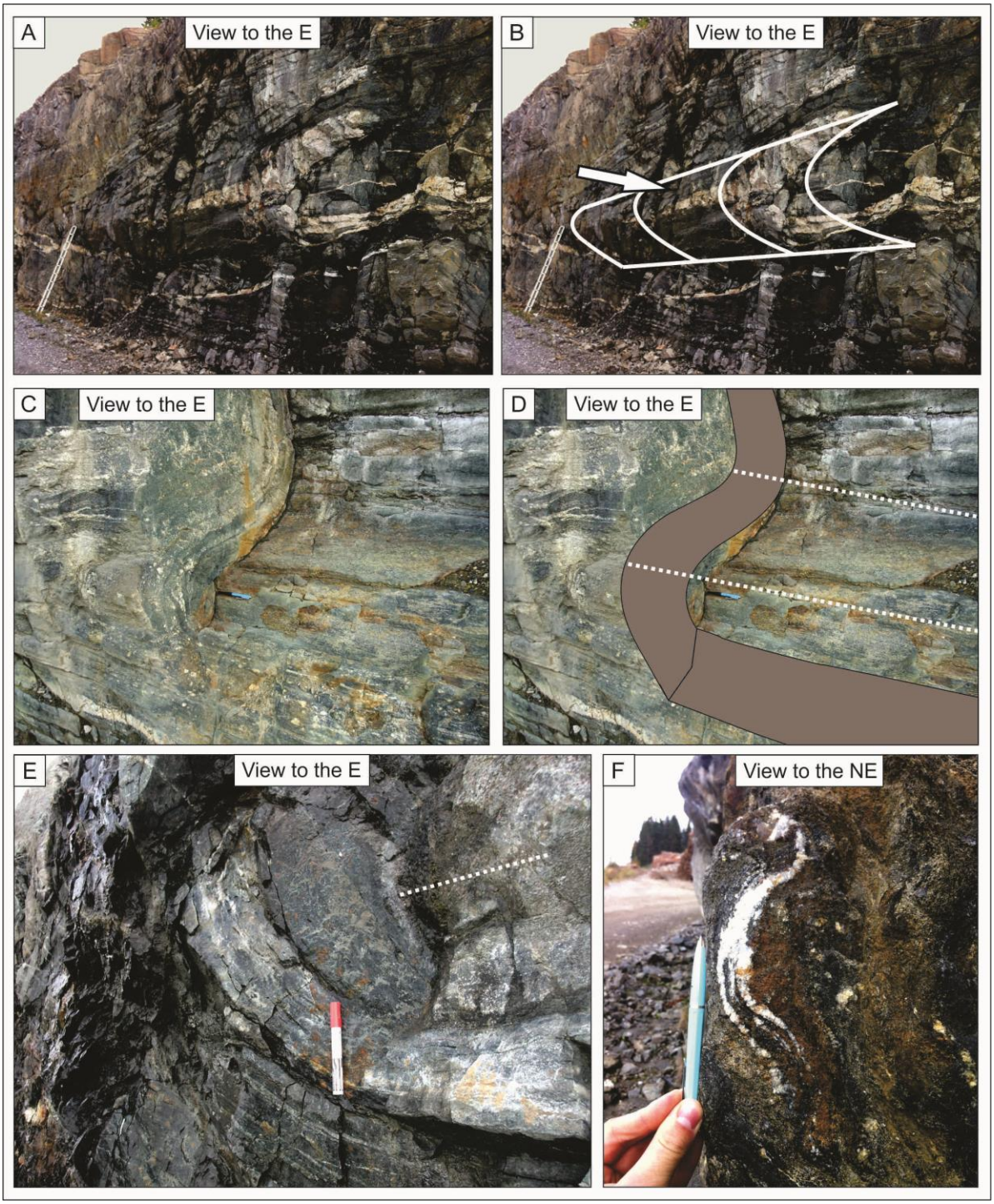

Figure 5.7: A) Fold 17 trending coaxially with the strike of the ORC. B) Sketch of fold 17 where a pegmatite is displaying isoclinal folding. C) Fold 17 showing folded highly strained zones. D) Sketch of C showing the HSZ folded by fold 17. With lines indicate fold axes. E) Folded foliation in fold 11. F) Folded pegmatites parallel to strike of the ORC (NE-SW).

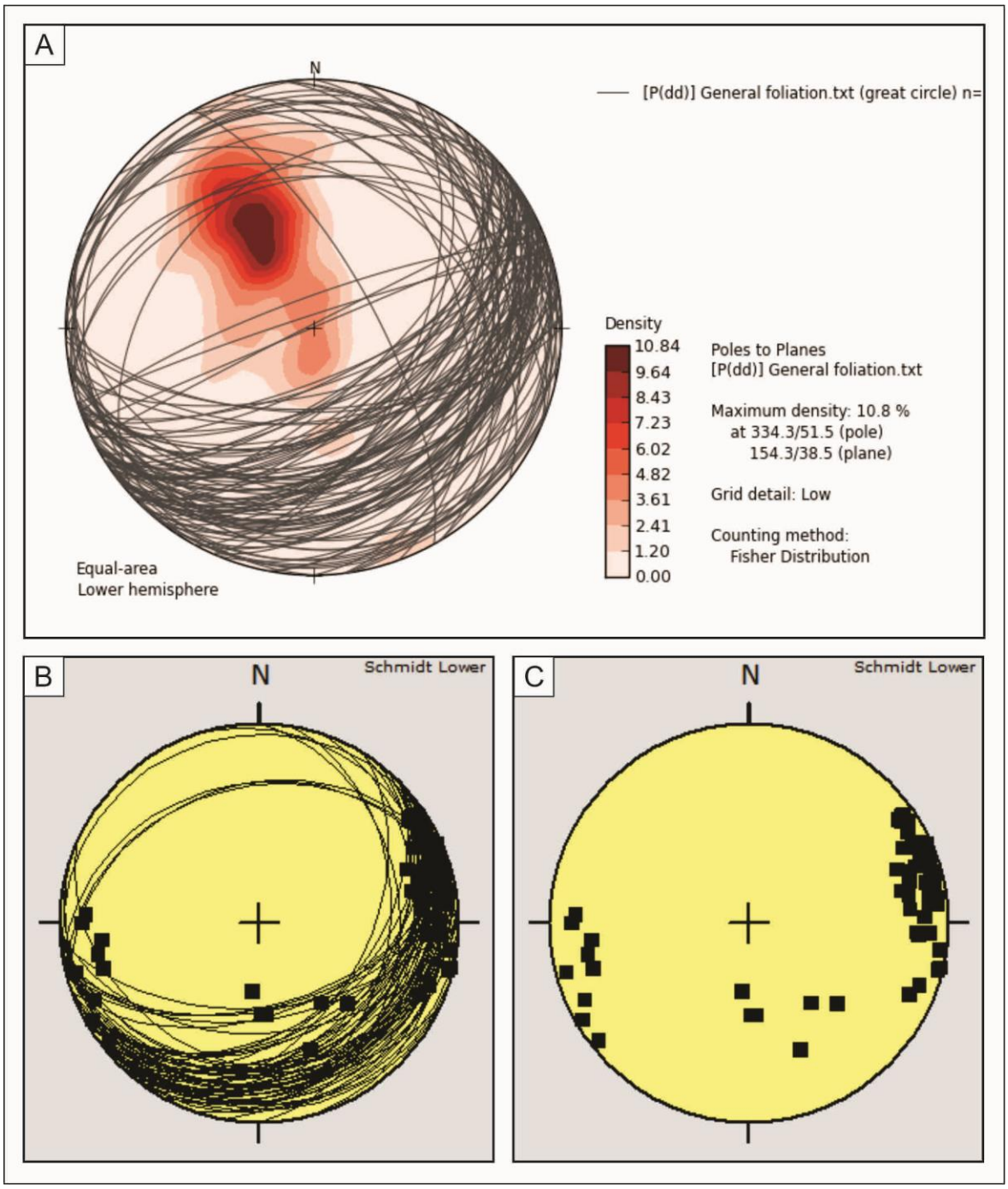

Figure 5.8: A) Foliation orientation at ORC displaying a strong trend dipping towards the SE. B) Stereonet of measured folds. Great circles: axial plane. Solid squares: fold axis. C) Stereonet showing only the total number and orientation of the ORC fold axes.

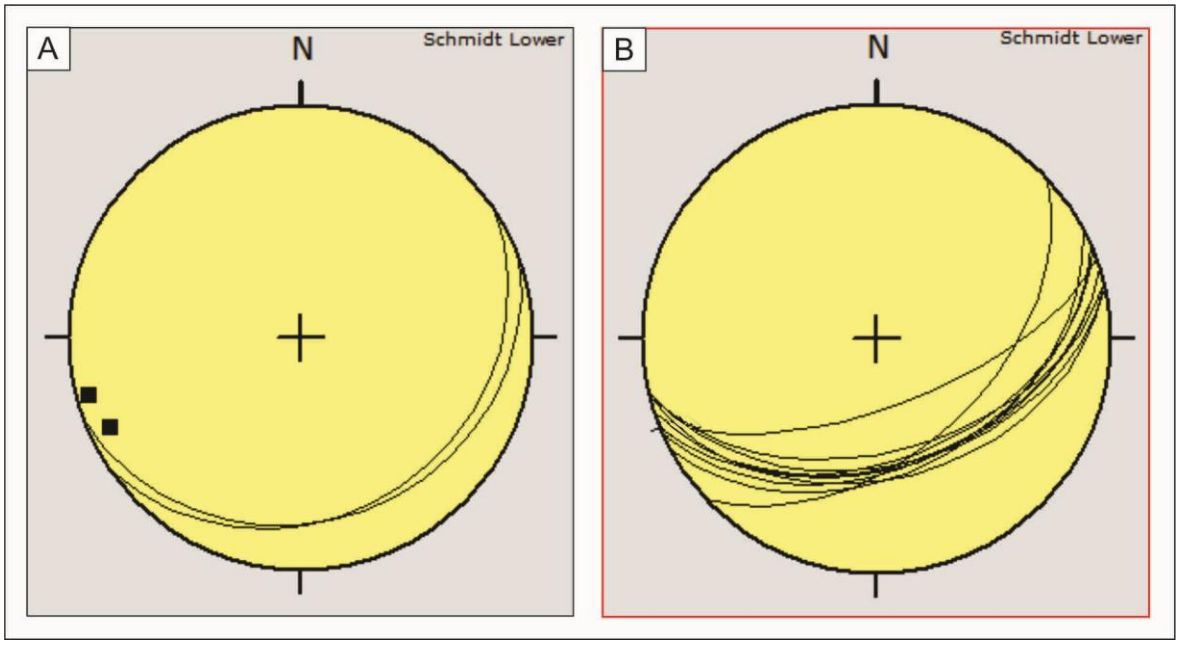

Figure 5.9: A) Axial planes plotted as great circles and fold axes as black dots representing fold 19,5. B) Orientation of ductile shear zone 23, which is similar to the axial planes of fold 19,5 in A.

5.1.5. Ductile shear zones

Mesoscopic observations

The ORC contains a total of seven ductile shear zones. These shear zones cut through all structures within the ORC, except the brittle-ductile and brittle faults. All shear zones have associated shear foliations (Figure 5.10 and Figure 6.2). Three distinct sub-groups of ductile shear zones can be identified based on orientation and kinematics:

1. Set of four oblique-slip normal faults, with top-to-the NE transport (Figure 5.10D)
2. Set of low-angle, dip slip detachment faults with top-to-the SSE transport
3. Oblique-slip thrust fault with top-to-the NNW transport (Figure 5.10D)

Both sub-groups 1 and 2 contain a pervasive mineral stretching lineation given by the alignment of amphibole. The pegmatites described above are sheared and folded by the different types of ductile shear zones. The geometries produced by the folding and deformation of the pegmatites is crucial to establish the kinematics of the shear zones. Combining mineral lineations with shear zone folds confirm that all ductile shear zones except shear zone 23 belongs to an extensional regime.

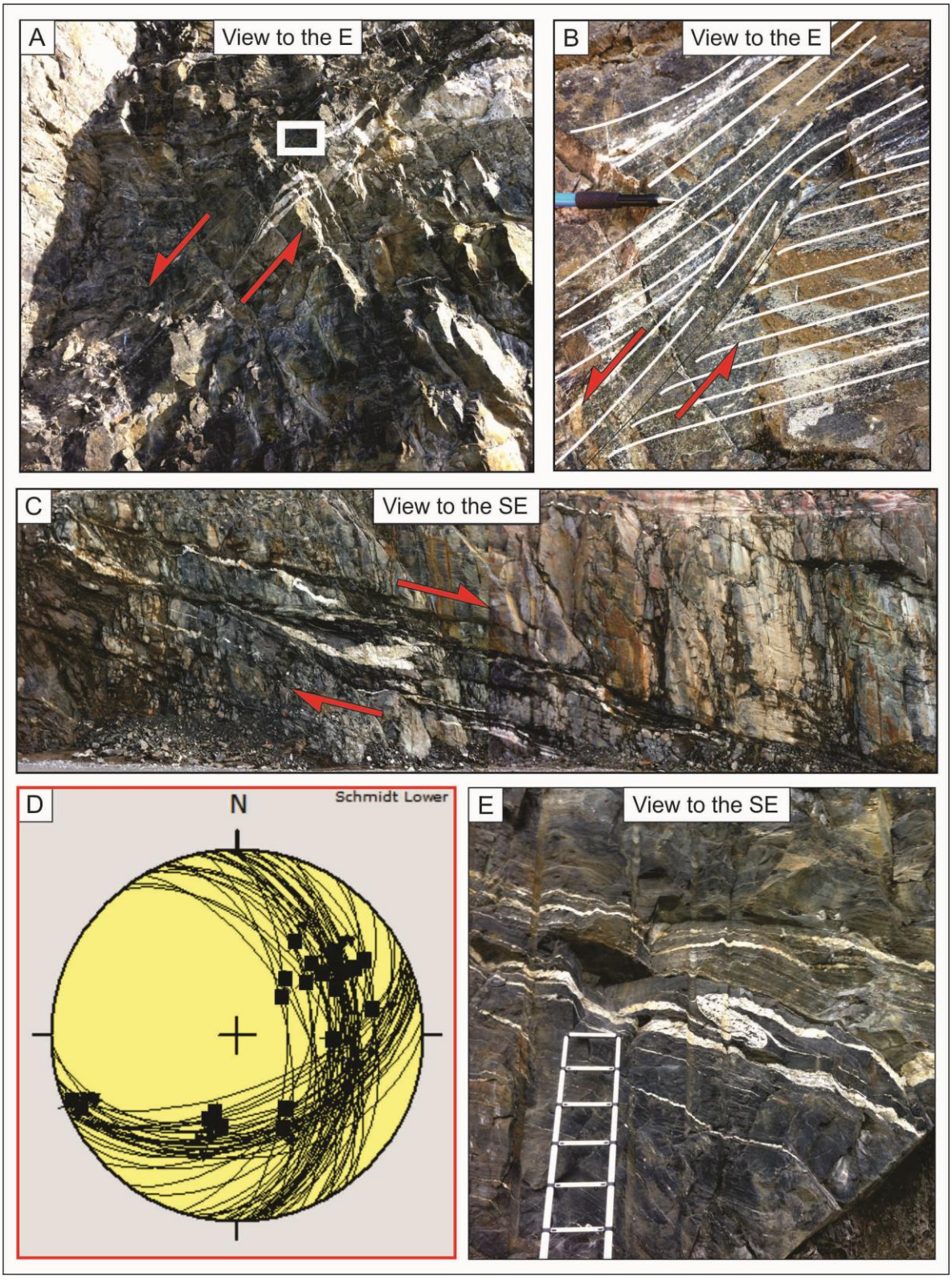

Figure 5.10: A) Ductile shear zone showing pegmatite sills transposed into shear zones. B) Close-up of picture A white rectangle where the ductile shear zone foliation is married with white lines. C) Ductile shear zone showing pegmatites that are deformed into drag folds and isoclinal folds indicating that the shear zone is extensional. D) Stereonet showing orientation and dip of all ductile shear zones. E) Ductile thrust with folded generation 2 pegmatites, indicating oblique thrusting.

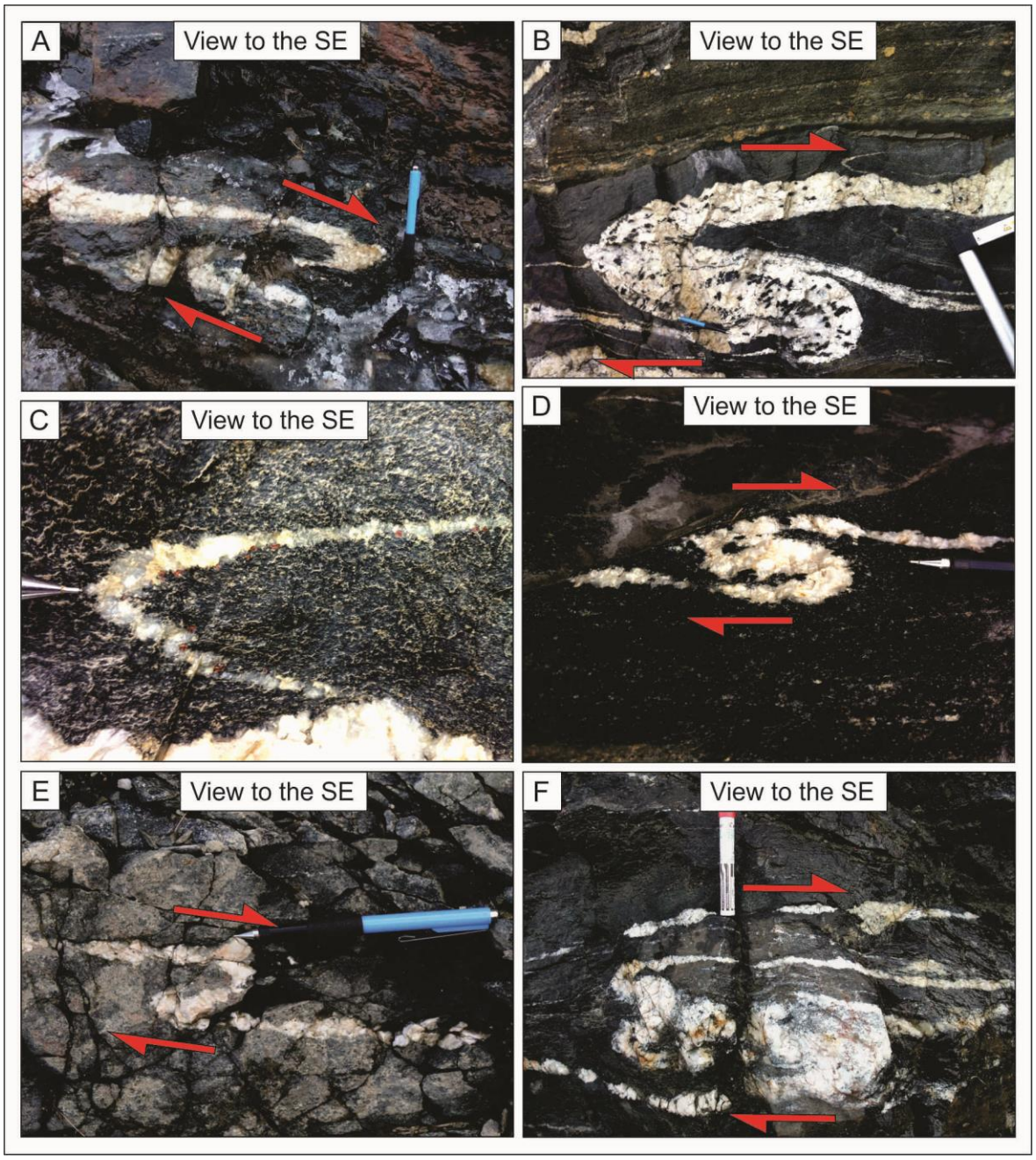

Figure 5.11: A) Drag fold within ductile shear zone 16B, supporting the fact that this is an extensional shear zone. B) Folded pegmatites are interpreted to show top-to-the N thrusting of shear zone 23. Hornblende crystals occur as xenoliths within the folded pegmatite. C) Folded pegmatite with garnets on the inner side of the fold located just above the fold in picture B. D) 1,5 m below ductile thrust 23 is an isoclinal drag fold indicating relatively high strain. E) Drag fold within shear zone 16B, supporting the extensional interpretation. F) Highly rotated relict boudin indicating sinistral sense of shear.

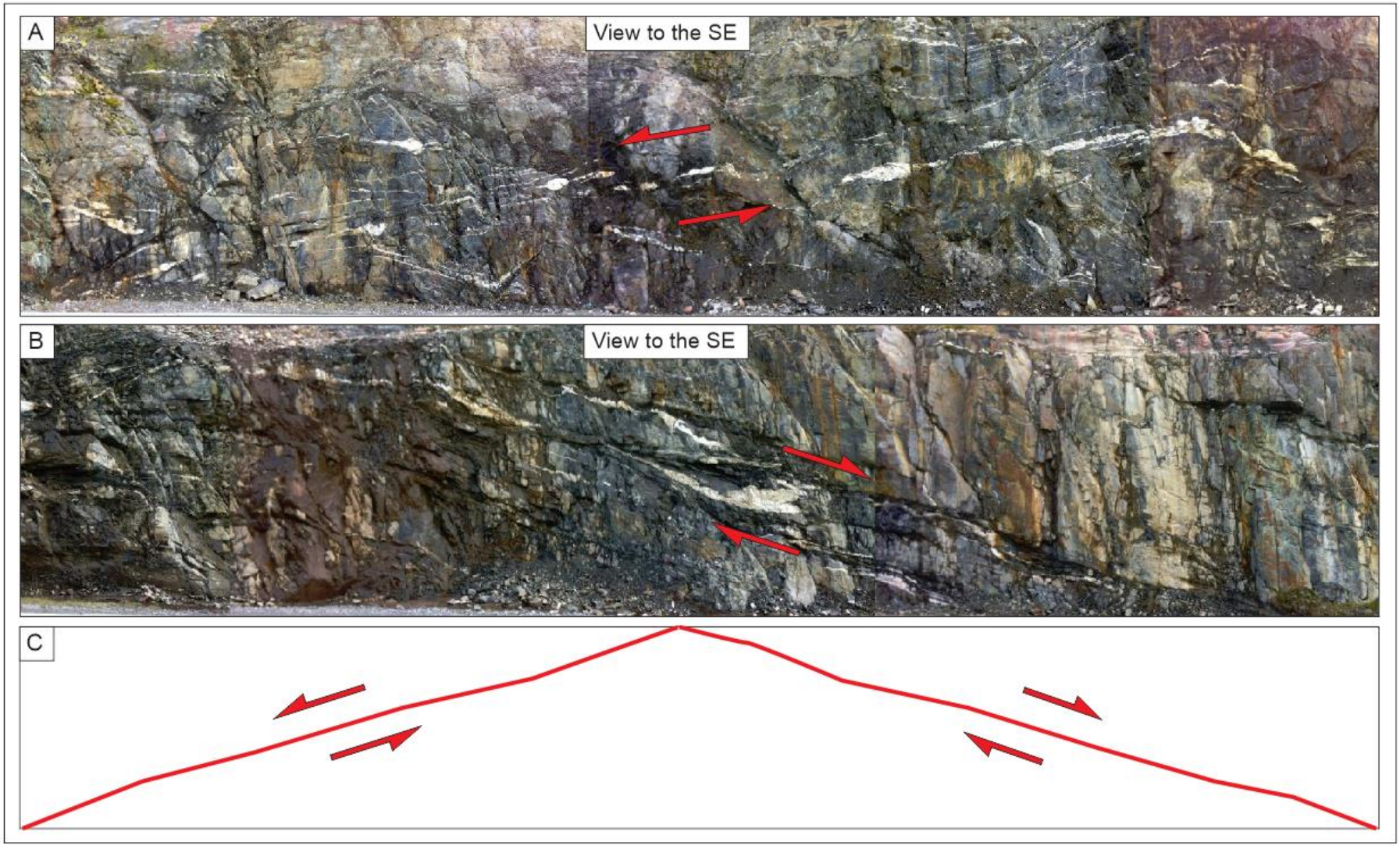

Figure 5.12: A) A possible conjugate set of ductile shear zones is observed from the 60m marker all the way to the 140m marker. Ductile shear zones 16A and 16B are brittly reactivated with top-to-the SE extension. B) Immature shear zone show ENE-WSW extension with large amounts of transposed pegmatites. C) Interpretative sketch showing the two ductile shear zones combined.

Mineral lineations, consisting of oriented amphibole grains in combination with asymmetric folds and a number of other kinematic indicators support the kinematic interpretation. The geometry of folds above ductile shear zone 23 shows fold axes oriented NE-SW yielding thrust kinematics (Figure 5.11).

Sub-group 2 and 3 are represented by ductile shear zones 16A and 16B and ductile thrust 23, all dipping towards NE. These shear zones share the same orientation (see fault stereonets in cross section: 16A, 16B and 23B). Ductile shear zone 23 is interpreted as a thrust, which share a common orientation with ductile shear zones 16A and 16B dipping towards the SE. There might also exist a set of conjugate ductile zones within the ORC **(**Figure 5.12**)**. These sets have the same dip but in opposite directions. The immature ductile shear zone presented in Figure 5.12A was detected too late for further investigation.

Ductile shear zones systematically deflect pegmatites of generation 2 (cross section: ductile shear zones 6 and 18B, 50m and 158m), and therefore post-dates generation 2 (Figure 5.13). The ductile shear zones are spatially developed close to pegmatite-rich domains, often trending parallel to shear foliation (Figure 5.13).

Ductile shear zones postdate all pegmatites because they deform relict pegmatite sills into the shear zone. The un-sheared part of the pegmatite, situated outside the shear zone, are still oriented parallel to foliation. Shear zone folds and mineral lineation support the shear sense of the ductile shear zones suggested by the deflection of transposed pegmatites. During extensional ductile shearing σ_1 must have been oriented vertically and at a low angle during the formation of ductile thrust 23. Shear zones 16A and 16B may have started out as ductile thrust during the compressional phase and later reactivated as normal shear zones during the extensional phase.

Microscopic observations

Thin section 102_1 is taken from ductile shear zone 15 and includes plagioclase bands with poikilitic porphyroblasts of garnet. A bookshelf structure of garnets can be observed in a fine-grained matrix consisting of plagioclase, hornblende and quartz (Figure 5.14). Garnets were deformed in a brittle fashion, whereas the hornblende phenocrysts define the foliation. Thin section 102_2 shows feldspars formed into boudins that are thinned into 0,1 mm bands.

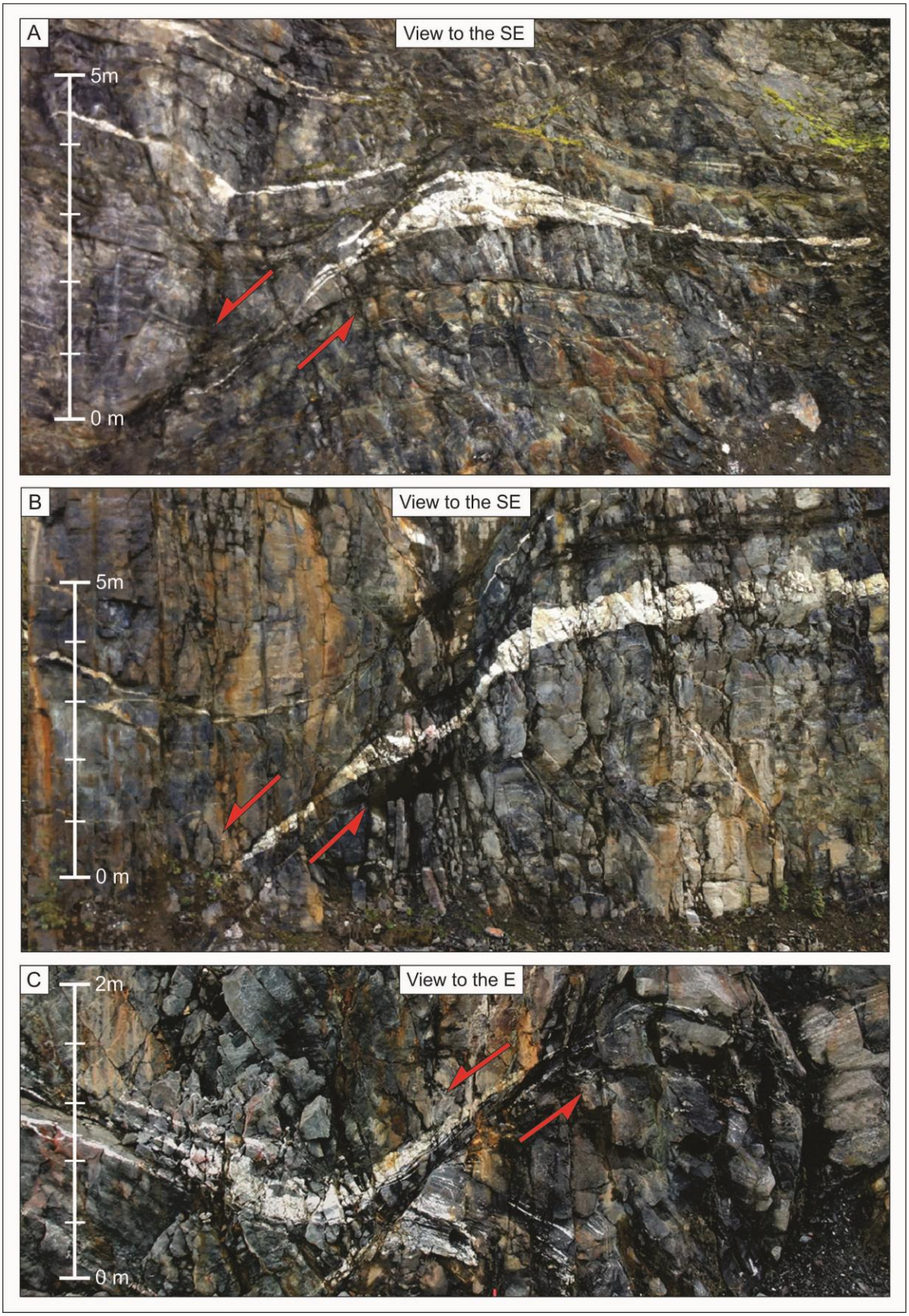

Figure 5.13: Sub-group 1: A) Transposed pegmatite within shear zone 6 with a minimum displacement of 4 m. B) Pegmatite transposed by shear zone 18B with minimum 5 m displacement. C) Pegmatite displaced just under 2m by shear zone 9.

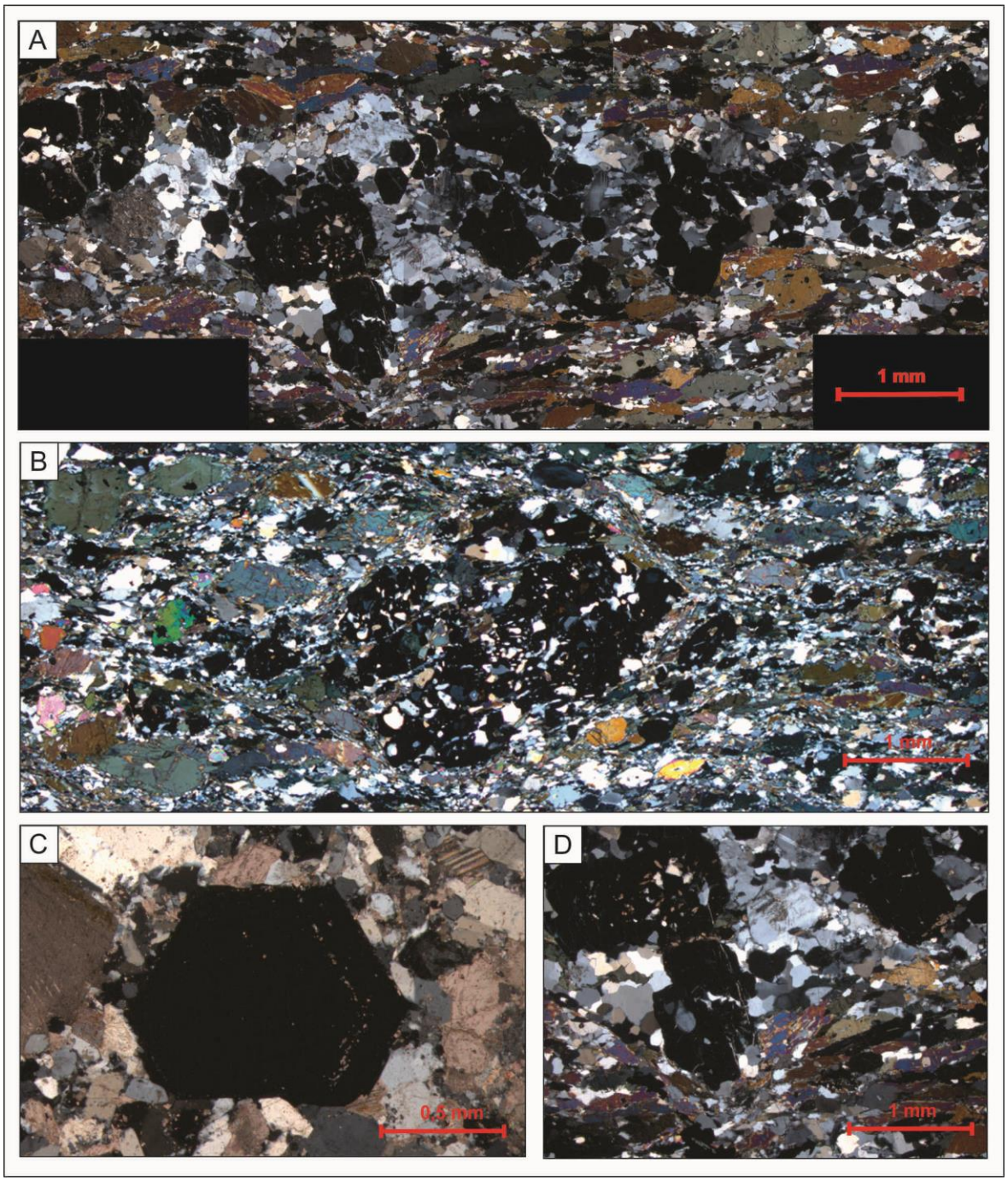

Figure 5.14: A) Large garnet clasts surrounded by feldspar grains. B) Brittly deformed garnet in a bookshelf structure surrounded by feldspar, quartz and epidote. C) Euhedral garnet that has undergone zonational growth. D) Inclusions of sphene within garnets from shear zone 15.

5.1.6. Brittle-ductile faults

Mesoscopic observations

Faults within the ORC are classified as brittle-ductile when they show a combination of brittle and ductile textures. They are all extensional structures and show two distinct orientations:

1. Top-to-the W/NW oblique-slip
2. Top-to-the NE oblique slip.

Both orientations display an average dip of ca. 50° (Figure 6.2B). The first 220 m of the ORC (from the left to the right within the ORC-cross section) are characterized by group 1. From 220 m to 240 m in the cross section, the section is characterised by a set of faults that can be ascribed to group 2. Lineations in group 2 show several different orientations, but the majority indicate oblique slip at ca. 45 degrees plunge towards NE.

Microscopic observations

Only thin sections of brittle-ductile faults that have experience fully brittle reactivation have been analysed. These contain invariably cataclasitic fault rocks. The cataclasites consists of plagioclase, quartz, chlorite, calcite and sphene and are shaped as angular fragments with only a few slightly rounded clasts (Figure 5.27D and E). The presence of secondary calcite and chlorite indicates fluid interaction within the fault cores.

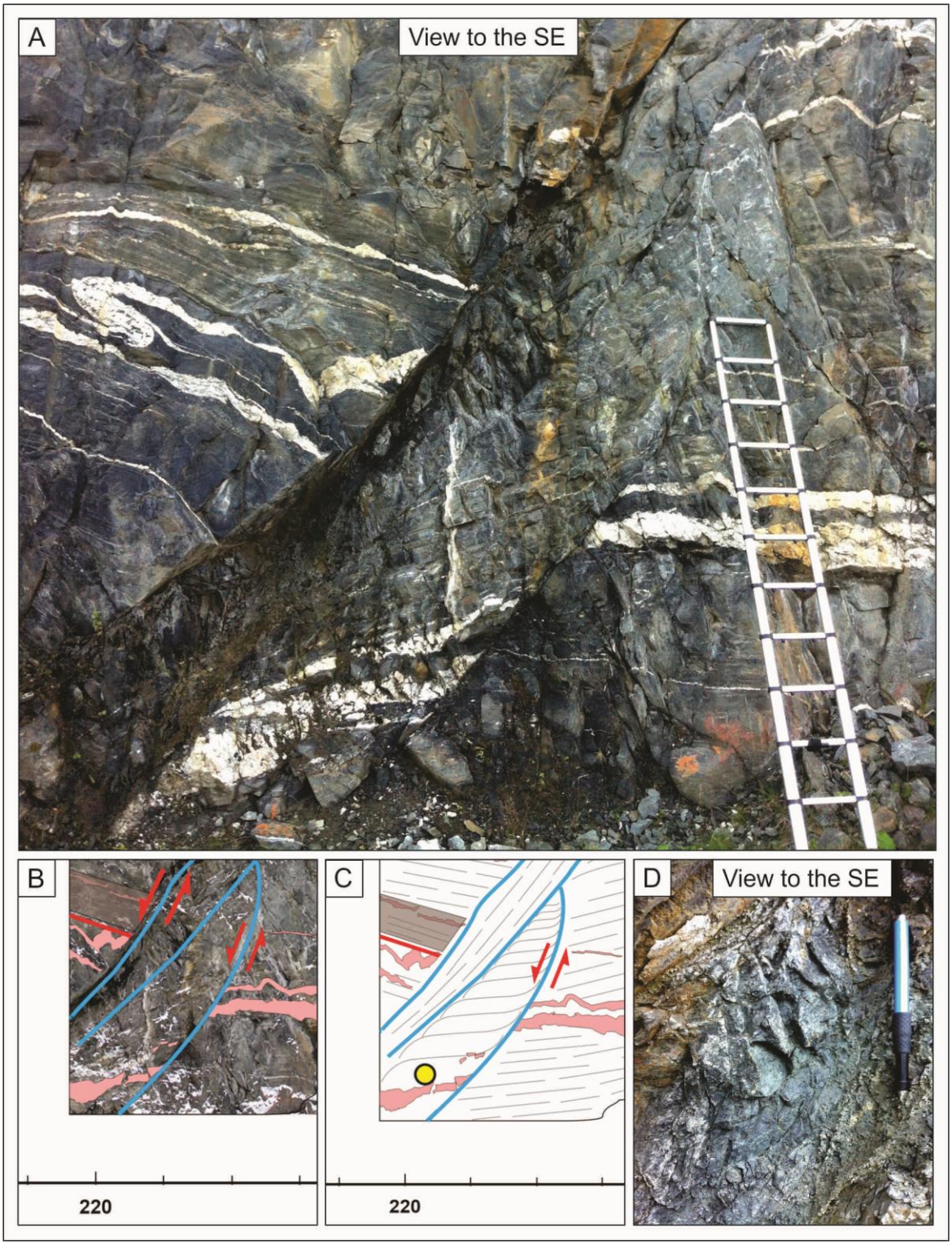

Figure 5.15: A) Photo showing several discrete brittle-ductile faults and transposed pegmatites. Ladder for scale. B) Brittle-ductile normal faults 24A and 24B marked for A, pegmatites are marked in pink. C) Sketch of B showing sigmoidal foliation. D) Close-up of fault core 24A situated in contact with hanging wall and showing angular sheared rock with gouge in between.

5.1.7. Brittle faults

Mesoscopic observations

The brittle faults of the ORC, marked in green in the ORC-cross section (Appendix 4), cut through the entire ORC and affect all lithologies postdating all the structures described above. Brittle faults contain both fault cores defined by cataclasites and gouge with mostly angular fragments and damage zones extending into both the hanging wall and the footwall (Figure 5.27B). The faults can be sorted according to three main geometric and kinematic groups:

1. Top-to-the W oblique-slip normal faults
2. Top-to-the NE oblique-slip normal faults
3. Brittle faults oriented parallel to the foliation.

With the exception of fault 8, 12A, 12B, 20A, 27, 28 (striking NNW-SSE at ca. 75° dip), all brittle faults dip at about 55-60 degrees and show displacement between 2 cm and 70 cm (Figure 5.17**)**. Due to no apparent displacement and fault planes dipping at ca. 80°, brittle faults 3B, 4, 12A, 13, 14, 27, 28, 29A may be interpreted as purely extensional fractures, that is, joints. They are observed in greater density in the more massive part of the ORC (cross section: 240-260 m), where there are less relict structures to be found. Some of the extensional fractures (12A, 13 and 14) could not be reached due to the height of the road cut. These faults were therefore not examined in great detail.

Brittle faults 7A, 7B, 12B and 20A and 20B (see Figure 5.17) cut through the pegmatites, folds, foliation, brittle-ductile faults, ductile shear zones and high strain zones. Ductile shear zones, however, are often not cut through by brittle faults, but if suitably oriented are reactivated in brittle fashion along preferential slip planes. Brittle-ductile faults have large fault cores consisting of sheared rock and gouge, which indicate extensive pure brittle overprinting. Brittle faults 19A, 20B and 24A cut the HSZ (see cross section: 172 m, 196 m and 220 m). These crosscutting relationships indicate that brittle faults, both reactivated and newly-formed, post-date all other structures at the ORC.

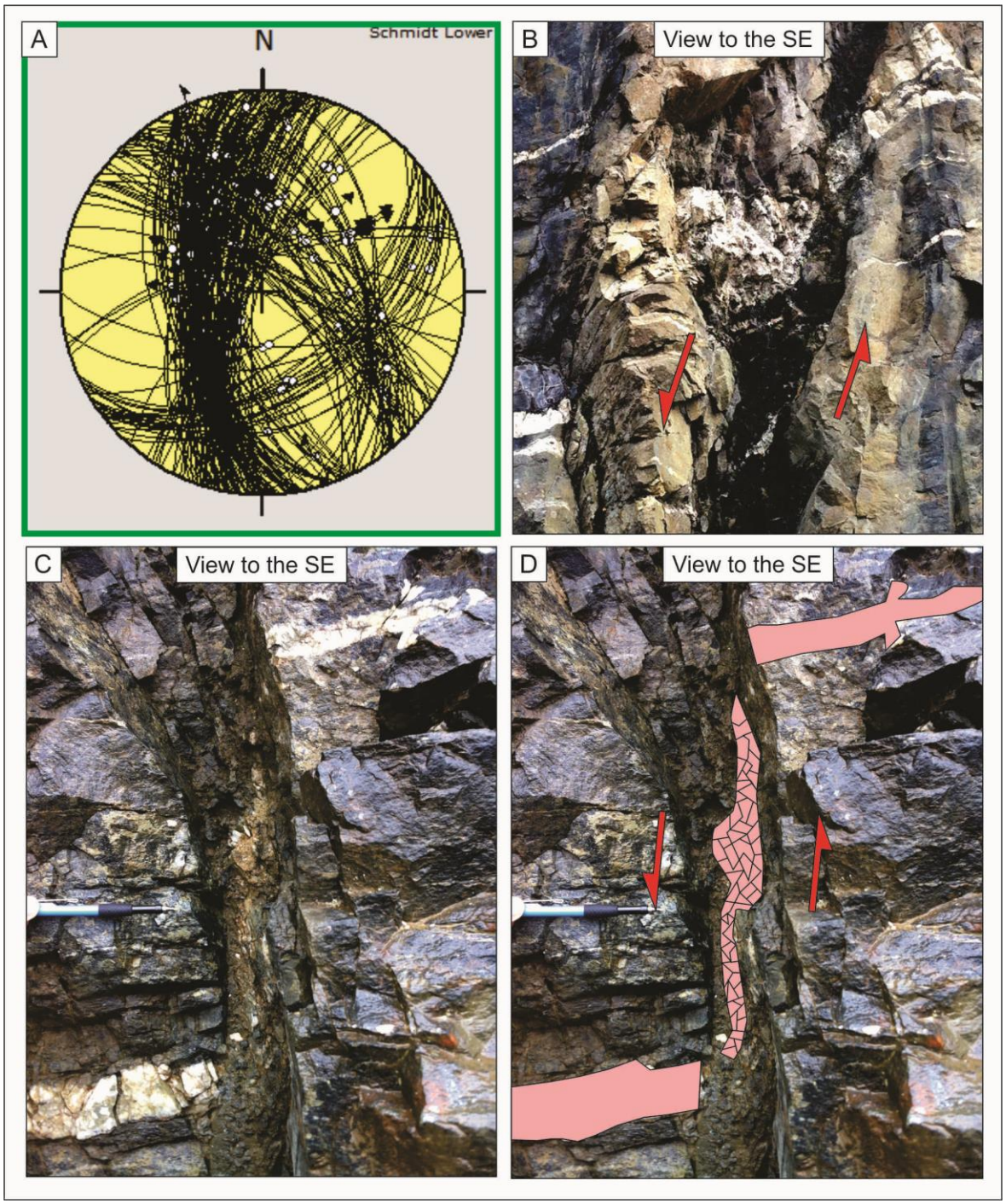

Figure 5.16 A) Summary stereoplot of all brittle faults within the ORC. B) Fractured and displaced pegmatite within the brittle fault core of fault 22A. C) Sheared pegmatite within fault 8 showing displacement of ca. 24 cm. D) Sketch of the same fault with the fractured pegmatite marked in pink.

Microscopic observations

Thin sections from brittle faults show two distinctly different fabrics. Thin section 18_3 is from a pegmatite dike of generation 2, which is 13 cm thick and oriented perpendicular to the foliation. The thin section consists mainly of porphyroclastic calcite averaging 0,7 mm within thin cataclastic zones containing small quartz and minor anhedral plagioclase grains averaging 0,3 mm. The thin section shows alternating, mineralogically homogeneous, domains (calcite) and heterogeneous domains (calcite, plagioclase and quartz). One faulting episode and a late fracture event can be observed (Figure 5.30). The fault is represented by two larger cataclastic zones with fault material averaging 0,5 mm in grain size. The cataclastic zones occur in bands separated by zones of porphyroclastic calcite. These are parallel to the fault plane observed at the outcrop and therefore represent the main deformation event. The porphyroclastic calcite shows deformation twins of different sizes. A small set of fractures shows 0,2 mm displacement across feldspar grains that lie within the cataclastic zone. These fractures are filled with calcite and therefore post-date the main cataclastic event (Figure 5.30). Fractures filled with precipitated calcite, combined with country rock lithology, is evidence of major fluid rock interaction and brittle fracturing of older pegmatite intrusions.

The sub-vertical orientation of the faults and fractures support the theory of faults representing a late phase of exhumation of the region with coeval aqueous fluid injection along these faults (Figure 5.16). This exhumation must have occurred coevally with extension with a vertical σ_1. Brittle fault 1 (Figure 5.29) shows evidence of reactivation during two events indicated by continuous fractures running through both clastic calcite grains and matrix.

The matrix of thin section 172_1 consists of fine-grained fragments of quartz and plagioclase with porphyroclasts of quartz and feldspar clasts making up the matrix. Large 2,5 mm plagioclase crystals show extensive recrystallization with sausseritization. Cataclastic fragments (d=0,7 mm) consist of mainly plagioclase, chlorite, and quartz. Hornblende crystals occur as minor grains in the very fine-grained matrix.

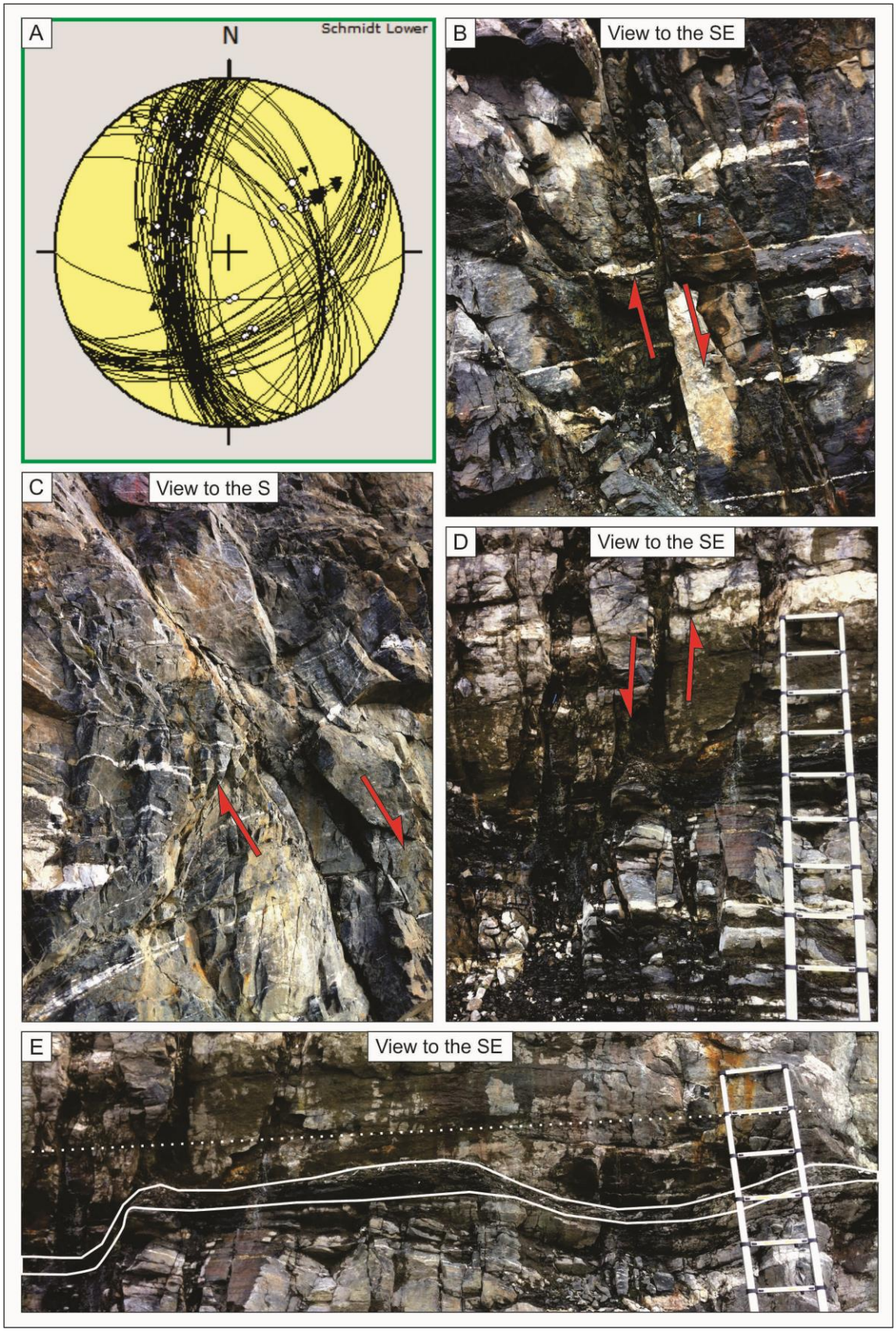

Figure 5.17: A) Summary stereonet of all brittle faults excluding faults 8, 12A, 12B, 20A, 27 and 28, which can be characterized as joints. B) Pegmatites (partially folded in right corner) are displaced by fault 8. C) Fault 7B cutting through highly folded host rock. D) Pegmatites running parallel to the folded foliation are displaced by brittle fault 20B. E) Fault 21s (cross section: 198 m) fault core is marked with a white line. The fold axis of fold 17 (cross section: 181-297 m) is marked with a dotted line.

The lack of angularity of the largest clasts indicates extensive grinding and the presence of an aqueous fluid is indicated by secondary chlorite and epidote mineralisation. A clast within the thin section contains quartz with preserved evidence of grain boundary migration through recrystallization during its earlier ductile deformation.

5.2. Brittle reactivation of relic structures

There is clear evidence of extensive and important brittle reactivation of many previous structures within the ORC and, therefore, this evidence is considered separately in this section. The scale of the brittle overprint varies along the ORC. Brittle reactivation is very clear in faults that are sub-optimally oriented for brittle faulting and where large amounts of sheared rock and gouge are present. Brittle reactivation of structures within the ORC can be divided into three general groups based on the presence of relict structures such as ductile shear zones, folding and pegmatites:

1. Brittle faults that reactivate older ductile shear zones
2. Brittle faults that reactivate due to pegmatite intrusions
3. Brittle faults that reactivate due to relic folds

These three types of reactivated structures are presented in accordance with their group in the rest of chapter 5. Several parameters are studied for each fault to help compare and systematise the brittle reactivation within different structures:

- Fault zone geometry
- Fault core geometry and composition
- Fault plane characteristics
- Displacement
- Grain size
- Presence of fluids

5.2.1. Brittle reactivation of ductile shear zones

Mesoscopic observations

Ductile shear zones of the ORC consist of both extensional and compressional shear zones with two very consistent dip directions: ENE and 2. SSE, both dipping at ca 40°. They consist of a tabular mylonitic layer of around 30 cm in width (Figure 5.13), which deflects the general foliation of the ORC is deflected by the extensional shear zones (Figure 5.20). A shear zone parallel foliation including pegmatites is present within all the ductile shear zones.

All of the ductile shear zones found in the ORC show brittle reactivation along the contact between the bent external foliation and the shear mylonitic foliation (Figure 5.18). Some shear zones are reactivated both along the upper and lower contact to the undeformed footwall and hanging wall (Figure 5.22). None of the ductile shear zones shows reactivation within the core foliation itself.

The brittly reactivated fault core consists of lens shaped fault rock domains (seen very clearly in shear zone 15, 16A and 16B, cross section: shear zones 15, 16A and 16B, Figure 5.18). Larger 5-7 cm lens-shaped blocks show significant mechanical disruption into smaller lenses (Figure 5.19). Brittle reactivation fault cores do not exceed 7 cm in thickness. Damage zones are very narrow and are mostly confined to an envelope of 5-6 cm width on both sides of the fault core (Figure 5.18).

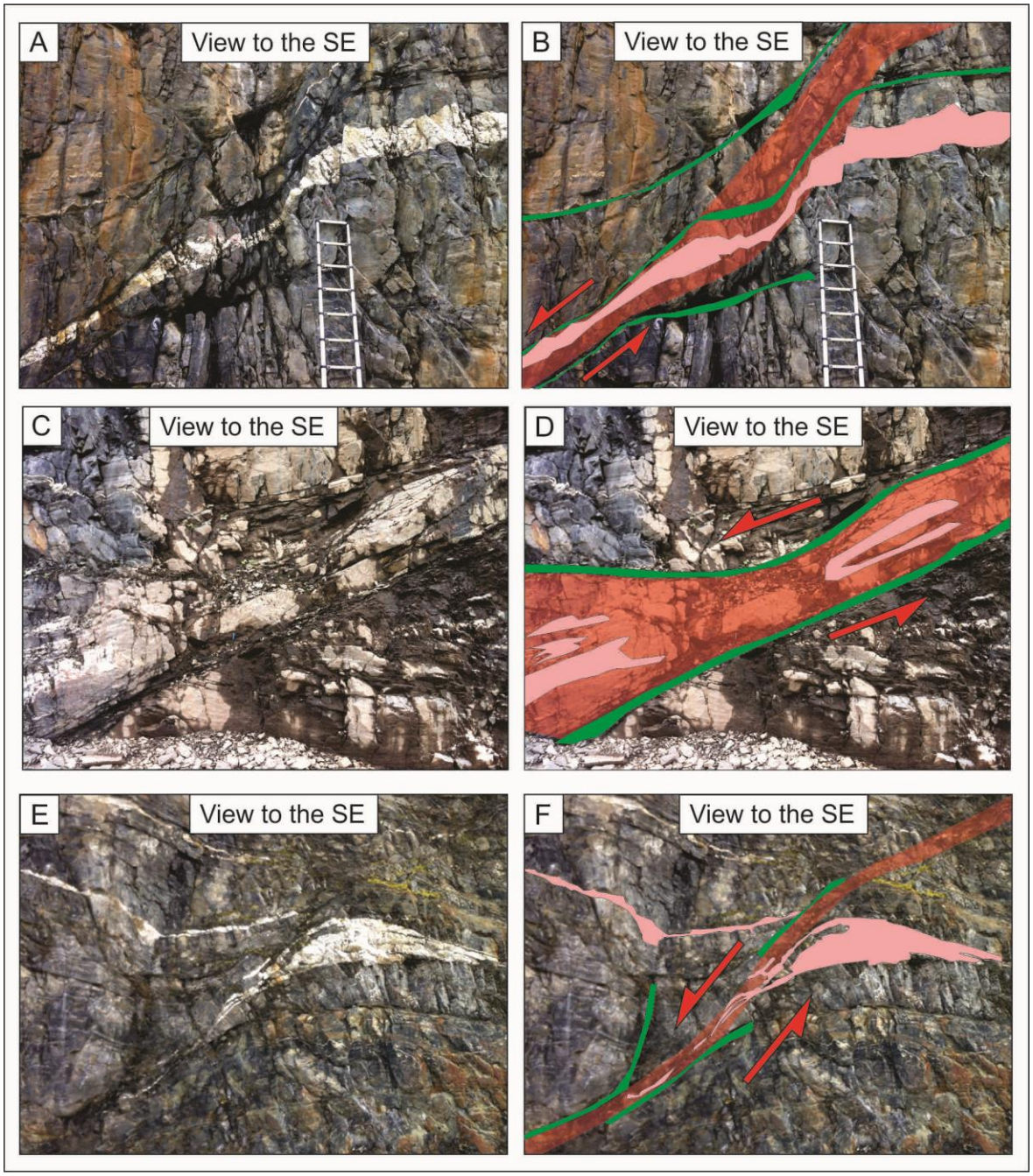

Figure 5.18: A) Ductile shear zone 5 shows shear zone foliation, transposed pegmatite sill and brittle fault reactivation. B) Sketch of the same fault indicating that brittle reactivation is constrained to the contact between footwall, hanging wall and the shear zone foliation. C) Picture of ductile shear zone 15. D) Sketch of picture C displaying shear zone foliation in red and reactivated brittle fault cores in green. The brittle fault cores are in contact with the hanging-wall and footwall. E) Ductile shear zone 6 with transposed pegmatites oriented parallel to the shear foliation. F) Sketch of figure E showing pegmatites in pink and brittle reactivation in green. The brittle reactivation is displayed in short brittle segments, which has not developed into one brittle fault plane.

The pre-existing ductile shear zones are not totally tabular (cross section: ductile shear zones 6 and 18B) and are therefore not brittly reactivated continuously along their length. The brittle fault network rather forms a discontinuous, anastomosing array whose components are connected together by fractures (Figure 5.18B and F).

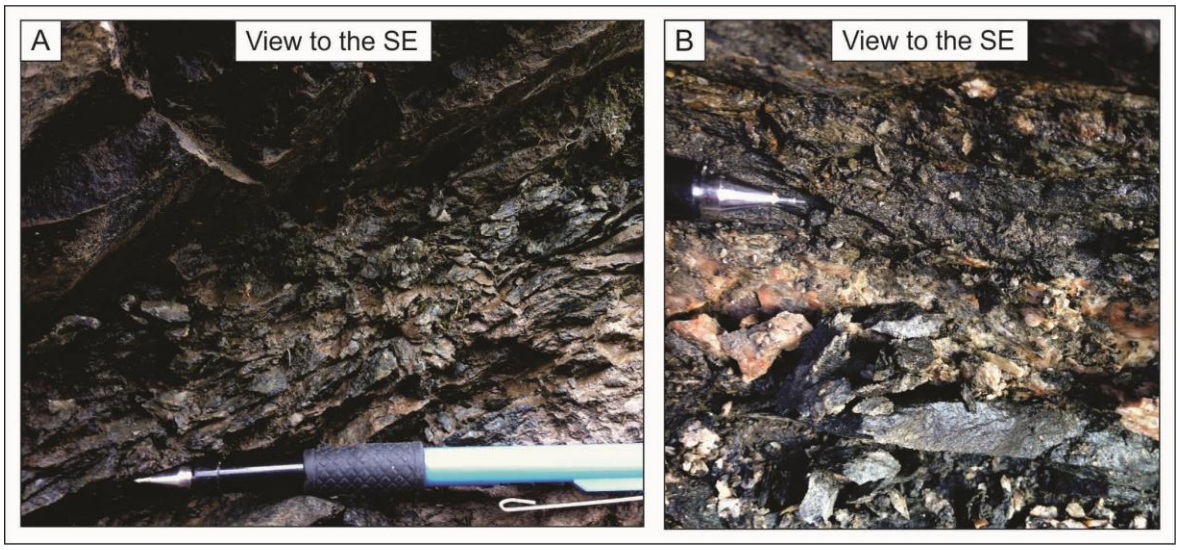

Figure 5.19: Brittle reactivation of ductile shear zones. A) Close-up of brittly reactivated fault core of ductile shear zone 15 with lens-shaped fault core material. B) Brittle reactivation of ductile shear zone 16B with same fault core texture as in A.

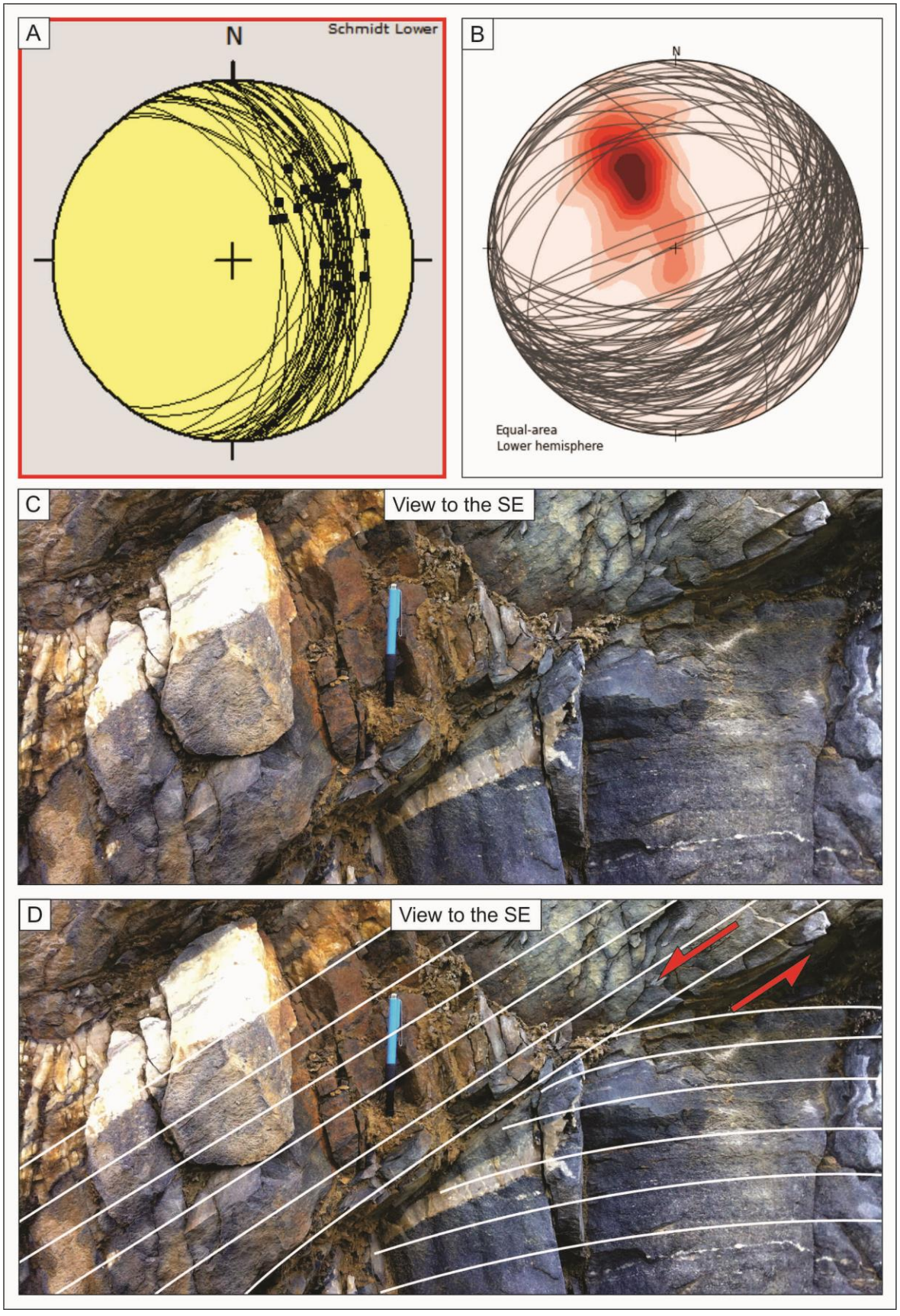

Figure 5.20: A) The stereoplots show the shear zone foliation of the extensional ductile faults. B) The stereoplot of the general foliation within the Orkanger fault shows a different foliation orientation. C) Ductile shear zone 18B with the general foliation deflected downwards within the footwall. E) Sketch of the same shear zone with foliation marked by white lines.

Figure 5.13 shows very well the ductile displacement on ductile shear zones spanning from 1,8-5 m. Displacement due to brittle reactivation was not measurable because the shear zones do not intersect the pegmatite veins, which could have been used as brittle displacement-markers. The correlation between displacement and brittle reactivation was not investigated. The grain size within the ductile shear zones is fine grained. Some ductile shear zones show evidence of a remnant fluid phase that was arrested by the shear foliation, trapping it within the footwall. Evidence of the fluid phase occur as a massive quartz vein that was not able to fully penetrate the shear foliation of the ductile shear zones which acted as fluid barriers (Figure 5.21).

Shear zone 23 is the only compressional shear zone observed within the ORC (cross section: 218 m). The shear zone is characterized by two different lithologies, a dark-coloured variant of the amphibolite host rock juxtaposed against a grey coloured variant. Both lithologies contain feldspar clasts and amphibolite in alternating bands where thin, white levels consist of fine-grained feldspar and quartz. Between the two different lithologies there is evidence of brittle reactivation (Figure 5.22D and Figure 5.18). The brittle fault plane contains no fault material and only an extremely thin slip surface is observed. The slip plane is slightly folded with a fold axis oriented NE-SW. The fault plane curvature pre-dates the brittle reactivation because folds of that orientation are cut by the brittle faults.

The weakest domain in the reactivated ductile shear zone studied, appears to be the angular discontinuity between the ductile shear zone foliation and the differently oriented foliation of both footwall and hanging wall. Pegmatites within the shear foliation may allow reactivation through lithological contrasts.

Microscopic observations

Ductile shear zone 15 in the ORC has been sampled along a continuous traverse (Figure 5.22C). Four samples in total, represent the footwall, the shear zone and the hanging wall. All samples within the traverse were oriented to allow the determination of potential kinematic indicators (Figure 5.23) and are described and interpreted below.

Shear zone 15: hanging wall

Oriented thin section sample 101_1 is taken from the hanging wall and consists mainly of

feldspar grains averaging 0,22 mm in size and hornblende grains averaging 0,7 mm. Feldspar grains up to 0,7 mm are found clustered together with angular garnets. Feldspar and garnet boudins are enveloped by symmetric and asymmetric hornblende crystals (Figure 5.24). Hornblende and plagioclase grains are concentrated along domainal layers. Even though there are several kinematic indicators, such as shear bands and sigma clasts, it was not possible to determine unequivocally the sense of shear. This might indicate that the rock accommodated a component of pure shear and did not develop any monoclinic asymmetry.

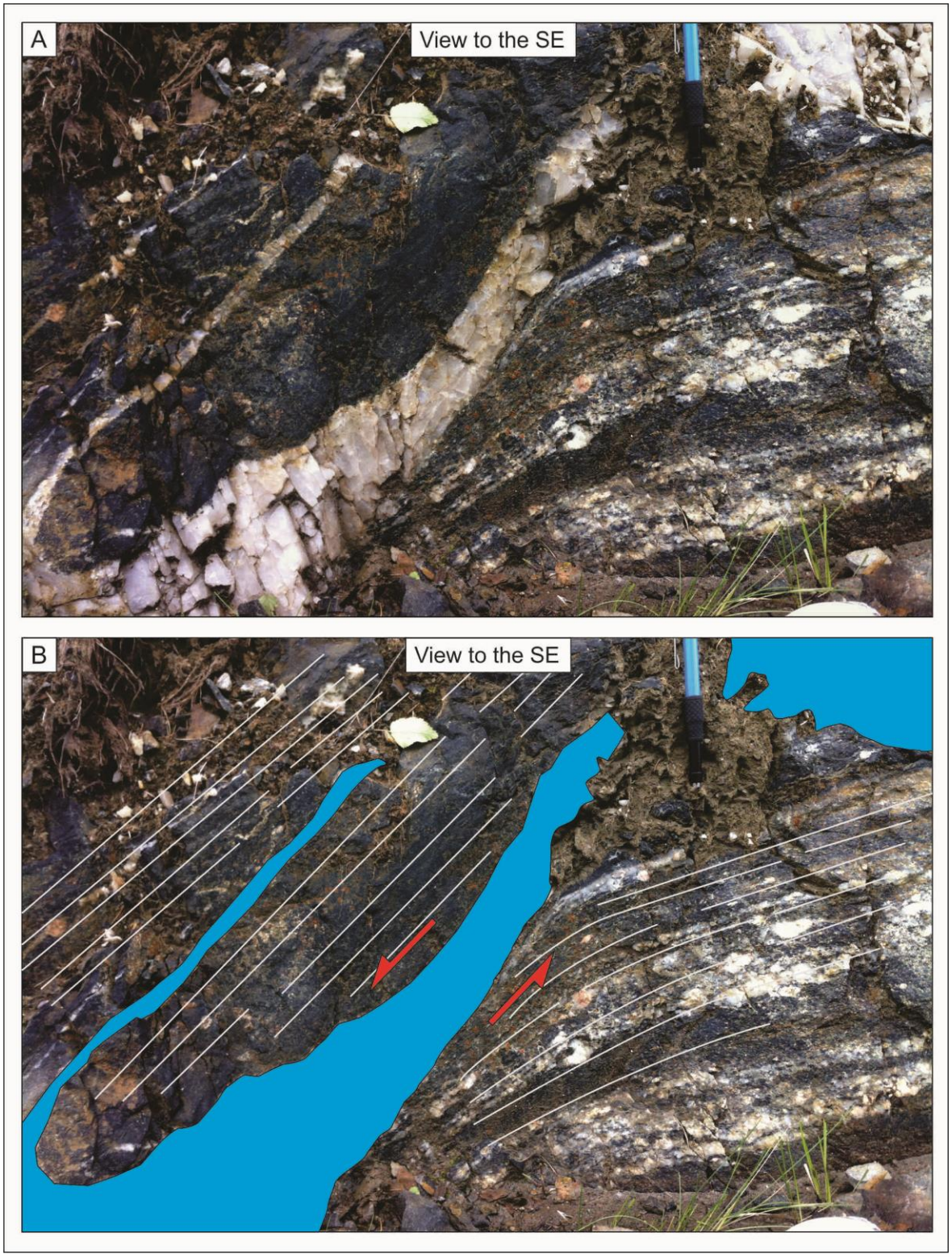

Figure 5.21: Evidence of shear zone foliation acting as fluid barrier in ductile shear zone 18B. Quartz-vein is oriented parallel to the shear zone and partly blocked by the shear zone foliation leading to precipitation between the shear zone foliation and the footwall foliation (HSZ).

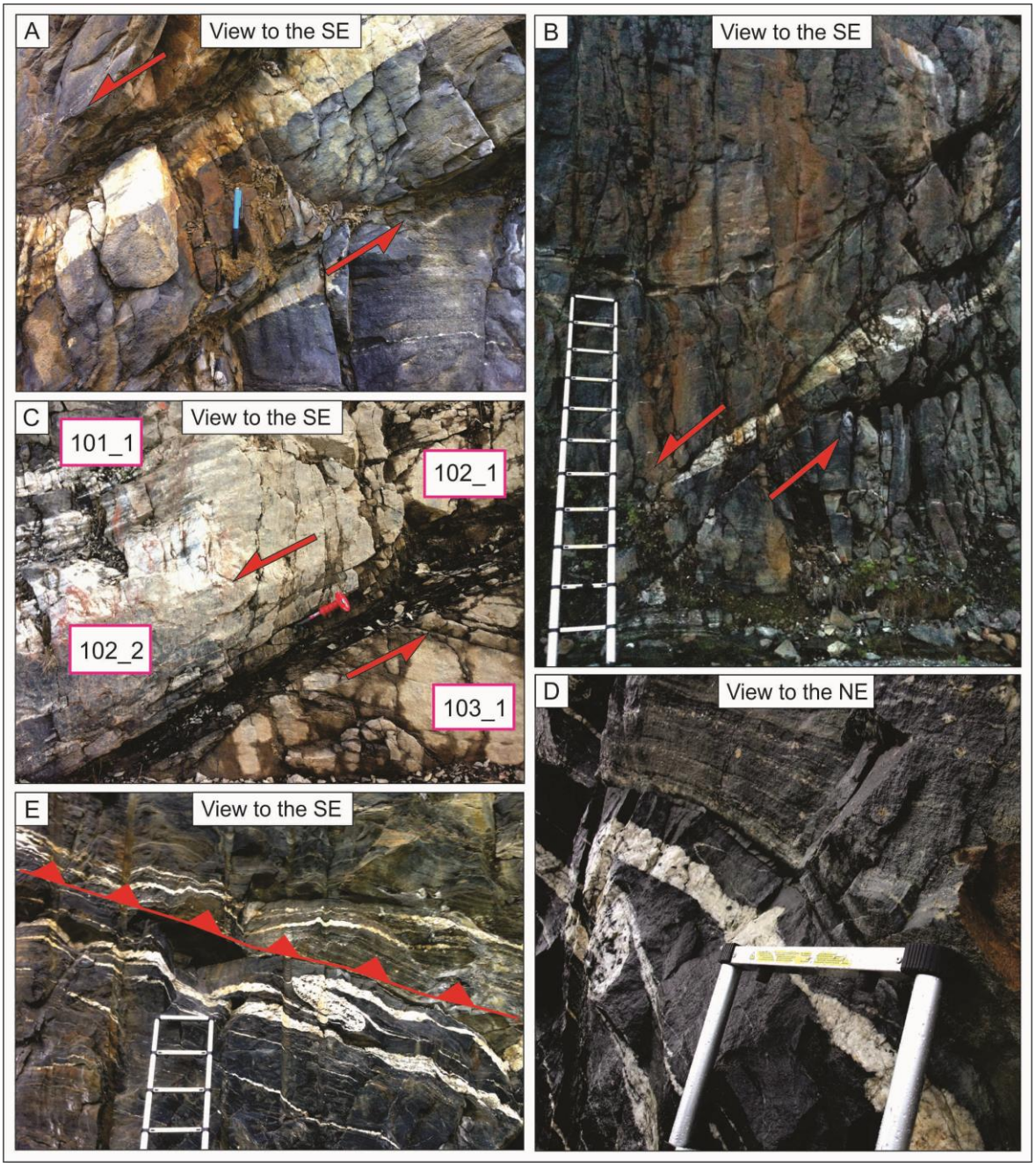

Figure 5.22: Brittle reactivation of different ductile shear zones. A) Ductile shear zone 18B showing close up of both brittle fault cores on each side of the shear zone. B) Showing the total length of ductile shear zone 18B. C) Close-up of brittle reactivation fault core in ductile shear zone with thin section samples marked in white boxes 15. E) Ductile shear zone 23 with thrust-markers indicated in red. D) Close-up of picture E showing a thin fault plane that can represent brittle-ductile or brittle reactivation.

Shear zone 15: core zone

Sample 102_1 is taken from the actual shear foliation of the shear zone core (Figure 5.22 and Figure 5.25). The thin section consists mainly of hornblende, plagioclase and garnets. Hornblende occurs as sigma clasts and as thin needles making up the foliation with an average grain size of 0,07 mm. Plagioclase grains average 0,03 mm and are concentrated in plagioclase-

rich domains. Thin section 102_1 shows extensive evidence for strain localisation through the presence of lens-shaped hornblende and plagioclase showing evidence of grain size reduction relative to the hanging wall. Shear bands running diagonally, averaging 5 mm in length, indicate a dextral sense of shear, which is consistent with the displacement of transposed pegmatites observed at the outcrop. Sigmoidal hornblende clasts show dextral sense of shear adding support for ductile NE-SW extension (Figure 5.25).

Oriented thin section 102_2 also represents the core of shear zone 15. Hornblende has an average grain size of 0,5 mm with some grains as big as 2,1 mm in a coarse grained segment. Plagioclase averages 0,17 mm as both interstitial and as part of feldspar and garnet rich segments. Plagioclase grains have undergone grain size reduction from 0,22 mm to 0,17 mm when compared to the hanging wall (thin section 101_1) and footwall (thin section 103_1) mineralogy, indeed indicative of high strain localization. The coarse plagioclase grains (averaging 2,8 mm) occurring together with rounded garnets are probably part of a relict transposed pegmatite. Hornblende crystals are lens-shaped and surrounded by small-grained plagioclase clasts (Figure 5.25). Bands of small feldspar and garnet grains are still present but less pronounced than in the footwall. Several deformation structures are recognised within the thin section, such as pressure shadows with recrystallized quartz and sigmoidal hornblende crystals. The shear sense remains inconclusive as sigmoidal grains show both dextral and sinistral shear sense. The brittle reactivation of the shear zone is located 40 cm from the sample towards the hanging wall and runs parallel to the shear foliation.

Shear zone 15: footwall

Oriented thin section 103_1 is sampled from the footwall of shear zone 15 (cross section: 103 m, Figure 5.22C) and its compositional banding is made up of four distinct sections of hornblende, plagioclase, and epidote (Figure 5.26). These segments, oriented parallel to the general foliation of the footwall, vary substantially in grain size. Plagioclase has a specifically small grain size of 0,22 mm indicating grain size reduction. The lower one third of the thin section contains 16 % epidote, which is not observed in the other thin sections of the traverse. The hornblende crystals present are deformed into symmetric lenses. These lenses,

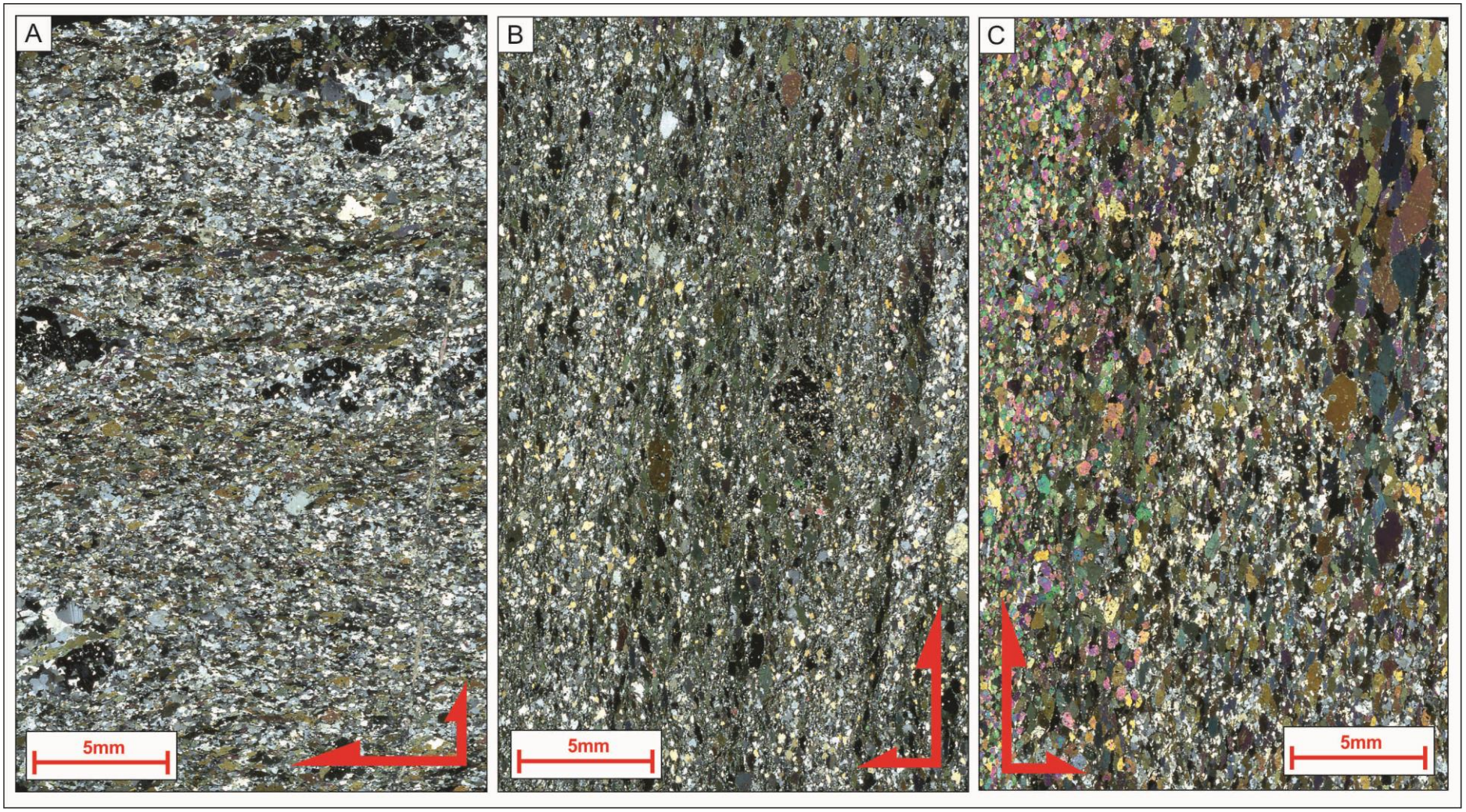

Figure 5.23: Each picture include the total size of the thin section. A) Thin section of sample 101_1 representing the hanging wall of ductile shear zone 15. B) Thin section is made from sample 102_1 and represents the shear foliation ductile shear zone 15. C) Thin section cut from sample 103_1 and represents the footwall of the ductile shear zone. Epidote can be seen in lower part of the thin section, indicative of fluid interaction.

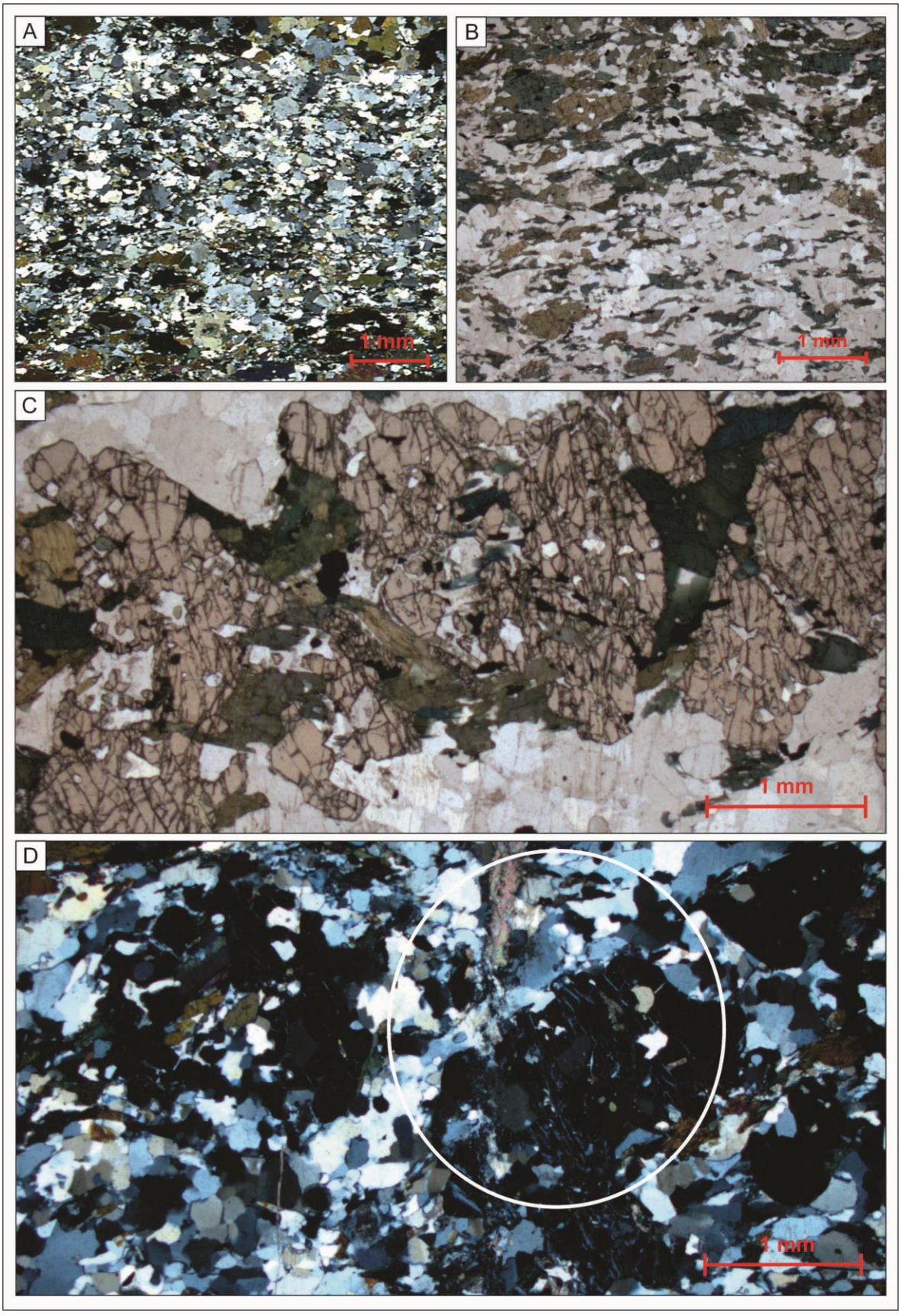

Figure 5.24: All photomicrographs are of thin section 101_1 representing the hanging wall of ductile shear zone 15. A) Coarse grained plagioclase wrapped by minor amounts of symmetric hornblende grains. B) Fractured garnet in a matrix consisting entirely of plagioclase. C) Highly fractured garnet in light brown colour with hornblende in between. D) Calcite vein (top) oriented vertically that connect to isotropic garnet with chlorite coating. X-pl.

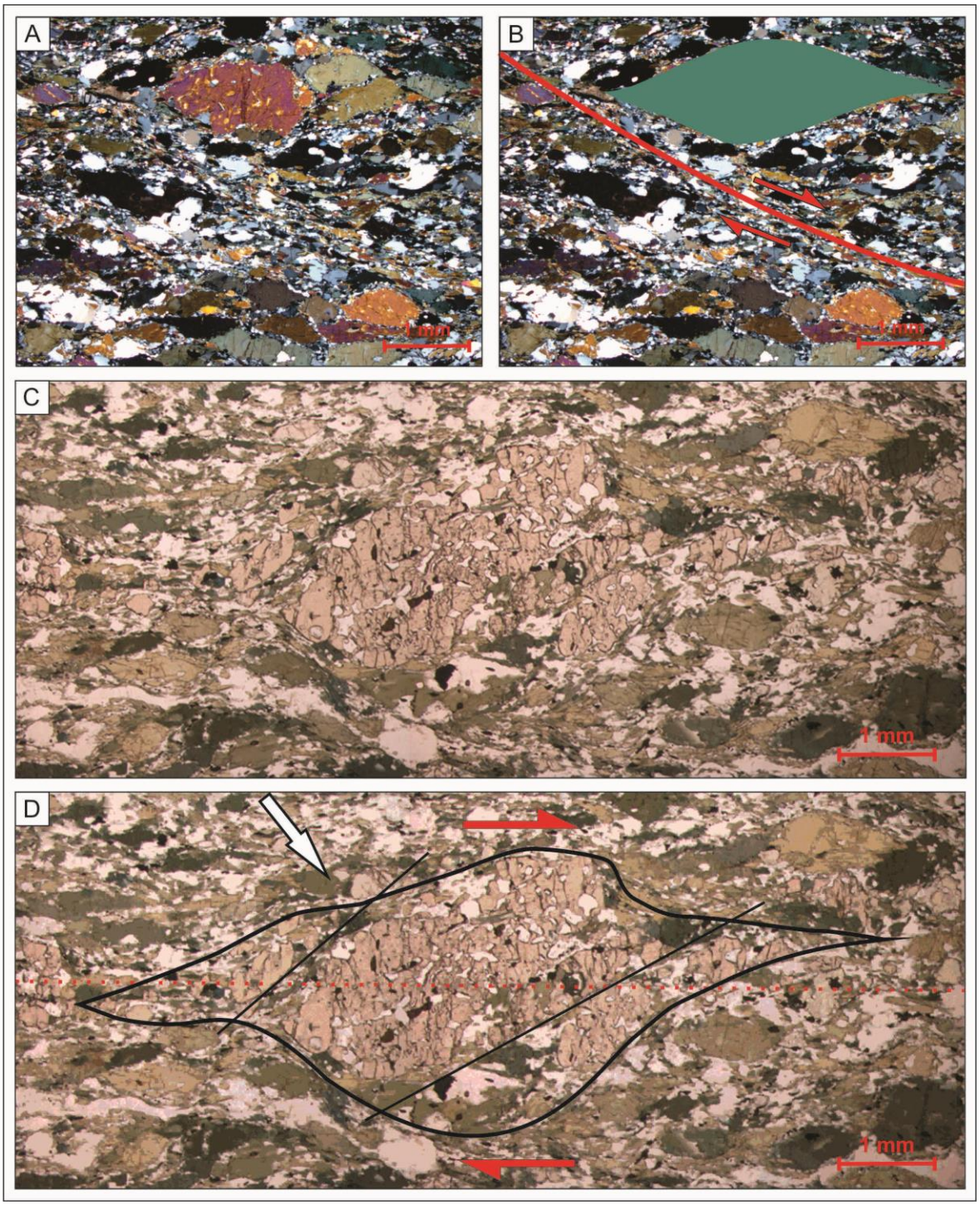

Figure 5.25: All photomicrographs represent thin section 102_1 (Figure 5.22C). A) Thin section with fine grained plagioclase with large symmetric feldspar-clasts in the top of the picture. X-pl. B) Sketch of picture A showing dextral shear sense by both the shear band and sigma clast. This is consistent with mesoscopic observations of shear zone 15 yielding top-to-the NE extension. X-pl. C) Photomicrograph-stitch showing a garnet clast surrounded by feldspar and minor quartz (in white). D) Sketch of picture C indicating bookshelf-structure of the garnet sigma clast, which is indicative of brittle faulting within the dextral shear zone.

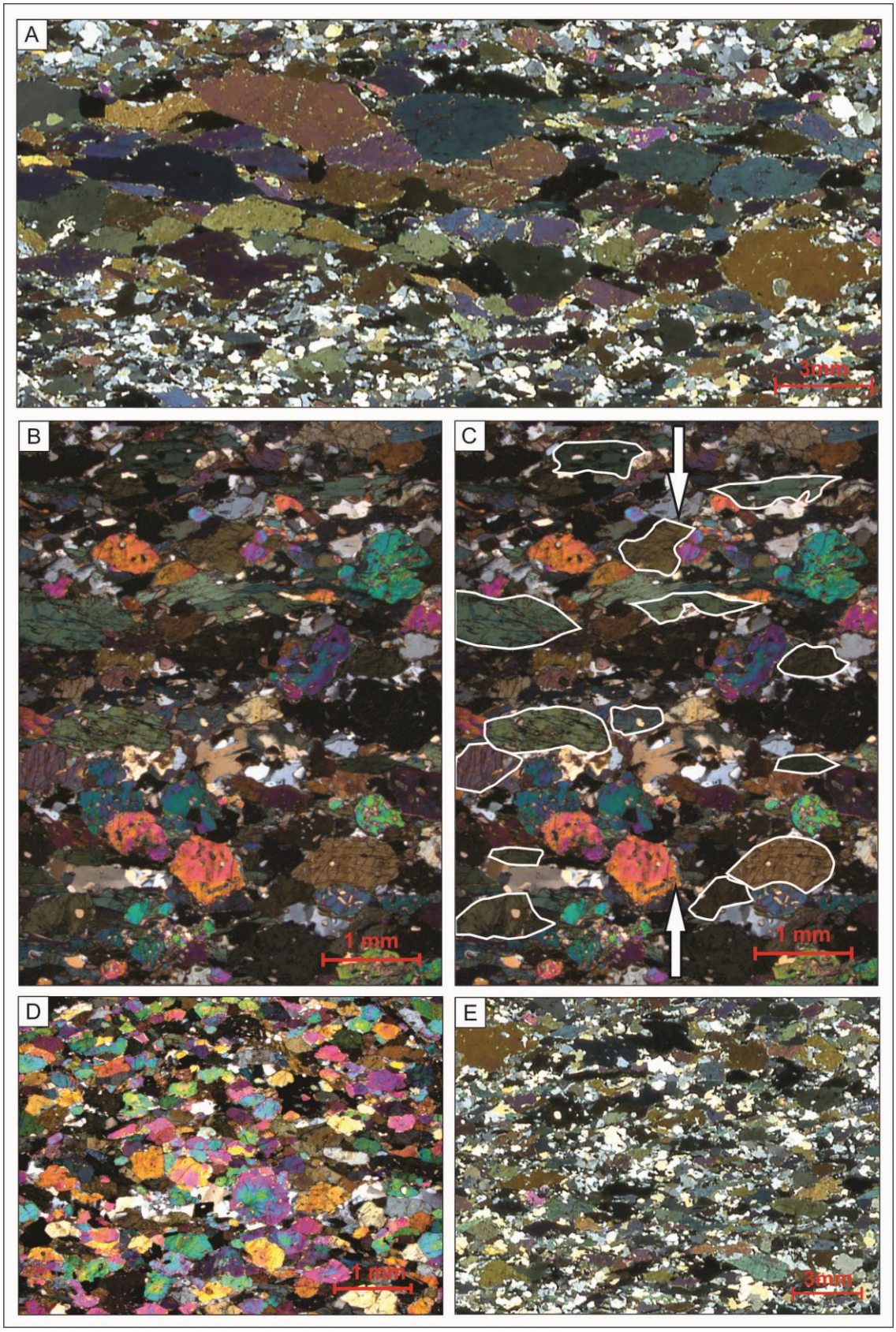

Figure 5.26: All photomicrographs are of thin section 103_1 (Figure 5.22C). A) Large grained symmetric hornblende yielding inconclusive shear sense. B) General look of more hornblende rich section showing asymmetric hornblende clasts as well as euhedral epidote with inclusions. C) Sketch of picture B showing the symmetric hornblende clasts. Largest compressive stress tensor is oriented vertical, indicated by white arrows. D) Epidote rich segment of the lower 1/3 of the thin section indicative of fluid interaction. E) Thin section is made up of more coarse grained feldspar that the shear zone foliation (see scale) of ductile shear zone 15.

averaging 0,022-1,4 mm, lie packed together in two distinct bands oriented parallel to each other.

The presence of more symmetrically deformed hornblende crystals within the footwall (thin section 103_1) of shear zone 15 is indicative of high strain pure shear flattening. A vertical σ_1 yields pure shear flattening, which is also consistent with the overall extensional regime of shear zone 15. The small grain size of plagioclase in the footwall, averaging 0,3 mm, supports the high strain which would have led to extensive grain size reduction during dynamic recrystallization. No reactivation was observed within the footwall, probably due to the horizontal orientation of foliation. The high content of epidote (16%) within the thin section points towards a fluid phase percolating within the footwall, interacting with the amphibolite schist. This is not seen within the shear zone itself or in the hanging wall, indicating that the shear zone acted as a fluid barrier, trapping fluids within the footwall. Uplift, fluids and retrograde metamorphism probably allowed for the growth of epidotes.

5.2.2. Brittle reactivation of brittle-ductile faults

Mesoscopic observations

Several brittle-ductile faults (cross section: faults 10, 11, 19A, 19B and 25) show highly curvilinear fault planes, which dip at 70° at the bottom of the road cut, but tend to flatten out towards the top. The steeply dipping parts of the fault planes are also commonly parallel to a weakly developed shear foliation but elsewhere cut the foliation discordantly with a sub-vertical attitude. Brittle-ductile fault cores vary in geometry and composition. They can be divided into two groups:

1. Fault cores with variable thickness along the fault plane and containing significant amounts of gouge material.
2. Fault cores that show constant thickness and whose fault rocks do not exceed 5 cm in thickness and consist of angular fractured country rock.

Fault 19A (cross section: 170 m) is mapped as a brittle-ductile fault with top-to-the SW kinematics and cuts through the whole vertical extension of the road cut. Its primary fault core is overprinted by the products of major brittle reactivation. Fault 19A represents group 1 and

starts out with a 6 cm fault core at the top of the road cut, which increases in width to 35 cm at the bottom of the section (Figure 5.27). It contains large amounts of gouge and fractured rock. Fault 25 (cross section: 227 m) is a typical example of group 2, with a constant fault zone width. The fault core material consists mainly of sheared rock with a prominent shear foliation with a parallel discrete fault plane running through. The displacement caused by this discrete fault has weakly transposed the foliation in contact with the discrete fault. The fault cores are particularly pronounced along the contact between the hanging walls and the fault core of faults 24A and 25 (cross section: faults 24A and 25).

The fault planes occur mostly as continuous slip surfaces cutting through the outcrop. Exceptions to this build-up include small fault segments that connects the main fault plane (see cross section: e.g. lower part of fault 24B and 25). The lower part of fault 24B shows evidence of deflected foliation which is likely the result of synchronous ductile extensional shearing and brittle normal faulting along both the hanging wall and the foot wall (Figure 5.15C). Multiple small fault planes are indicators of an anastomosing fault architecture (see Figure 5.15). Fault cores consist of very limited amounts of cataclasite, juxtaposed against semi-consolidated and consolidated fault rocks. Highly fractured lensoidally-shaped rock fragments are interpreted to be the damage zone. When moving farther away from the faults, less densely fractured country rock is common. This indicates that strain was localized into no more than 70 cm, with an average of 15 cm. Displacement varies from 45 cm - 107 cm, as measured through fault-displaced pegmatites of generation 1.

The grain size of the fault core material varies greatly from microscopic to blocks with sizes of up to 20 cm in diameter (see cross-section in appendix 4). The variation in fault core material size is especially significant in fault 19A, with an average grain size of 0,5 cm. Euhedral calcite crystals in the fault plane are found within fault 2 and 19A. The extensive fracturing and width of the fault core indicates that the calcite crystals must have precipitated during a period of fault inactivity due to their near perfect rhomb shapes. Quartz and pyrite are also found precipitated onto the fault planes in several brittle-ductile faults (Figure 5.28). All brittle-ductile faults that are not sub-vertical show extensive fracturing and thick damage zones. The amount of fractures increases equally in both the footwalls and the hanging walls of the faults, thus suggesting symmetric strain accommodation on either side of the fault core. It should be noted that these fractures may all be linked to extensive brittle reactivation as many of the fractures are sub-

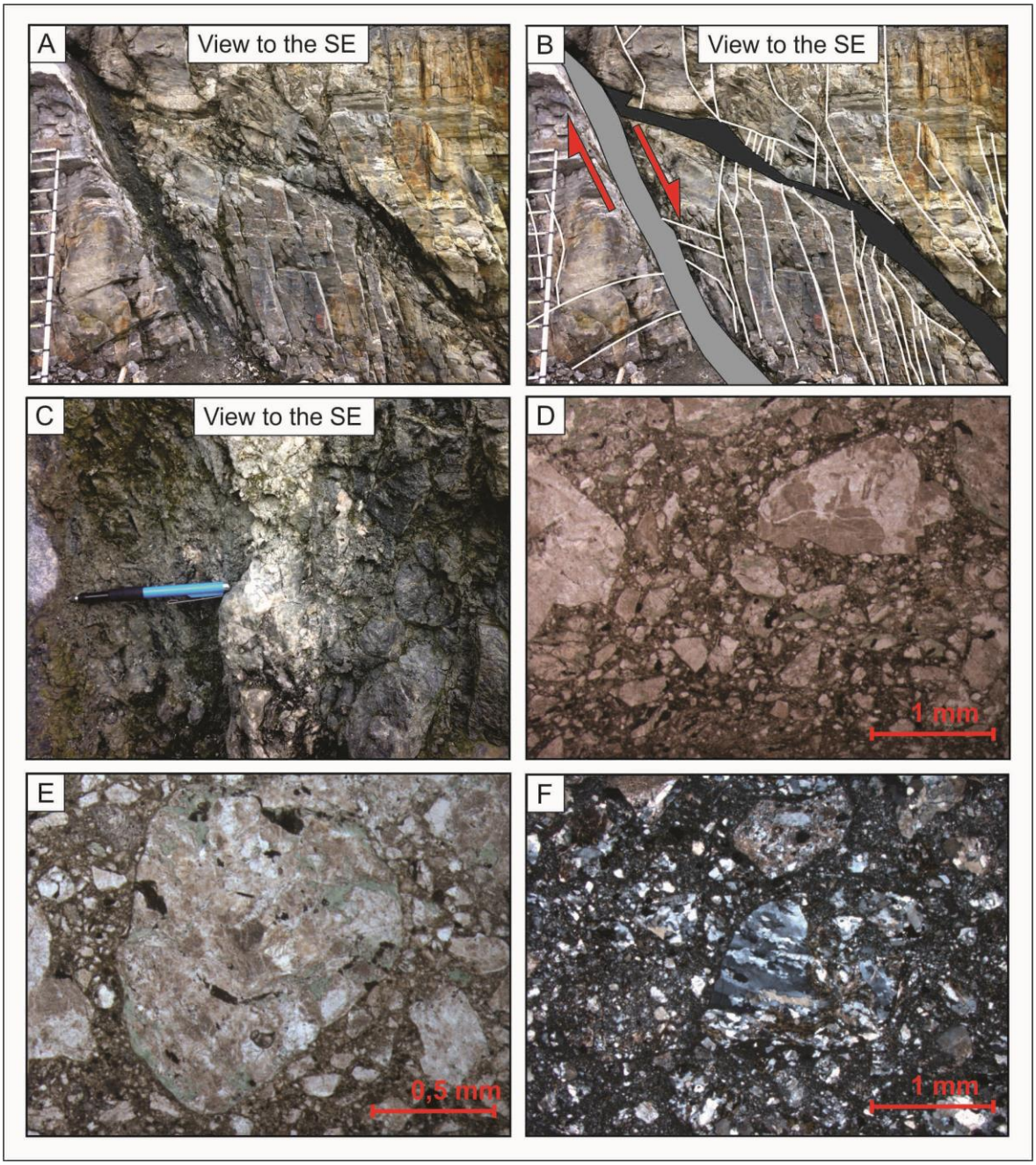

Figure 5.27: A) Full scale photo of fault 19A. B) Two distinct types of fault core material are found in fault 19 with section A showing a fault core with gouge material as well as more sheared rock. Gouge is not present in the connected fault B. C) Field photo showing a continuous change in fault rock material from slip plane in to the damage zone (to the right). D) Photomicrograph of the core of Fault 19A showing cataclastic material in which was in contact with the slip plane with very sharp and angular rock fragments (bottom of picture) and the evolution into more rounded clasts as one moves away from the slip plane. E) Photomicrograph of rounded clast with chlorite filled cracks along the edge of the clast. F) Photomicrograph of rounded clast with large quartz grains indicating preserved GBM. X-pl.

vertical and can be seen in large amounts throughout the ORC.

In summary, brittle reactivation seems to be limited only to those brittle-ductile fault cores with an earlier shear foliation. Slip along brittle-ductile faults was concomitant with large amounts

of circulating fluids in contrast to the ductile shear zones that only rarely show clear evidence of fluid-rock interaction. Extensive brittle reactivation has overprinted many of the brittle-ductile textures (e.g. cross-section: brittle-ductile fault 19A). Statically crystallized euhedral crystals of sulphide and calcite indicate periodic fault quiescence, allowing crystal growth along the fault planes.

Microscopic observations

There are no thin sections of the brittle-ductile faults as they all show heavy brittle reactivation in the form of cataclasis. The following thin section therefore only document the brittle reactivation of a brittle-ductile fault.

Sample 228_1 is from brittle-ductile fault that shows compositional banding of feldspar and hornblende. Strain is localized into the centre of the thin section where hornblende and small-grained feldspar occur interchangeably. Hornblende grains are elongated and occur as sigma-clasts that envelop larger porphyroclasts of feldspar indicating a dextral sense of shear, supporting the top-to-the ENE extension of brittle-ductile fault 25. Feldspars averaging 2 mm in size are located outside the zone of localized strain and are eight times larger than feldspars found within the localized strained zones. The presence of large feldspar grains indicates the some relative grain size reduction by dynamic recrystallization. There is no evidence of brittle mechanical comminution.

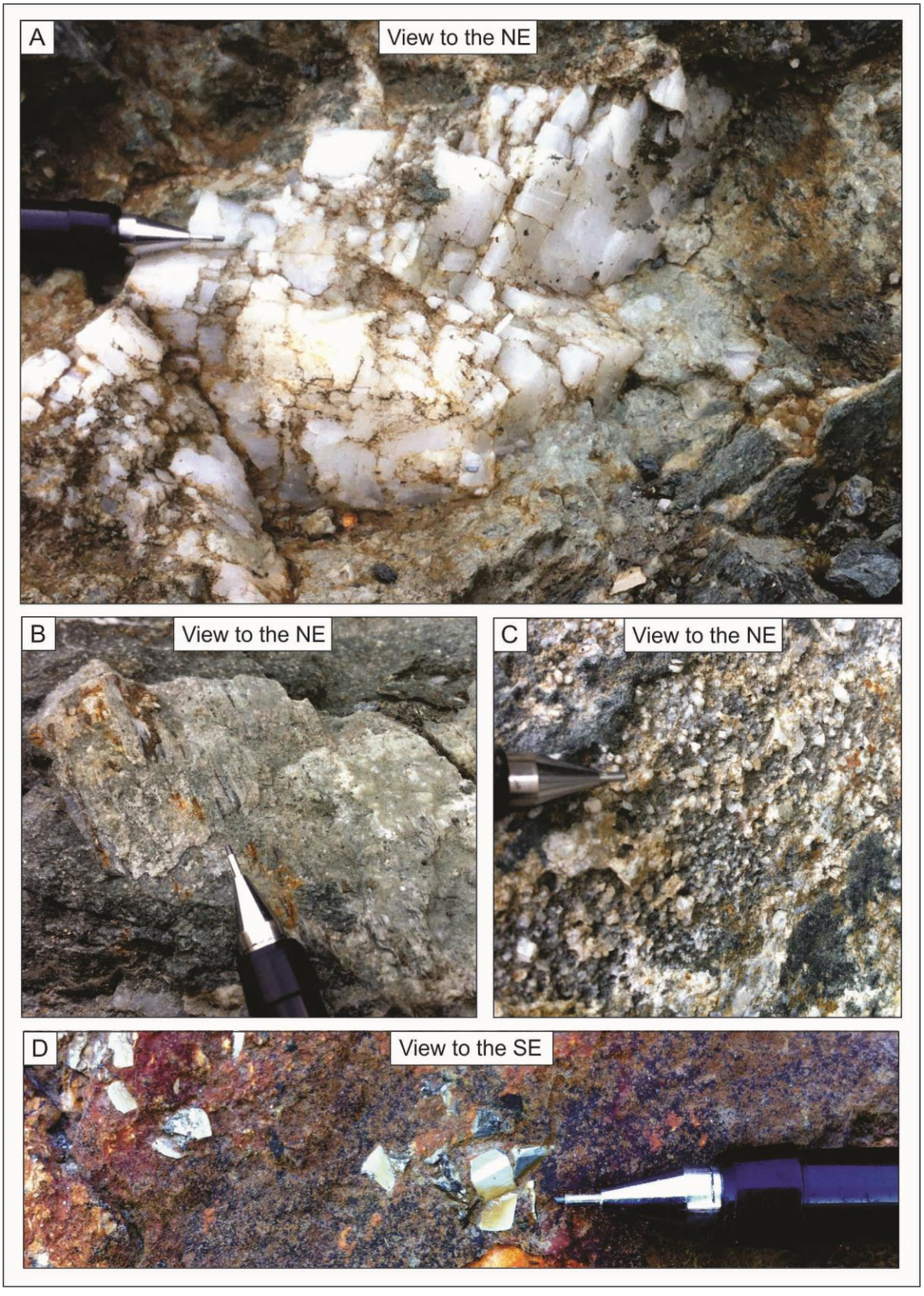

Figure 5.28: A) Brittle-ductile fault 10 shows small cavities within the footwall where euhedral calcite crystals may have grown during fault quiescence. B) Cataclasite developed along the fault plane, but not damaged the fragile calcite crystals. C) Brittle ductile fault plane 19A showing quartz, which probably precipitated during an episode of fluid flow in the fault core. D) Picture showing a brittle-ductile fault of fault group 2 with euhedral pyrite crystals along the fault plane.

5.2.3. Brittle reactivation of pegmatites

Mesoscopic observations

Pegmatites are deflected and transposed into many of the reactivated ductile shear zones. Pegmatites oriented parallel to the shear foliation of ductile shear zones have been the preferential focus of reactivation by brittle faults (cross section: ductile shear zones 6, 15, 16A, 16B, 18B and 23). When present within a shear zone, pegmatites show clear examples of brittle reactivation close to their contacts with the host rock amphibolite (Figure 5.18). Brittle fault 1 (cross section: 18 m) shows a unique orientation of a pegmatite vein which is not seen anywhere else within the ORC. The dike runs almost perpendicular to the general foliation and follows the main trend of the brittle faults in the ORC.

The fault core of fault 1 is 13 cm thick (the total width of the relict pegmatite dike) with elongated feldspar clasts of 0,5-6 cm evenly distributed within the fault core (Figure 5.29). Calcite crystals are also observed within the fault core. Along the contact between the footwall and the fault core there is a thin coating of quartz, evidence of a possible secondary fluid phase. Sulphides are found within the cataclasite, which may be due to reworking of the fault core during fault activity together with percolating fluids.

Fluids do not seem to have been able to penetrate the shear foliation, where deformed pegmatites are transposed into the shear zone (Figure 5.1, Figure 5.21 and Figure 5.22). The pegmatites allow the calculation of displacement based on brittle transposed pegmatite veins. Fault 22A shows a pegmatite displaced 1,3 m (cross section: 202m, Figure 5.16B). On the other hand, where pegmatites are reworked by brittle faults, extensive indication of fluid interaction is present (Figure 5.30).

In summary, pegmatites are invariably transposed in all ductile shear zones and show brittle reactivation along the contacts to the host rock. Sulphides, quartz and calcite crystals point towards the involvement of aqueous fluids percolating through the cataclastic fault cores developed at the expense of the pegmatites.

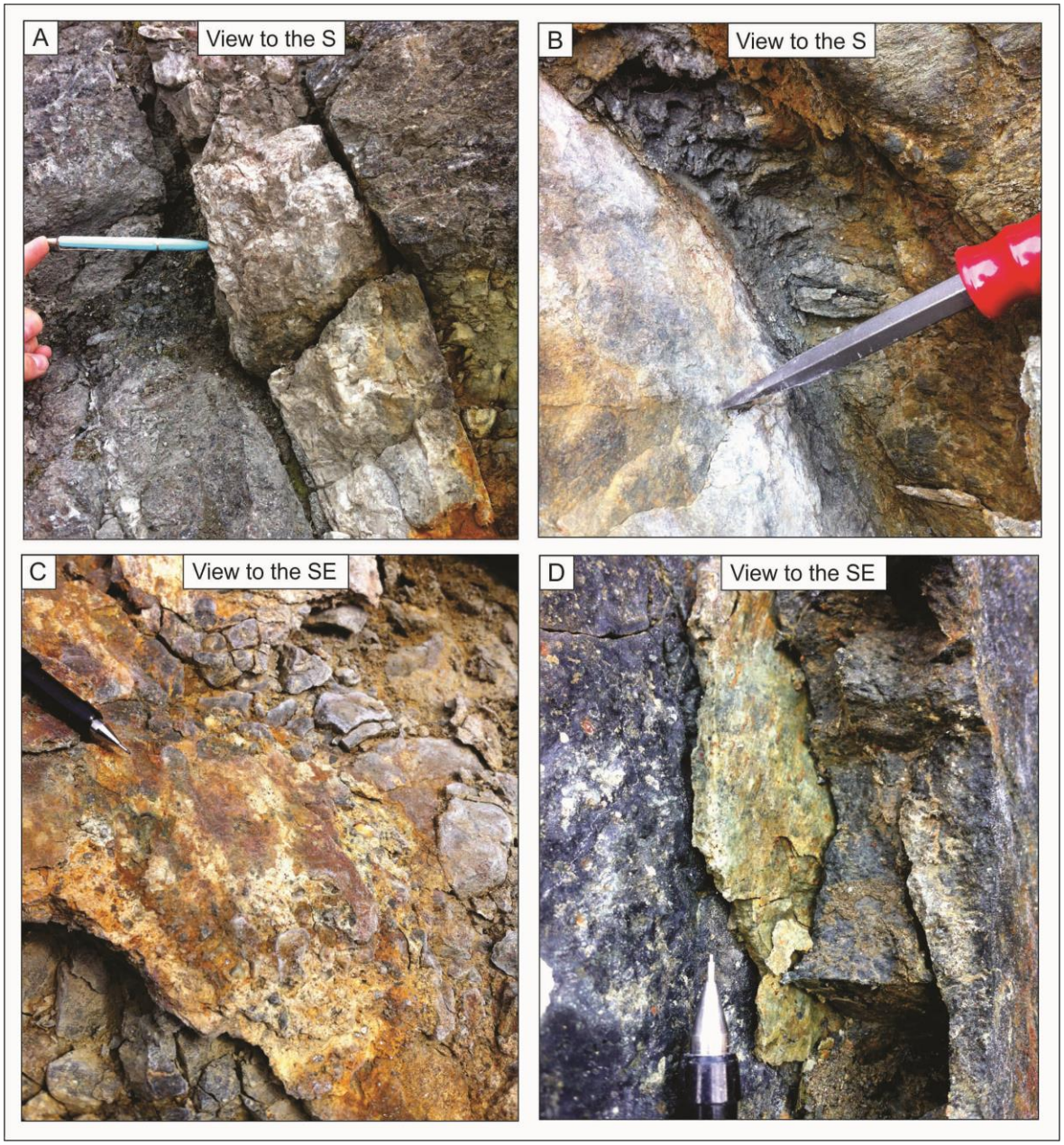

Figure 5.29: Both A and B depict fault 1, reactivated along a remnant pegmatite dike (generation 2). A) Fault 1. Cataclastic core consisting of old pegmatite minerals and some amphibolite. Several different lineation orientations were found (see stereoplot in appendix 4, Fault 1). B) Incohesive cataclastic fault core of fault 1. Orange coating indicate extensive fluid interaction. C) Cataclastic material within fault 7B is orange and is most likely the product of fluid interaction. Small sulphide crystals are also seen within the matrix. D) Picture of fault 20B with a cataclastic fault core consisting of epidote.

Microscopic observations

Sample 18_1 represents the thin section of a cataclasite from brittle fault 1 (cross section: 19m). It is a porphyritic rock consisting of 75% crystals of varying size and 25% of fine grained crushed feldspar, quartz and calcite. Due to extensive cataclasis there exists no foliation or layering. Porphyroblasts of calcite and poikiloblastic plagioclase dominate the larger grains indicating the presence of an aqueous fluid phase.

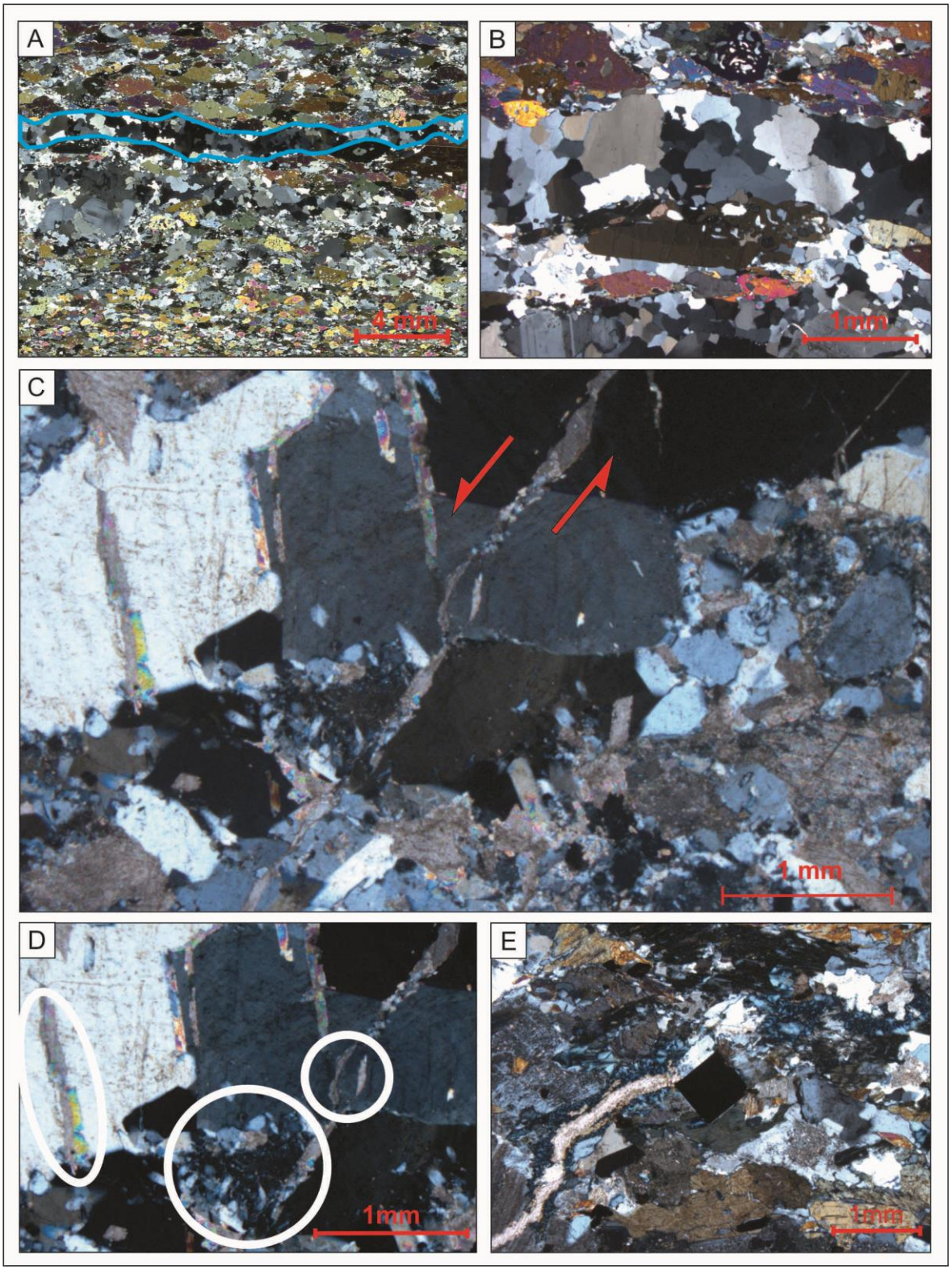

Figure 5.30 Photomicrographs of pegmatites and amphibolite host rock. A) Fluid flow is evident through extensive presence of epidote within thin section 169_2. Epidotes are constrained to an area beneath recrystallized quartz veins. B) Totally recrystallized quartz vein that has undergone dynamic recrystallization indicating temperatures over 400°C. C) Cataclasite of remnant pegmatite with a later secondary fracture phase fracturing both the feldspar grains and matrix (thin section 18_3). D) Presence of muscovite (left circle), chlorite (middle circle) and calcite (right circle) within veins support secondary fracturing and presence of fluids (thin section 18_3). E) Thin section 20_1 represent the hanging wall of fault 1 (cross section: 18m) and shows several fluid precipitation-events within a vein oriented diagonally in the picture. Chlorite (dark blue) is found in the vein walls with calcite making up the core of the vein. At the end of the vein, a perfect cubic sulphide crystal is displayed. All figures with X-pl.

5.2.4. Brittle reactivation of high strain zones (HSZ)

Mesoscopic observations

Domains of the host garnet amphibolite forming the ORC contain white bands with feldspar-augens. Some are still connected by thin white bands of feldspar and quartz (Figure 5.3). Visually, the augen gneiss, with its feldspar augen, is distinctly different from the dark fine-grained amphibolite that make up the general lithology of the ORC. The augen gneiss segments of the ORC display a mylonitic fabric (Figure 5.31), which is oriented parallel to foliation throughout the ORC. HSZ are transposed into both ductile extensional shear zones 16A and 16B, and ductile thrusts (ductile shear zone 23). Strain partitioning into these HSZ produces contacts where HSZ and moderately deformed rock lie adjacent to each other. Within these contacts brittle faults have developed with discrete fault planes, but without fault cores (cross section: ductile shear zone 23). The paper-thin discrete fault plane is parallel to the whole HSZ adjacent to ductile shear zone 23.

Microscale observations

Several thin sections of the HSZ are taken throughout the ORC. These include thin sections 169_1, 194_1, 220_1 and 229_1 and display several similarities such as the amount and grain size of feldspar and small amounts of hornblende. All thin sections display compositional banding texture with segments made up of hornblende and plagioclase. The average amount of plagioclase in the thin sections is ca. 30% higher than in the amphibolite (considered to be the host rock of the ORC). There is also ca. 50% less hornblende within the thin section of the HSZ. There is evidence of relatively high strain displayed through compositional banding and grain size reduction of plagioclase. The amount of strain is less than that of ductile shear zone 15, which showed a far more intense grain size reduction (Figure 5.23).

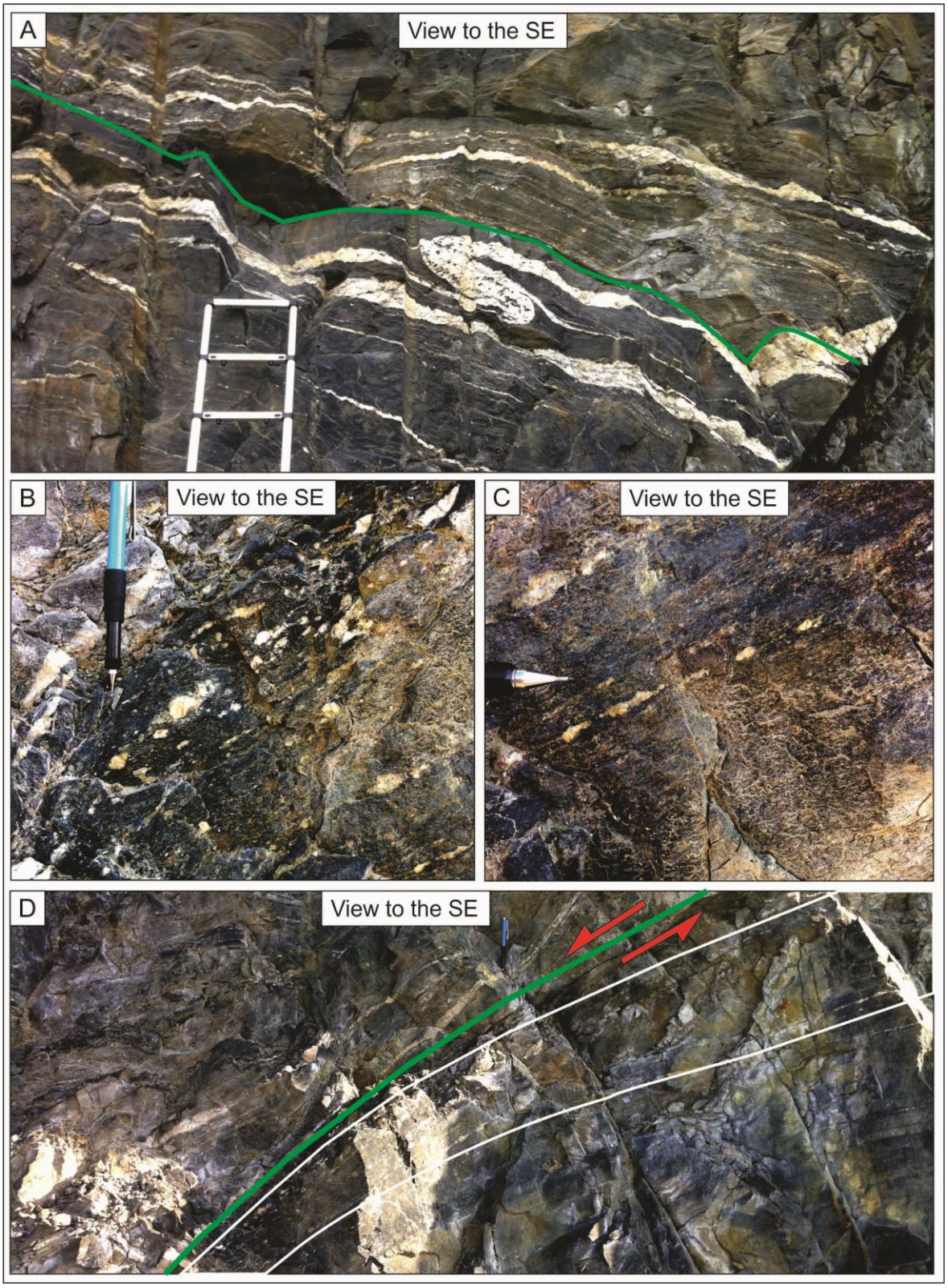

Figure 5.31: A) Ductile thrust 23 showing clear evidence of two differently strained segments of rock with a discrete brittle fault in between. B) Close-up of deformation within ductile shear zone 18B showing deformed feldspar clasts with thinned bands of generation 1 intrusion. C) Another close up of shear zone 18B showing an array of plagioclase crystals that are stretched into small clasts parallel to the LS-tectonite. D) Ductile shear zone 6 where one can see the HSZ, which lies parallel to the brittle reactivation.

5.2.5. Effect of folds on brittle reactivation

Where folding is intense, there exists large brittle-ductile faults, which are brittly reactivated. The setting of fault 10 (cross section: 77 m) is an example of how folds appear to have localised brittle strain. Both the footwall (fold 13) and hanging wall (fold 12) are relict fold structures with fault 10 cutting through both fold limbs and fold hinge. Brittle fault 7B shows the same orientation and kinematics, i.e., top-to-the W normal faulting, (Figure 5.32) as fault 10 and cuts through fold 7 (cross section: 60) in the same way as brittle-ductile fault 10 cuts through fold 11 and 13. This is also displayed nicely in fault 20B cutting sub-perpendicularly through recumbent fold 17, oriented sub-parallel to the ORC (cross section: 180-200 m).

The damage zones of faults cutting fold structures are large. Segments of country rock are trapped within faults with several slip planes (see brittle-ductile fault 10). Fault 10 has one consistent fault plane. The amount of displacement within this fault may be as little as 6 cm shown by the displacement of a semi-fractured pegmatite. The fault consists of gouge and 1 mm grains. Evidence of extensive fluid interaction was observed through the presence of calcite, quartz and pyrite crystals on the fault plane. Damage zone fractures have been concentrated within the hanging wall.

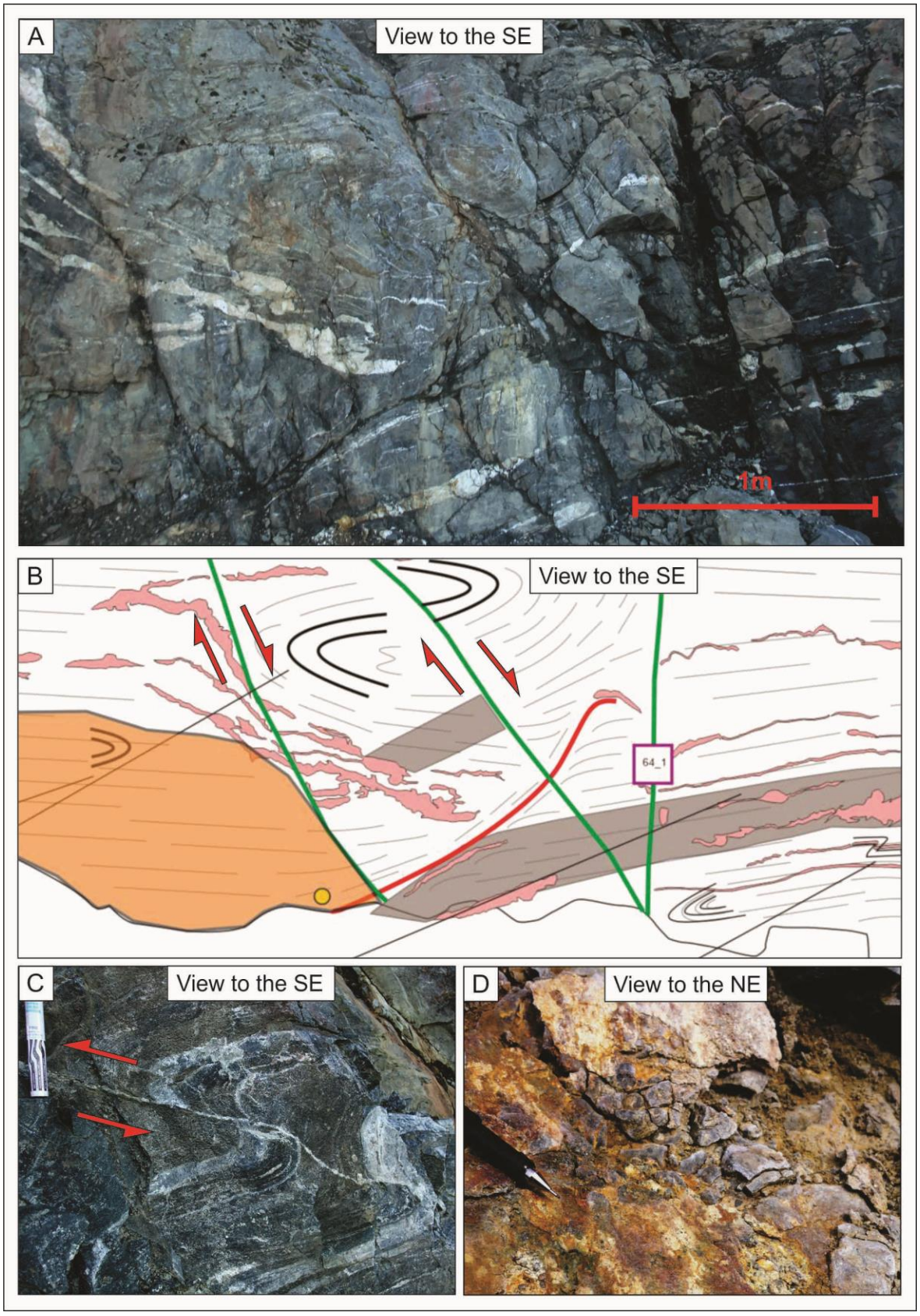

Figure 5.32: A) Large scale fold (fold 13) is cut through by brittle faults running through both the hinges and limbs. B) Sketch from the ORC map sketch showing brittle faults cutting through highly folded amphibolite schist C) Fold 6, which is interpreted to represent the same folding phase, is cut through the hinge by a thin pegmatite vein. D) Rusty cataclastic material within fault 7B indicating the presence of fluids.

5.3. Paleostress inversion in the Orkanger Road Cut

A paleostress analysis was done on brittle structures within the ORC. The brittle faults of the ORC have been refined and regrouped manually in Win_Tensor to reconstruct stress fields of the geological past. The angle of misfit was not allowed to be higher than 30°, which is the largest misfit angle mechanically possible. The paleostress inversion yielded three mechanically probable sub-groups of brittle faults. These faults are presented in Figure 5.33. The first trend represents a stress field with a sub-vertical σ_1, which is in concordance with Andersonian fault theory. This produces NE-SW-extension with fault planes being coated with both epidote and quartz (Figure 5.33A).

The second trend displays a stress field representing non-Andersonian stress-conditions. With σ_1 oriented sub-horizontally the stress field yielding a conjugate set of faults represented by dextral faults oriented N-S and sinstral fault oriented NE-SW (Figure 5.33B). The fault planes of this sub-group are consistently coated with chlorite. The third sub-group represents a stress field with a vertical σ_1, consistent with Andersonian fault theory. This stress field yields NNW-SSE extensional oblique slip with both epidote- and chlorite-coated fault planes (Figure 5.33C).

Based on these stress fields there seems to be no correlation between axial planes and the stress fields of the paleostress analysis. This is because the main trend of the axial planes is oriented N-E (Figure 5.8), which is perpendicular to the different fault groups striking in a NNW-SSE fashion.

Around 120 fault planes without lineations were not included in the inversion, because they would not influence the results. Some fault planes, with lineations, were separated from the constructed paleostress-fields because they did not fit mechanically well with the three sub-group models (Figure 5.33D).

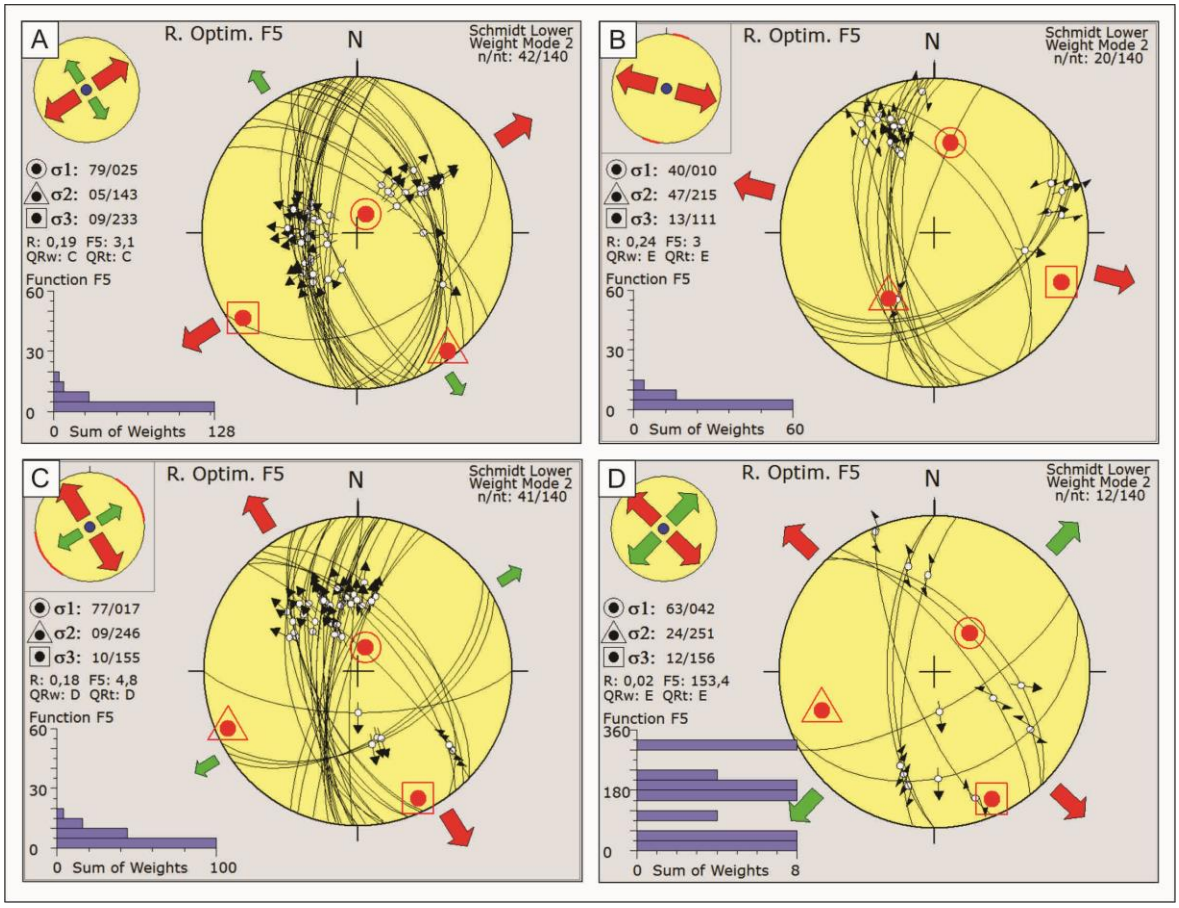

Figure 5.33: All figures are stereoplots produced by the fault slip inversion method. A) Stereoplot yielding NE-SW extension with quartz- and epidote coating. B) N-S-extension of faults with consistent chlorite coating of the fault plane. C) NW-SE extension with only quartz coating. D) Stereoplot consisting of the remaining faults that did not fit the different fault groups.

6. Discussion

6.1. Tectonic evolution of the Orkanger Road Cut

The chronological evolution of the Orkanger Road Cut is complex, but by utilising the systematic structural observations documented, it is possible to unravel the tectonic evolution. A significant variety of structures spanning over more than 400 million years has accommodated extensive fracturing and faulting (and disruption of the primary physical continuity of the outcrop) along the road cut, increasing the level of difficulty in interpreting the different structural events. Below, a thorough discussion of each deformation structure, brittle reactivation and a paleostress analysis is presented.

6.1.1. Host rock

The country rock of the ORC shows consistent evidence of equilibration under amphibolite facies metamorphic conditions. Studies by Hacker and Gans (2005) on the metamorphic conditions of the area was carried out along the E39 only 1,9 km from the ORC. They described an amphibolite schist yielding peak T conditions of 712+- 69 °C and pressures of 11,7+-1,2 kbar. The mineralogical composition of the samples are the same as for the ORC and consists of hornblende, plagioclase, garnet and quartz (Figure 5.26E). The proximity between the two locations, both belonging to the same tectonic unit, the Seve Nappe (or Blåhø, the Norwegian equivalent), and similar mineralogy allows the extrapolation of Hacker and Gans's results to the ORC. Hacker and Gans (2005) suggested that the Seve Nappe of the Trøndelag region experienced burial and exhumation of 40-50 km from lower crustal regions, which would explain the high-grade metamorphic conditions of the ORC. The host rock is generally an S-tectonite, although locally L-S fabrics can also be recognised in some of the shear zones of the ORC.

The ORC shows abundant evidence for pure shear outside of the more clearly simple-shear dominated ductile shear zones. Mesoscopic observations include thin pegmatites with symmetric boudin shapes, supported by microscopical evidence showing symmetric non-rotated plagioclase clasts (Figure 5.26C). Chauvet and Séranne (1994) observed similar

conditions and considered them as resulting from an early phase of extension in the early Devonian. This lead to the exhumation of the Seve Nappe in the Trøndelag region aided by the extensional HDF (Osmundsen et al., 2005a).

6.1.2. Pegmatites

Key observations of the ORC pegmatites reveal that the regional foliation, oriented sub-horizontally throughout the ORC (in spite of local variations due to folding and localised shearing), was intruded by three sets of pegmatites labelled as generation 1, 2 and 3. Generation 1 is only observed as highly transposed within the HSZ. The largest and most prominent pegmatites, generation 2, intruded parallel to the foliation whereas generation 3, which contains much thinner intrusions, cut discordantly through the main fabric elements of the outcrop (Figure 5.4). Generation 2 displays pronounced boudinage and folding, while generation 3 pegmatites are only slightly folded. These structures are also observed by Nordgulen et al. (2002) on the Kollstraumen Detachment Fault to the NE. Group 2 cuts sub-vertically through both structures and must therefore be a younger generation (as already concluded above), supported by the fact that it is not deformed to the same extent.

Pegmatite intrusions within the Trøndelag Region have been interpreted to be part of the orogen-scale plutonic event of early Silurian age (435 Ma ago; e.g. Hacker and Gans (2005)). Grimmer et al. (2015) observed the presence of what they considered as decompression-related melts intruding into the Seve Nappe, dated at 429-434 Ma. These pegmatites are believed to be cogenetic with a pluton that intruded into the Baltic margin, which was tectonically segmented and emplaced upon the Baltic Shield together the Seve Nappe. This constrains the pegmatite age between 435 and 429 Ma, just 7-20 Ma before the nappe emplacement (Hacker and Gans, 2005).

The ORC contains pegmatite-rich (e.g. cross section: 40-140 m) sections and pegmatite poor sections (cross section: 40-155 m and 230-273 m). The pegmatite-poor segments are represented by the 0-40 m markers and from the 240-300 m markers in the cross section. These segments are also poor in faults and fractures, but are interpreted to represent the same lithology. There are two possible explanations for this uneven pegmatite distribution:

1. Pegmatite-poor domains lie close to large faults (cross section: shear zone 18B) that most likely have accommodated large displacements, thus juxtaposing large parts of the tectonostratigraphy that were initially widely separated and thus not exposed to the same intrusion.

2. The country rock of the pegmatite-poor sections may have a less pronounced foliation, which would impede foliation-parallel intrusion.

The first explanation is more plausible, as the host rock (foliated amphibolite) is the same throughout the whole ORC.

6.1.3. Folding history

The folds of the ORC can be divided into four different clusters based on their inter-limb angles (Appendix 2). Subgroup A, B and C are consistent with fold axes trending NE-SW with shallow axial planes (Figure 5.8). Subgroup D differs from the three former based on the steeper axial planes. Subgroup D is from folds situated close to ductile shear zones and may therefore be affected by fault block rotation. This is likely the case within the ORC because faults and shear zones show large displacements and block rotation is indeed recognizable (cross section: shear zone 16A, 16B and 18B, Figure 5.13).

Even though the folds can be divided into four sub-groups, the main trend of the fold axes is NE-SW (parallel to the outcrop face) and believed to represent one folding event. This orientation is coaxial to the NE-SW extension direction of the MTFC (Osmundsen et al., 2006) and the very penetrative structural grain of the entire Fosen Peninsula region.

Axial planes dip shallowly to both the NW and SE. The folds of the ORC therefore fit geometrically with the model of extension-parallel folding that occurred during the terminal phase of compression in the late Devonian (Chauvet and Séranne, 1994; Krabbendam and Dewey, 1998). Seranne (1992) discussed the possibility of the reorientation of fold axes due to the presence of the MTFC and its NE-SW strike. A ductile strike-slip phase may have rotated the fold axes from their original positions, which would explain why some of the fold axes are oriented in a more ENE-WSW manner within the ORC.

The folding of the ORC may have developed just as ductile extensional shearing initiated during the Early Devonian. Through the study of late Palaeozoic kinematics, Seranne (1992) suggested contemporaneous folding and extension, also known as extensional folding, within the MTFC. The ductile shear zones of the ORC cut consistently through the folds, which places the folding event before the ductile extension, and not contemporaneously as observed by (Seranne, 1992). Even though there must be a difference in timing, the folds of the ORC are most likely part of this extension parallel folding.

Field observations at the ORC reveal a set of rootless folds (fold 23 and 24) that, due to extreme transposition, show no continuous limbs. These folds may be part of an older generation of folds (cross section: 238-255 m). The fold axes of these folds show similar ENE-WSW orientation, which is consistent with the other ORC folds. The original fold axis orientation of these detached folds is most probably reoriented during the NW-SE extension.

6.1.4. Ductile shear zones

All ductile shear zones of the ORC are mesoscopically similar regarding both orientation and geometry (Figure 5.13). Microscopic studies of plagioclase grains within the shear zones show extensive evidence of grain size reduction in contrast to the footwall and hanging wall, where grain size is at least three times larger (Figure 5.24, Figure 5.25, Figure 5.26). The two distinct groups of shear zones identified (top-to-the ENE oblique extension and top-to-the SW oblique extension) are likely the results of different shearing episodes (see Figure 6.2).

Orogenic extension of the Caledonides within the central and northern parts of the Trøndelag region is subdivided into two different temporal events (Braathen et al., 2002). This extensional phase was coupled with extension parallel folding, believed to be linked to the terminal phase of the orogenic phase. In the early Devonian, at medium-grade metamorphic conditions, ductile, low-angle shear zones cut through the nappe stack with overall top-to-the WSW kinematics, showing local implications of top-NE ductile extension, which is also observed by Seranne (1992). The observed top-NE ductile extension fits well with the top-ENE extensional shear zones of the ORC, displayed in Figure 5.20. The slightly more east-verging geometry of the ductile shear zones in the ORC may be due to late block rotation, post-dating the extensional shear zones.

Kendrick et al. (2004) studied extensional NE-SW trends through kinematic indicators within ductile shear zones of the Trøndelag metamorphic core complex. Further, Braathen et al. (2002) interpreted these shear zones to be connected to a proto-version of the MTFC, which may constrain the age of the similarly oriented ductile shear zones of the ORC to an early Devonian age.

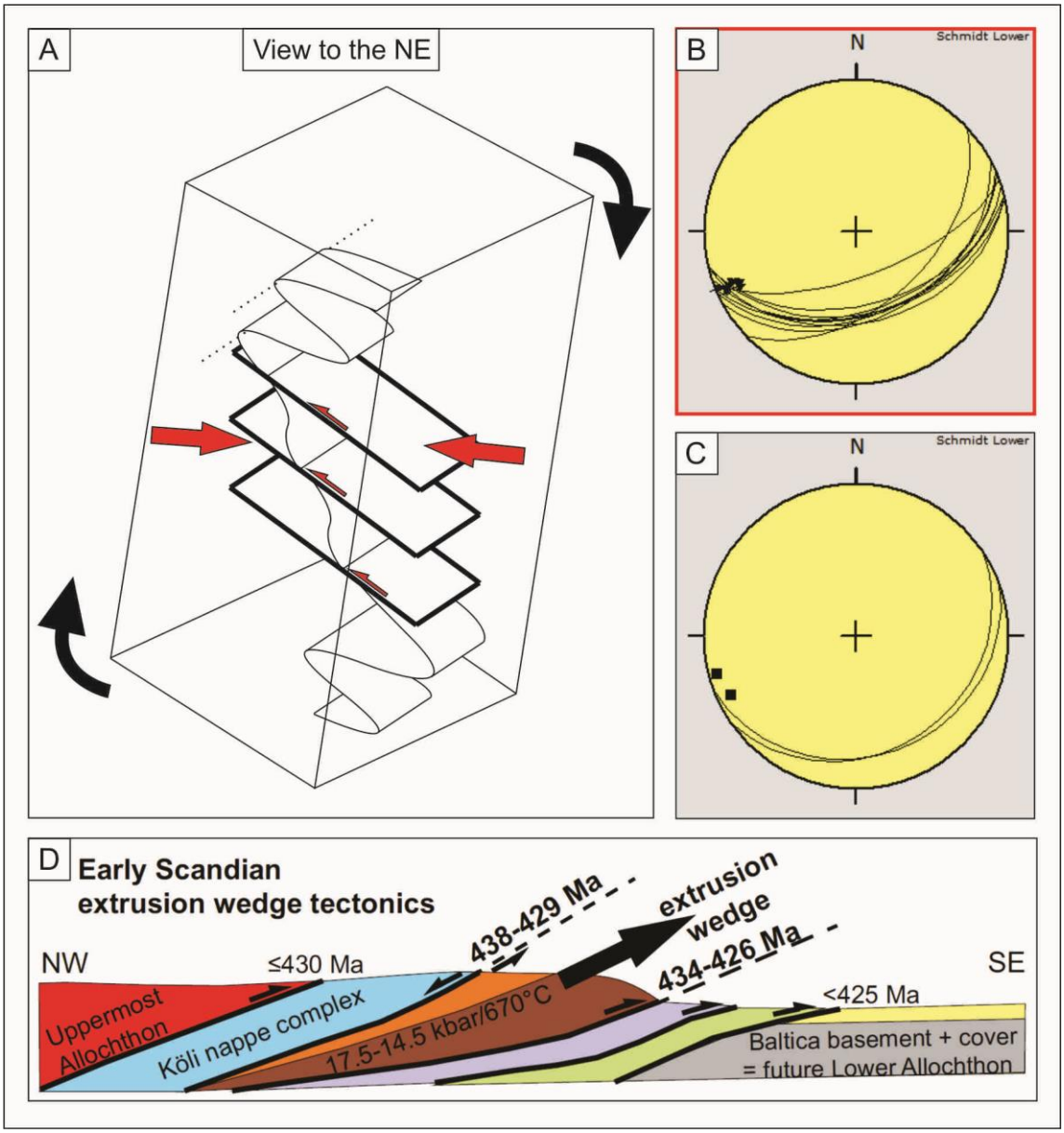

Figure 6.1: A) Sketch of the evolution of ductile thrust 23 within the ORC. Thrust-kinematics may have been a part of the roof-contact of an extrusion wedge of the Seve Nappe in Sweden. The top-to-the-NW thrusting fit the extrusion wedge that extruded towards SE. The orientation of the folds and the ductile shear zone is probably affected by fault block rotation (black arrows) due to extensive fault displacement of faults in the vicinity. B) Stereonet showing the orientation of the ductile thrust 23 (dots represent later brittle reactivation and should not be considered in this discussion).C) Stereonet with orientation of fold 19,5 with shallow axial plane and fold axes (together with mesoscopical observations) indicating NNW thrusting. D) Extrusion wedge model presented by Grimmer et al. (2015) showing the Seve Nappe in brown, extruding towards the SE with opposite kinematics in the lower and upper contact (indicated by black arrows).

Extrusion wedge

Shear zone 23 (cross section: 217 m) represents an oblique thrust and is the only compressional shear zone documented in the ORC. It is a combination of genetically linked ductile shear zones and asymmetric, verging folds. Its folds could not be measured directly at the outcrop due to their high location in the rock face and obliquity, but a rough estimate indicate E-W oriented fold axes. This yields a strange thrust direction of top-to-the NNW.

The thrust was probably linked to the general trend of folds oriented NE-SW, by allowing ductile reverse shear zones to form along fold limbs. This caused structures where the limbs of the folds are transposed and reactivated as proper ductile shear zones (Figure 6.1A). The segments between each thrust preserve a fold hinge or strongly deflected and steepened foliation.

Grimmer et al. (2015) developed an extrusion wedge model for the Seve Nappe in the Jämtland-Västerbotten segment (Figure 6.1D). The extrusion wedge model involves extension in the roof contact of the extruding wedge with simultaneous thrusting in the lower contact (Figure 6.1D). Pegmatites intruding into the extrusion wedge, consisting of amphibolite and kyanite mica schist, have been dated to 434 Ma and 429 Ma. This evidence may be correlated with observations at the ORC. Thrust 23 may be a part of a roof-section of the western part of the extrusion wedge seen in Sweden. Pegmatites intruded into amphibolite, dated at Tråsåvika and Fanrem (assumed to be related to the ORC-pegmatites) are dated to 431 Ma and 421 Ma (Tucker et al., 2004; Robinson, 2008). The resemblance of both age and host rock lithology, together with observations made by Grimmer et al. (2015) is striking. Together with fitting fold kinematics of fold 19,5 the ductile thrust may have recorded the roof-contact kinematics of the Swedish extrusion sketched in Figure 6.1A. The unusual orientation of the whole thrust, with folds, may very well be due to block rotation by the big brittle-ductile fault 24B to the right of the thrust (marked by bent arrows in Figure 6.1A).

6.1.5. Brittle-ductile and brittle faulting

The brittle-ductile faults of the ORC are observed throughout the ORC as either top-to-the ENE dip-slip or top-to-the WSW oblique-slip extensional faults. The brittle-ductile faults cut through all structures and are only post-dated by purely brittle faults (Figure 6.3). Brittle-ductile faults

of the ORC probably represent faults developed at brittle-ductile conditions during denudation and subsequent exhumation of the MWGR.

Brittle faults occur all along the ORC as sub-vertical faults with variable displacement and fault core composition. Crosscutting relationships constrain them as the youngest structures within the ORC (Figure 5.16 and Figure 5.17). They accommodated ENE-WSW extension and may be linked to the extensional phase of the MTFC, which shows NE-SW extension, also observed by Kendrick et al. (2004).

They are the result of both neo-formation and reactivation of inherited remnant structures, as discussed in the paleostress analysis section. Quartz, epidote, sulphides, chlorite and calcite found within the brittle faults and reactivated relict structures imply extensive fluid circulation (Figure 5.29B). Brittle faults with fractured fault zones are indeed excellent fluid conduits. The large variety of secondary minerals found within the faults point towards several fluid circulation events during the exhumation of the Seve Nappe and the ORC. Osmundsen et al. (2006) observed epidote- and quartz-coated fracture sets close to the Austrått Formation, exhumed from brittle-ductile conditions due to the HDF. Quartz and epidote must have precipitated at deeper crustal levels while sulphides, chlorite and calcite precipitated at more shallow crustal levels consistent with the obvious exhumation of the ORC. Late Palaeozoic and Mesozoic brittle faults continued deformation through first dextral strike-slip faults and then as sinistral faults (Seranne, 1992). A more thorough examination of the orientations of the brittle faults is done by paleo-stress analysis.

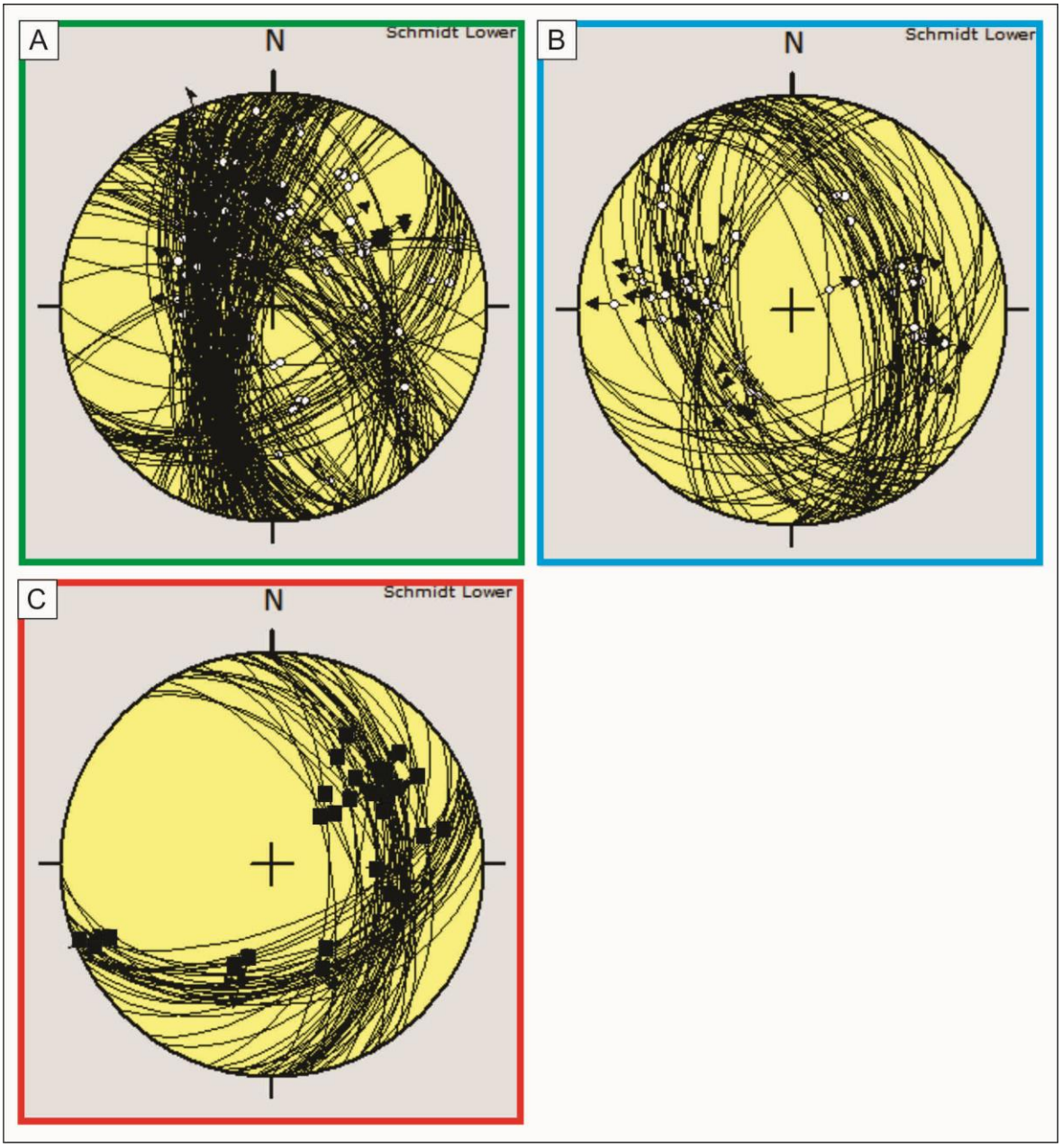

Figure 6.2: All great circles and lineations shown in the stereonets represent faults within the ORC. A) Summary fault plot of brittle faults with three distinct fault groups. The most pronounced fault group strikes N-S, while another group is striking NW-SE with a third striking NE-SW. B) Summary fault plot of brittle-ductile faults with two distinct fault groups showing ENE-WSW extension. C) Summary of ductile shear zones showing two distinct orientations of shear zones showing ENE-WSW oblique slip extension and NW-SE oblique slip of both compressional and extensional regimes.

The relative age of all the structures within the ORC is shown below. The figure is based on all observations made in field and through microscopic examination (see Appendix 1).

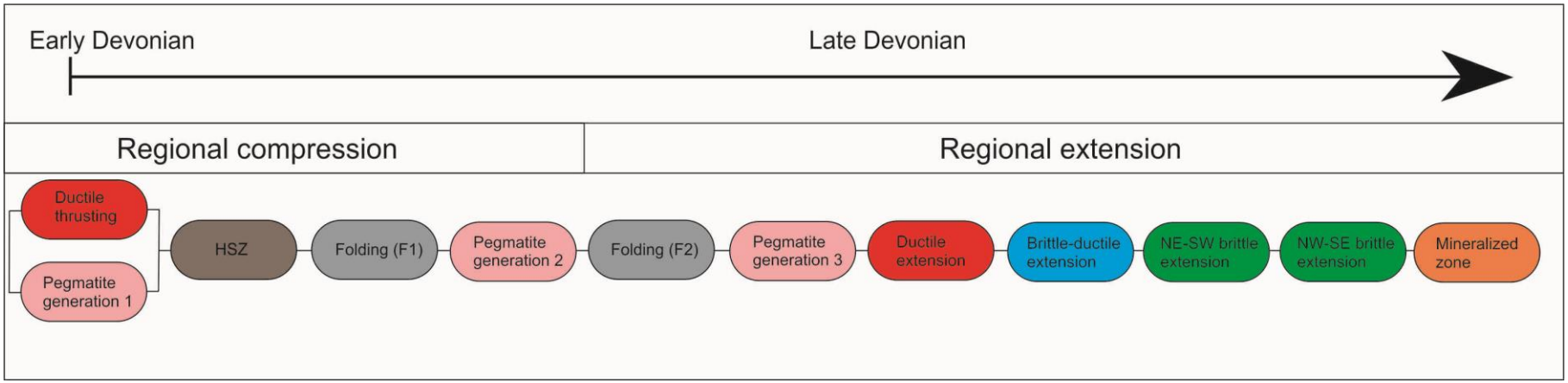

Figure 6.3: Showing the relative age of all the main structures within the ORC. The coeval ductile thrusting and pegmatite intrusion gave way for the generation of the HSZ of the ORC. This was followed by a folding phase (F1) that is displayed as rootless folds in the ORC today. This was followed by extensional folding through the translation of the HDF and overall extensional phase of the Scandian Orogeny during the Late Devonian. This was followed by an intrusion event that cut the folds of F2. This was followed by ductile extensional shear zones which transposed generation 3 pegmatites. Brittle-ductile structures develop, cutting older structures, which probably belongs to the exhumation of the Seve Nappe due to the extensional phase of the MTFC. Brittle NE-SW extensional faults develop as the exhumation progresses and the main palaeo-stressfield of the regions shows NE-SW extension. A set of NW-SE brittle extensional faults developed as the HDF left a void that gave local NW-SE extension within the margins of the HDF. The extensive brittle faulting generated heavy fluid interaction and created mineralized zones in segments of the ORC (Figure 5.1).

6.2. Mechanisms of brittle reactivation: Lessons learned from the ORC

There are numerous studies of brittle reactivation within the Trøndelag region (Braathen et al., 2002; Redfield et al., 2005b). Excluding the case of only a set of newly nucleated brittle faults, reactivation is indeed common within the ORC. It can be genetically linked to three main types of inherited, relict structures, even though reactivation occurs in other structures as well. These three main inherited features that steered brittle strain localization are ductile shear zones, folds and pegmatites and their differences will be discussed below.

6.2.1. Ductile shear zones

The most prominent localization of brittle reactivation took place along Caledonian ductile shear zones. These share a similar orientation throughout the ORC with an average dip of around 45° and with transposed pegmatites aligned parallel to the mylonitic shear foliation.

Lithological (that is, competence) differences and geometrical misorientation of the shear zone foliation and the general foliation are the key parameters that seem to make brittle reactivation possible along the inherited shear zones. The rheological difference at the lithological contact represents an obvious plane of weakness where strain may easily localize (Figure 5.19). Etheridge (1986) recognised three distinct parameters controlling the reactivation of ductile faults: the strength of the shear zone, host rock lithology and the orientation of the active stress-field. It should be noted that, in addition to parameters presented by Etheridge (1986), the misorientation of the foliation within the shear zone contact must play a significant role in brittle reactivation, which is well backed by shear zone reactivation displayed in Figure 5.18.

The grain size reduction of both hornblende and plagioclase documented in shear zone 15, relative to the footwall and hanging wall, represents a weakened zone (cross section: 105 m). Experiments on different materials done by Tullis and Yund (1985) and De Bresser et al. (2001) show that strain weakening is generated through grain size reduction and the generation of ductile shear zones. The hardened shear zone (the zone of reduced grain size) may have aided

brittle reactivation. The oriented shear zone foliation, an optimally oriented stress field together with mechanical competence contrast through grain size reduction of both plagioclase and hornblende is the most likely explanation of brittle reactivation of ductile shear zones within the ORC.

6.2.2. Folding history and reactivation

The MTFC underwent extension-parallel folding which involved NE-SW extension with σ_1 oriented horizontally during the orogenic collapse in the early Devonian. The NW-SE compression of the Trøndelag Gneiss Core Complex allowed for ductile folding leading to a set of mega scale up-right folds with local tight folding (Chauvet and Séranne, 1994).

Multiple folding events are recognized within the ORC. Several folds, fold 7, 11, 13 and 17 (cross section: 60m and 180m) are cut by brittle structures within the ORC, which seem to concentrate into highly folded zones. This is displayed by brittle faults 7B, 20A and 21 cutting through the limbs of the folds, which fold axes are oriented coaxial to the strike of the ORC (Figure 5.32). Brittle faulting parallel to the axial planes and parallel to the foliation of the fold limbs is possible from a mechanical point of view. Tight folding will lead to the development of axial plane cleavage, which are planes of weakness oriented parallel to the axial plane. This is not the solution for the reactivation of folds within the ORC. The faults cut the folds almost perpendicular to the fold axis, excluding reactivation along axial plane cleavage. A potential explanation may be that the folds were mechanically weakened during the exhumation in the late Devonian, which led to the concentration of late brittle faulting in these early structures.

A conceptual model of brittle reactivation in inherited structures represented by pegmatites, shear zone and folds has been developed through the careful study of remnant structures in the ORC (Figure 6.4). Fault group 1 is represented by brittle reactivation of remnant pegmatites. The starting point of fault group 1 is a pegmatite cutting foliation sub-perpendicularly (representative of generation 2, but includes also generation 3 pegmatites). These pegmatites are faulted in the reactivation phase where the fault core is concentrated in the contact between the amphibolite host rock and the intrusion with extensive fluid rock mixing. When the fault undergoes fault quiescence, the fault has matured to consist of the total width of the relic pegmatite. During fault quiescence, the fault core and damage zone becomes impermeable due

to the precipitated fluids, such as vein quartz and calcite. The fault core material consist of mostly angular fragments of pegmatite.

Fault group 2 involves a relict ductile shear zone consisting of a well developed shear zone foliation with deflected foliation of both the hanging wall and footwall. During the reactivation-stage, contacts of the geometric misorientation between the deflected external foliation and the shear foliation concentrate brittle faulting (Figure 5.22). A mature fault core may develop within the reactivated zones, which show consistent lens shaped fault core material. Very little evidence of fluid interaction has been found within the shear zones, indicating that the shear zone foliation acts as a fluid barrier, although reactivated fracture-zones are most likely to have been fluid conduits.

Fault group 3 involves highly folded host rock. In the reactivation-stage the folds concentrate brittle faults. The brittle faults cut through fold hinges and limbs at random orientations (but consistently with the imposed stress field at the time of brittle faulting). Stage 3 (fault quiescence) represents the mature fault core consisting of sheared country rock and gouge. Calcite and pyrite indicate the presence of abundant fluid interaction with fault rock material.

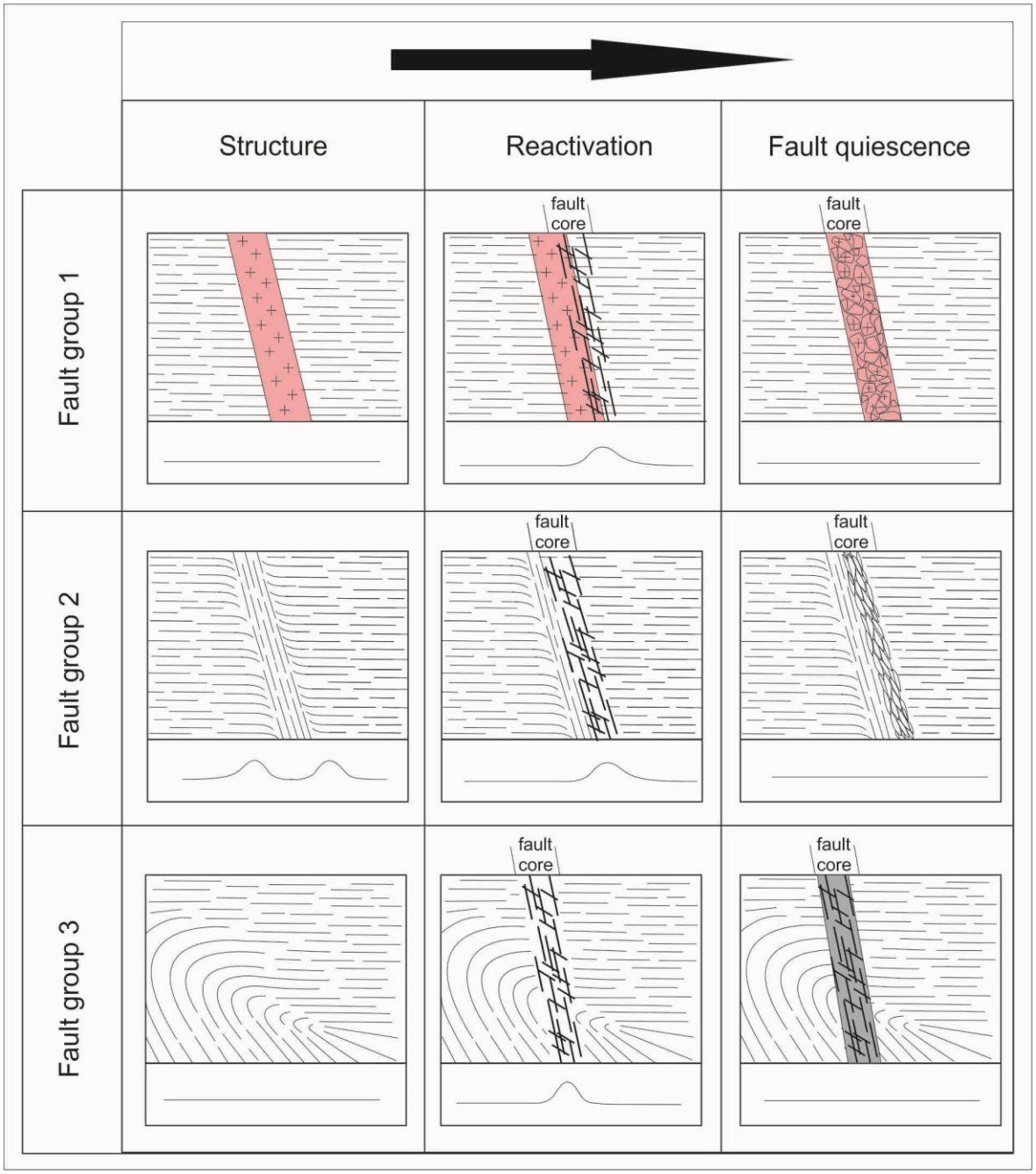

Figure 6.4: Conceptual model of how different types of inherited structures may have promoted localised brittle reactivation on a mesoscopic scale in the ORC. Fault group 1 represents the case of a pegmatite intruding sub-vertically through the amphibolite host rock. Brittle faults develop within and along the contact of the two lithologies and evolve into a cataclasite. Fluid circulation along the highly dilatant fault core is important as documented by neo-crystallisation of calcite and quartz within the cataclasite. Fault group 2 represents the case of an extensional ductile shear zone. In stage two, brittle faulting localizes within and along the shear zone boundary aided by the geometric misorientation between the deflected external shear zone foliation and the shear foliation. This reactivation is common for both the hanging wall as well as the footwall contact. Very little fluid interaction was observed in the fault core itself, probably due to the relatively impermeable anisotropy of the foliated shear zone mylonitic core. The product is a thin brittle fault core consisting of sheared lens shaped fault rock fragments. The pre-existing shear foliation controls the shape and size of these fragments. Fault group 3 represents the case of tightly folded foliation. Stage two involves brittle faults cutting through fold hinges and limbs at random orientations (but consistently with the imposed stress field at the time of brittle faulting). Stage three represents the mature fault core consisting of sheared country rock. Calcite and pyrite indicate the presence of remnant abundant fluid interaction with fault rock material.

6.3. Paleostress inversion of brittle faults

The paleostress field of the late Devonian led to the denudation and exhumation of the Trøndelag gneissic core complex, aided by detachments such as the HDF. The extensional movement of this detachment was NE-SW, which is coaxial to the extensional orientation of the MTFC (Seranne, 1992; Osmundsen et al., 2006). In addition to ductile-brittle NE-SW extension, later ductile NW-SE compression led to the tightening of upright extensional parallel folding within the MTFC. The paleostress field of the post-Caledonian MTFC has therefore been controlled by both extension and compression under both ductile and brittle conditions (Chauvet and Séranne, 1994; Braathen et al., 2000; Osmundsen et al., 2006). Evidence of paleo-stress fields is found within the ORC. Through paleo-stress inversion, three mechanically different fault sets were found indicating both paleo stress fields and possible neo-tectonic stress fields. These include NE-SW extension, a weak NE-SW compression and a NNE-SSE extension.

The misfit angle of the faults was not allowed to exceed 30°. This is because reactivation of pre-existing surfaces of weakness in normal faults is theoretically possible with a maximum of ca. 30° from their ideal position (Ranalli, 2000).

NE-SW extension

The NE-SW extension (almost vertical σ_1) generated by the inversion procedure followed here fits very well with the overall paleo stress-field of the MTFC, oriented NE-SW with a vertical σ_1 (Figure 5.33). Further, the fault planes of this sub-group contain both quartz and epidote mineralization, which are regarded as typical for relatively high temperature conditions. This indicates that those faults developed deep in the crust and were brought up to the surface through denudation and exhumation as presented by Drake et al. (2009) in (Figure 6.5). Thus, the coating of the fault planes also supports the Late-Palaeozoic stress field oriented NE-SW which is consistent with work done by Osmundsen et al. (2006). Fault plane mineralisation of epidote is common all over the MTFC and considered to be of late Devonian age by e.g. (Roberts, 1998; Osmundsen et al., 2006; Olsen et al., 2007). The fault sub-group is coherent with Andersonian fault theory with σ_1 oriented vertically and the other two principal stresses horizontally.

Generation	Main related event and/or age
1. Mylonite; quartz, epidote, muscovite, chlorite, albite ± K-feldspar, calcite	Waning stages of the Svecokarelian orogeny (>1750 Ma)
2a. Cataclasite; epidote, quartz, chlorite ± K-feldspar, albite	Probably 1750–1620 Ma
2b. Cataclasite; K-feldspar, chlorite, quartz, hematite, albite ± illite	
3a. Quartz, epidote, chlorite, calcite, pyrite, fluorite, muscovite ± K-feldspar, hornblende	Intrusion of Götemar and Uthammar granites related to the
3b. Prehnite ± calcite, fluorite	1.47–1.44 Ga Danapolonian orogeny
3c. Calcite, laumontite, adularia, chlorite, quartz, illite, hematite	
4. Calcite, adularia, laumontite, chlorite, quartz, illite, hematite ± albite, apatite	Sveconorwegian orogeny (1.1–0.9 Ga)
Cambrian sandstone (near surface)	Early Cambrian extension
5. Calcite, adularia, chlorite, hematite, fluorite, quartz, pyrite, barite, gypsum, clay minerals, apophyllite, harmotome, REE-carbonate (probably bastnäsite), ± galena, chalcopyrite, laumontite, sphalerite, analcime	Caledonian orogeny at 440–400 Ma.
6. Calcite, pyrite, clay minerals, goethite (near surface)	Possibly Quaternary

Figure 6.5: Table representing high temperature fracture mineralisations at depth. 1 = oldest, 9 = youngest. Table after Drake et al. 2009.

NNW-SSE extension

The paleostress inversion also generated a sub-group of extensional NNW-SSE oblique slip faults (Figure 5.33). These fault planes are coated with both epidote and chlorite. With reference to the discussion above, the epidote coating most likely represents faults developed early in the exhumation phase while the chlorite is probably the product of reactivation of the same faults. The NNW-SSE extension has only been reported by (Bunkholt, 2006). He interpreted this episode as a part of an extensional phase active at the same time as the NE-SW extension of the HDF. If the HDF is considered as a disc, its detachment towards the south would allow for NW-SE extension due to increasing space to the NW and SE. This is model, with its NW-SE extension, would also fit the sub-group of the ORC, because a large proportion of the structures within can be related to the MTFC.

NE-SW compression

A sub-group of faults shows NE-SW compression accommodated by sets of conjugate faults with σ_1 oriented sub-horizontally. In addition, chlorite fault plane mineralisation is displayed consistently on all fault planes, which occurs only in the uppermost sections of the crust (Figure 6.5). This result probably reflects a recent to neo-tectonic stress field acting later than both NE-SW and NNW-SSE extensional phases discussed in this chapter. This is supported by the work done by Roberts and Myrvang (2004) who considered the present day stress field to be NE-SW compression (horizontal σ_1) by studying borehole breakouts (Figure 6.6).

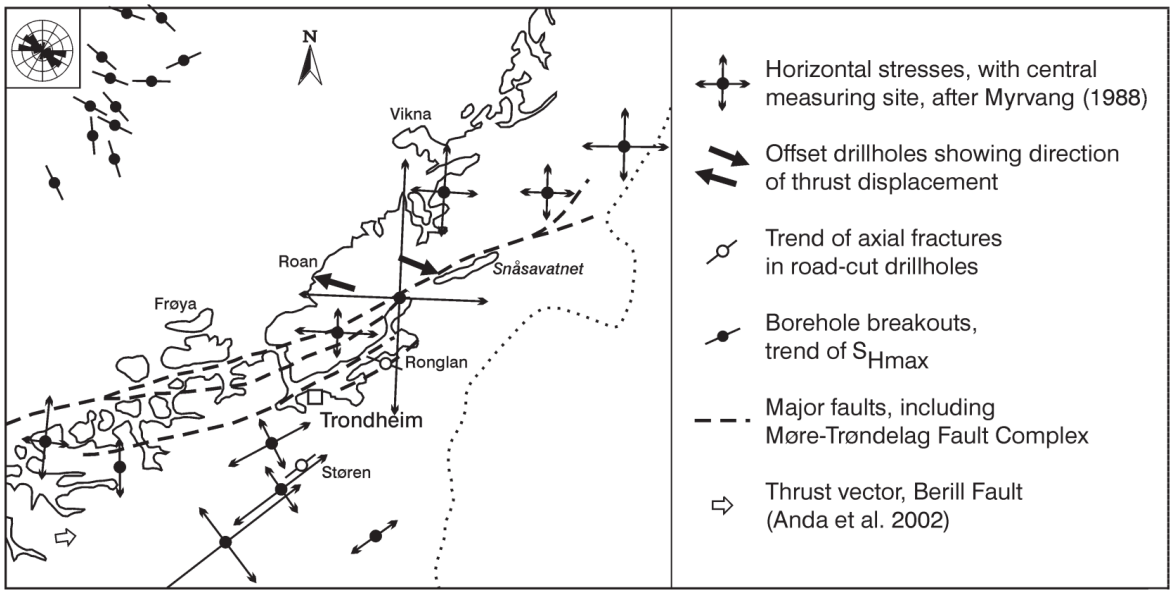

Figure 6.6: Map of Central-Norway showing rock-stress orientations. The neo-tectonic stressfield (NE-SW compression) active today in the ORC is seen SW of Trondheim. After Roberts and Myrvang (2004).

The paleostress inversion method used dictates that there should be no block faulting which is highly likely to have happened within the ORC. Anomalous orientations of brittle fault families are probably the product of extensive block rotation during faulting, which may have happened to segments including ductile thrust 23, which is cut by brittle fault 22B to the left and 24A to the right (cross section: 207-220 m).

Through the systematic analysis and discussion of the data presented in the results, we can draw several conclusions (presented below) about the structural evolution and brittle reactivation within the ORC.

7. Conclusions

- The Orkanger Road Cut preserves a rich and important record of structures that reflect the complex tectonic history of the Trøndelag region of the MWGR.

- The structural and chronological evolution of the Orkanger Road Cut can be described in the following order: formation of the country rock foliation, high strain zones, generation 1 pegmatite intrusion, F1 folding, generation 2 pegmatites, F2 folding, generation 3 pegmatites, ductile shear zones, brittle-ductile faults, brittle faulting and heavy fluid interaction.

- Thrust structures within the Orkanger Road Cut may represent remnants of the roof-contact of an extrusion wedge of the Seve Nappe in the Jämtland-Västerbotten segment in Sweden, supported by correlated pegmatite intrusions and kinematics at both localities.

- The folds of the ORC represent two folding phases: F1 and F2, where F2 represents the extension-parallel folding associated with the NE-SW extension of the MTFC.

- Based on fault core and damage zone thickness, the brittle-ductile faults show more extensive brittle reactivation than the ductile shear zones.

- Brittle faults reactivate and develop preferentially in the following pre-existing structures: ductile shear zones, strongly folded country rock segments and parallel to pegmatites.

- Paleostress inversion shows that brittle faults can be ascribed to three different brittle events. One showing NE-SW extension with high temperature mineral coating, representative of late Devonian extension along with the HDF. A second brittle faulting phase showing NW-SE extension that may describe the space left empty from the detached part of the HDF. A third fault group display NE-SW compression with a conjugate set of faults with chlorite coating, representative of a neo-tectonic stress field.

8. References

Andersen, T. B. 1998. Extensional tectonics in the Caledonides of southern Norway, an overview. *Tectonophysics,* 285**,** 333-351.

Andersen, T. B. & Jamtveit, B. 1990. Uplift of deep crust during orogenic extensional collapse: A model based on field studies in the Sogn-Sunnfjord Region of western Norway. *Tectonics,* 9**,** 1097-1111.

Andersen, T. B., Jamtveit, B., Dewey, J. F. & Swensson, E. 1991. Subduction and eduction of continental crust: major mechanisms during continent-continent collision and orogenic extensional collapse, a model based on the south Norwegian Caledonides. *Terra Nova,* 3**,** 303-310.

Andréasson, P.-G. & Gee, D. G. 1989. Bedrock geology and morphology of the Tarfala area, Kebnekaise Mts., Swedish Caledonides. *Geografiska Annaler. Series A. Physical Geography***,** 235-239.

Angelier, J. 1979. Determination of the mean principal directions of stresses for a given fault population. *Tectonophysics,* 56**,** T17-T26.

Bird, J. M. & Dewey, J. F. 1970. Lithosphere plate-continental margin tectonics and the evolution of the Appalachian orogen. *Geological Society of America Bulletin,* 81**,** 1031-1060.

Bott, M. H. P. 1959. The mechanics of oblique slip faulting. *Geological Magazine,* 96**,** 109-117.

Braathen, A., Nordgulen, Ø., Osmundsen, P.-T., Andersen, T. B., Solli, A. & Roberts, D. 2000. Devonian, orogen-parallel, opposed extension in the Central Norwegian Caledonides. *Geology,* 28**,** 615-618.

Braathen, A., Osmundsen, P. T., Nordgulen, O., Roberts, D. & Meyer, G. B. 2002. Orogen-parallel extension of the Caledonides in northern Central Norway: an overview. *Norsk Geologisk Tidsskrift,* 82**,** 225-242.

Bunkholt, H. S. 2006. *Fault-slip inversion inversion and palaeostress analysis above and below a post-Caledonian Extensional Detachment.* NTNU.

Bøe, R. & Bjerkli, K. 1989. Mesozoic sedimentary rocks in Edøyfjorden and Beitstadfjorden, central Norway: implications for the structural history of the Møre-Trøndelag Fault Zone. *Marine Geology,* 87**,** 287-299.

Caine, J. S., Evans, J. P. & Forster, C. B. 1996. Fault zone architecture and permeability structure. *Geology,* 24**,** 1025-1028.

Chauvet, A. & Dallmeyer, R. 1992. 40 Ar/39 Ar mineral dates related to Devonian extension in the southwestern Scandinavian Caledonides. *Tectonophysics,* 210**,** 155-177.

Chauvet, A. & Séranne, M. 1994. Extension-parallel folding in the Scandinavian Caledonides: implications for late-orogenic processes. *Tectonophysics,* 238**,** 31-54.

Chester, F. & Logan, J. 1986. Implications for mechanical properties of brittle faults from observations of the Punchbowl fault zone, California. *Pure and Applied Geophysics,* 124**,** 79-106.

Collettini, C., Chiaraluce, L., Pucci, S., Barchi, M. R. & Cocco, M. 2005. Looking at fault reactivation matching structural geology and seismological data. *Journal of Structural Geology,* 27**,** 937-942.
Corfu, F., Gasser, D. & Chew, D. M. New Perspectives on the Caledonides of Scandinavia and Related Areas. 2014. Geological Society of London.
Crider, J. G. & Peacock, D. C. 2004. Initiation of brittle faults in the upper crust: a review of field observations. *Journal of Structural Geology,* 26**,** 691-707.
Dawers, N. H. & Anders, M. H. 1995. Displacement-length scaling and fault linkage. *Journal of Structural Geology,* 17**,** 607-614.
De Bresser, J., Ter Heege, J. & Spiers, C. 2001. Grain size reduction by dynamic recrystallization: can it result in major rheological weakening? *International Journal of Earth Sciences,* 90**,** 28-45.
Delvaux, D. & Sperner, B. 2003. Stress tensor inversion from fault kinematic indicators and focal mechanism data: the TENSOR program. *New insights into structural interpretation and modelling,* 212**,** 75-100.
Dewey, J., Ryan, P. & Andersen, T. 1993. Orogenic uplift and collapse, crustal thickness, fabrics and metamorphic phase changes: the role of eclogites. *Geological Society, London, Special Publications,* 76**,** 325-343.
Dewey, J. F. 1969. Evolution of the Appalachian/Caledonian orogen.
Dewey, J. F. 1988. Extensional collapse of orogens. *Tectonics,* 7**,** 1123-1139.
Drake, H., Tullborg, E.-L. & Page, L. 2009. Distinguished multiple events of fracture mineralisation related to far-field orogenic effects in Paleoproterozoic crystalline rocks, Simpevarp area, SE Sweden. *Lithos,* 110**,** 37-49.
Eide, E. A., Torsvik, T. H. & Andersen, T. B. 1997. Absolute dating of brittle fault movements: Late Permian and late Jurassic extensional fault breccias in western Norway. *Terra Nova,* 9**,** 135-139.
Escher, A. & Watterson, J. 1974. Stretching fabrics, folds and crustal shortening. *Tectonophysics,* 22**,** 223-231.
Etheridge, M. 1986. On the reactivation of extensional fault systems. *Philosophical Transactions of the Royal Society of London A: Mathematical, Physical and Engineering Sciences,* 317**,** 179-194.
Fleuty, M. 1964. The description of folds. *Proceedings of the Geologists' Association,* 75**,** 461-492.
Fossen, H. 1992. The role of extensional tectonics in the Caledonides of south Norway. *Journal of structural geology,* 14**,** 1033-1046.
Fossen, H. 2010. *Structural Geology,* USA, Cambridge Univeristy Press.
Fossen, H. & Dunlap, W. J. 1998. Timing and kinematics of Caledonian thrusting and extensional collapse, southern Norway: evidence from 40 Ar/39 Ar thermochronology. *Journal of structural geology,* 20**,** 765-781.
Fossen, H. & Hurich, C. A. 2005. The Hardangerfjord Shear Zone in SW Norway and the North Sea: a large-scale low-angle shear zone in the Caledonian crust. *Journal of the Geological Society,* 162**,** 675-687.
Gabrielsen, R., Odinsen, T. & Grunnaleite, I. 1999. Structuring of the Northern Viking Graben and the Møre Basin; the influence of basement structural

grain, and the particular role of the Møre-Trøndelag Fault Complex. *Marine and Petroleum Geology,* 16**,** 443-465.
Gale, G. H. & Roberts, D. 1974. Trace element geochemistry of Norwegian Lower Palaeozoic basic volcanics and its tectonic implications. *Earth and Planetary Science Letters,* 22**,** 380-390.
Gapais, D. 1989. Shear structures within deformed granites: mechanical and thermal indicators. *Geology,* 17**,** 1144-1147.
Gayer, R. & Roberts, J. 1973. Stratigraphic review of the Finnmark Caledonides, with possible tectonic implications. *Proceedings of the Geologists' Association,* 84**,** 405-IN3.
Gee, D. 1975. A tectonic model for the central part of the Scandinavian Caledonides. *American Journal of Science,* 275**,** 468-515.
Gee, D. G. 1978. Nappe displacement in the Scandinavian Caledonides. *Tectonophysics,* 47**,** 393-419.
Gee, D. G., Janák, M., Majka, J., Robinson, P. & Van Roermund, H. 2013. Subduction along and within the Baltoscandian margin during closing of the Iapetus Ocean and Baltica-Laurentia collision. *Lithosphere,* 5**,** 169-178.
Gerald, J. F. & Stünitz, H. 1993. Deformation of granitoids at low metamorphic grade. I: Reactions and grain size reduction. *Tectonophysics,* 221**,** 269-297.
Grenne, T., Ihlen, P. & Vokes, F. 1999. Scandinavian Caledonide metallogeny in a plate tectonic perspective. *Mineralium Deposita,* 34**,** 422-471.
Grimmer, J. C., Glodny, J., Drüppel, K., Greiling, R. O. & Kontny, A. 2015. Early-to mid-Silurian extrusion wedge tectonics in the central Scandinavian Caledonides. *Geology***,** G36433. 1.
Grønlie, A. & Roberts, D. 1989. Resurgent strike-slip duplex development along the Hitra-Snåsa and Verran Faults, Møre-Trøndelag fault zone, Central Norway. *Journal of structural geology,* 11**,** 295-305.
Hacker, B. R., Andersen, T. B., Johnston, S., Kylander-Clark, A. R., Peterman, E. M., Walsh, E. O. & Young, D. 2010. High-temperature deformation during continental-margin subduction & exhumation: The ultrahigh-pressure Western Gneiss Region of Norway. *Tectonophysics,* 480**,** 149-171.
Hacker, B. R. & Gans, P. B. 2005. Continental collisions and the creation of ultrahigh-pressure terranes: Petrology and thermochronology of nappes in the central Scandinavian Caledonides. *Geological Society of America Bulletin,* 117**,** 117-134.
Haggert, K., Cox, S. J. & Jessell, M. W. 1992. Observation of fault gouge development in laboratory see-through experiments. *Tectonophysics,* 204**,** 123-136.
Hanmer, S. 1986. Asymmetrical pull-aparts and foliation fish as kinematic indicators. *Journal of Structural Geology,* 8**,** 111-122.
Hippolyte, J.-C., Bergerat, F., Gordon, M. B., Bellier, O. & Espurt, N. 2012. Keys and pitfalls in mesoscale fault analysis and paleostress reconstructions, the use of Angelier's methods. *Tectonophysics,* 581**,** 144-162.
Hirth, G. & Tullis, J. 1992. Dislocation creep regimes in quartz aggregates. *Journal of Structural Geology,* 14**,** 145-159.

Hirth, G. & Tullis, J. 1994. The brittle-plastic transition in experimentally deformed quartz aggregates. *Journal of Geophysical Research: Solid Earth (1978–2012),* 99**,** 11731-11747.
Hudleston, P. 1973. Fold morphology and some geometrical implications of theories of fold development. *Tectonophysics,* 16**,** 1-46.
Hurich, C., Palm, H., Dyrelius, D. & Kristoffersen, Y. 1989. Deformation of the Baltic continental crust during Caledonide intracontinental subduction: Views from seismic reflection data. *Geology,* 17**,** 423-425.
Jaeger, J. C., Cook, N. G. & Zimmerman, R. 2009. *Fundamentals of rock mechanics*, John Wiley & Sons.
Kendrick, M., Eide, E., Roberts, D. & Osmundsen, P. 2004. The Middle to Late Devonian Høybakken detachment, central Norway: 40Ar–39Ar evidence for prolonged late/post-Scandian extension and uplift. *Geological Magazine,* 141**,** 329-344.
Kim, Y.-S., Peacock, D. C. & Sanderson, D. J. 2004. Fault damage zones. *Journal of structural geology,* 26**,** 503-517.
Kjøll, H. J., Viola, G., Menegon, L. & Sørensen, B. 2015. Brittle–viscous deformation of vein quartz under fluid-rich low greenschist facies conditions. *Solid Earth Discussions,* 7**,** 213-257.
Krabbendam, M. & Dewey, J. F. 1998. Exhumation of UHP rocks by transtension in the Western Gneiss Region, Scandinavian Caledonides. *Geological Society, London, Special Publications,* 135**,** 159-181.
Lacombe, O. 2012. Do fault slip data inversions actually yield “paleostresses” that can be compared with contemporary stresses? A critical discussion. *Comptes Rendus Geoscience,* 344**,** 159-173.
Lisle, R. J., Orife, T. O., Arlegui, L., Liesa, C. & Srivastava, D. C. 2006. Favoured states of palaeostress in the Earth's crust: evidence from fault-slip data. *Journal of Structural Geology,* 28**,** 1051-1066.
Marshall, D. & Mclaren, A. 1977. Deformation mechanisms in experimentally deformed plagioclase feldspars. *Physics and chemistry of minerals,* 1**,** 351-370.
Mckerrow, W., Mac Niocaill, C. & Dewey, J. 2000. The Caledonian orogeny redefined. *Journal of the Geological society,* 157**,** 1149-1154.
Milnes, A., Wennberg, O., Skår, Ø. & Koestler, A. 1997. Contraction, extension and timing in the South Norwegian Caledonides: the Sognefjord transect. *Geological Society, London, Special Publications,* 121**,** 123-148.
Mitra, G. 1984. Brittle to ductile transition due to large strains along the White Rock thrust, Wind River Mountains, Wyoming. *Journal of Structural Geology,* 6**,** 51-61.
Mosar, J. 2003. Scandinavia's North Atlantic passive margin. *Journal of Geophysical Research: Solid Earth (1978–2012),* 108.
Nasuti, A., Pascal, C. & Ebbing, J. 2012. Onshore–offshore potential field analysis of the Møre–Trøndelag Fault Complex and adjacent structures of Mid Norway. *Tectonophysics,* 518**,** 17-28.

Nasuti, A., Pascal, C., Ebbing, J. & Tønnesen, J. 2011. Geophysical characterisation of two segments of the Møre-Trøndelag Fault Complex, Mid Norway. *Solid Earth,* 2**,** 125-134.
Nemcok, M. 1995. A stress inversion procedure for polyphase fault/slip data sets. *Journal of Structural Geology,* 17**,** 1445-1453.
Nordgulen, O., Braathen, A., Corfu, F., Osmundsen, P. T. & Husmo, T. 2002. Polyphase kinematics and geochronology of the late-Caledonian Kollstraumen detachment, north-central Norway. *NORSK GEOLOGISK TIDSSKRIFT,* 82**,** 299-316.
Norton, M. 1986. Late Caledonide extension in western Norway: A response to extreme crustal thickening. *Tectonics,* 5**,** 195-204.
Norton, M. 1987. The Nordfjord-Sogn Detachment, W. Norway. *Norsk Geologisk Tidsskrift,* 67**,** 93-106.
Olsen, E., Gabrielsen, R. H., Braathen, A. & Redfield, T. 2007. Fault systems marginal to the More-Trondelog Fault Complex, Osen-Vikna area, Central Norway. *NORSK GEOLOGISK TIDSSKRIFT,* 87**,** 59.
Osmundsen, P. & Andersen, T. 2001. The middle Devonian basins of western Norway: sedimentary response to large-scale transtensional tectonics? *Tectonophysics,* 332**,** 51-68.
Osmundsen, P., Braathen, A., Nordgulen, Ø., Roberts, D., Meyer, G. & Eide, E. 2003. The Devonian Nesna shear zone and adjacent gneiss-cored culminations, North–Central Norwegian Caledonides. *Journal of the Geological Society,* 160**,** 137-150.
Osmundsen, P., Eide, E., Haabesland, N., Roberts, D., Andersen, T., Kendrick, M., Bingen, B., Braathen, A. & Redfield, T. 2005a. Exhumation and 'Old Red'basin formation in Central Norway: kinematics of the Høybakken detachment zone and the Møre–Trøndelag Fault Complex. *Journal of the Geological Society, London,* 162**,** 111-222.
Osmundsen, P., Eide, E., Haabesland, N., Roberts, D., Andersen, T., Kendrick, M., Bingen, B., Braathen, A. & Redfield, T. 2006. Kinematics of the Høybakken detachment zone and the Møre–Trøndelag Fault Complex, central Norway. *Journal of the Geological Society,* 163**,** 303-318.
Osmundsen, P. T., Braathen, A., Sommaruga, A., Skilbrei, J. R., Nordgulen, Ø., Roberts, D., Andersen, T. B., Olesen, O. & Mosar, J. 2005b. Metamorphic core complexes and gneiss-cored culminations along the Mid-Norwegian margin: an overview and some current ideas. *Norwegian Petroleum Society Special Publications,* 12**,** 29-41.
Passchier, C. & Simpson, C. 1986. Porphyroclast systems as kinematic indicators. *Journal of Structural Geology,* 8**,** 831-843.
Peacock, D. & Sanderson, D. 1991. Displacements, segment linkage and relay ramps in normal fault zones. *Journal of Structural Geology,* 13**,** 721-733.
Platt, J. 1986. Dynamics of orogenic wedges and the uplift of high-pressure metamorphic rocks. *Geological Society of America Bulletin,* 97**,** 1037-1053.

Platt, J., Whitehouse, M., Kelley, S., Carter, A. & Hollick, L. 2003. Simultaneous extensional exhumation across the Alboran Basin: implications for the causes of late orogenic extension. *Geology,* 31**,** 251-254.
Poirier, J. 1980. Shear localization and shear instability in materials in the ductile field. *Journal of Structural Geology,* 2**,** 135-142.
Pollard, D., Saltzer, S. & Rubin, A. M. 1993. Stress inversion methods: are they based on faulty assumptions? *Journal of Structural Geology,* 15**,** 1045-1054.
Ramberg, H. 1980. Diapirism and gravity collapse in the Scandinavian Caledonides. *Journal of the Geological Society,* 137**,** 261-270.
Ramberg I., B. I. N. A. 2006. *Landet Blir Til*, Norsk Geologisk Forening (NGF).
Ramsay, J. 1980. Shear zone geometry: a review. *Journal of structural geology,* 2**,** 83-99.
Ramsay, J. G. 1974. Development of chevron folds. *Geological Society of America Bulletin,* 85**,** 1741-1754.
Ranalli, G. 2000. Rheology of the crust and its role in tectonic reactivation. *Journal of Geodynamics,* 30**,** 3-15.
Reches, Z. E. 1978. Analysis of faulting in three-dimensional strain field. *Tectonophysics,* 47**,** 109-129.
Redfield, T., Braathen, A., Gabrielsen, R., Osmundsen, P., Torsvik, T. & Andriessen, P. 2005a. Late Mesozoic to Early Cenozoic components of vertical separation across the Møre–Trøndelag fault complex, Norway. *Tectonophysics,* 395**,** 233-249.
Redfield, T., Osmundsen, P. & Hendriks, B. 2005b. The role of fault reactivation and growth in the uplift of western Fennoscandia. *Journal of the Geological Society,* 162**,** 1013-1030.
Roberts, D. 1998. High-strain zones from mesoto macro-scale at different structural levels, Central Norwegian Caledonides. *Journal of Structural Geology,* 20**,** 111-119.
Roberts, D. 2003. The Scandinavian Caledonides: event chronology, palaeogeographic settings and likely modern analogues. *Tectonophysics,* 365**,** 283-299.
Roberts, D. & Gee, D. 1985. An introduction to the structure of the Scandinavian Caledonides. *The Caledonide orogen–Scandinavia and related areas,* 1**,** 55-68.
Roberts, D. & Myrvang, A. 2004. Contemporary stress orientation features in bedrocks, Trøndelag, central Norway, and some regional implications. *NGU Bulletin,* 442**,** 53-63.
Roberts, D. & Sturt, B. 1980. Caledonian deformation in Norway. *Journal of the Geological Society,* 137**,** 241-250.
Roberts, D. & Wolff, F. 1981. Tectonostratigraphic development of the Trondheim region Caledonides, central Norway. *Journal of Structural Geology,* 3**,** 487-494.
Robinson, P. a. R., David 2008. A Tectonostratigraphic transect across the central Scandinavian Caledonides, Storlien - Trondheim - Lepsøy.

Scholz, C. H. 1987. Wear and gouge formation in brittle faulting. *Geology,* 15**,** 493-495.
Segall, P. & Pollard, D. 1980. Mechanics of discontinuous faults. *Journal of Geophysical Research: Solid Earth (1978–2012),* 85**,** 4337-4350.
Selverstone, J., Morteani, G. & Staude, J. M. 1991. Fluid channelling during ductile shearing: transformation of granodiorite into aluminous schist in the Tauern Window, Eastern Alps. *Journal of Metamorphic Geology,* 9**,** 419-431.
Seranne, M. 1992. Late Paleozoic kinematics of the Møre-Trøndelag Fault Zone and adjacent areas, central Norway. *Norsk Geologisk Tidsskrift,* 72**,** 141-158.
Sibson, R. 1977. Fault rocks and fault mechanisms. *Journal of the Geological Society,* 133**,** 191-213.
Sibson, R. H., Robert, F. & Poulsen, K. H. 1988. High-angle reverse faults, fluid-pressure cycling, and mesothermal gold-quartz deposits. *Geology,* 16**,** 551-555.
Simpson, C. 1985. Deformation of granitic rocks across the brittle-ductile transition. *Journal of Structural Geology,* 7**,** 503-511.
Simpson, C. & De Paor, D. G. 1993. Strain and kinematic analysis in general shear zones. *Journal of Structural Geology,* 15**,** 1-20.
Stephens, M. & Gee, D. 1985. A tectonic model for the evolution of the eugeoclinal terranes in the central Scandinavian Caledonides. *The Caledonide Orogen—Scandinavia and Related Areas***,** 953-978.
Strand, T. 1961. The Scandinavian Caledonides; a review. *American Journal of Science,* 259**,** 161-172.
Sykes, L. R. 1978. Intraplate seismicity, reactivation of preexisting zones of weakness, alkaline magmatism, and other tectonism postdating continental fragmentation. *Reviews of Geophysics,* 16**,** 621-688.
Torsvik, T., Smethurst, M., Meert, J. G., Van Der Voo, R., Mckerrow, W., Brasier, M., Sturt, B. & Walderhaug, H. 1996. Continental break-up and collision in the Neoproterozoic and Palaeozoic—a tale of Baltica and Laurentia. *Earth-Science Reviews,* 40**,** 229-258.
Torsvik, T. H. 1998. Palaeozoic palaeogeography: a North Atlantic viewpoint. *GFF,* 120**,** 109-118.
Tucker, R. D., Robinson, P., Solli, A., Gee, D. G., Thorsnes, T., Krogh, T. E., Nordgulen, Ø. & Bickford, M. 2004. Thrusting and extension in the Scandian hinterland, Norway: New U-Pb ages and tectonostratigraphic evidence. *American Journal of Science,* 304**,** 477-532.
Tullis, J. & Yund, R. A. 1977. Experimental deformation of dry Westerly granite. *Journal of Geophysical Research,* 82**,** 5705-5718.
Tullis, J. & Yund, R. A. 1985. Dynamic recrystallization of feldspar: a mechanism for ductile shear zone formation. *Geology,* 13**,** 238-241.
Viola, G. & Ganerød, G. V. 2007. Structural characterization of deformation zones (faults and ductile shear zones) from selected drill cores and outcrops from the Laxemar area—Results from Phase 2. SKB P-07.

White, S., Bretan, P. & Rutter, E. 1986. Fault-zone reactivation: kinematics and mechanisms. *Philosophical Transactions of the Royal Society of London. Series A, Mathematical and Physical Sciences,* 317**,** 81-97.
Wibberley, C. A., Yielding, G. & Di Toro, G. 2008. Recent advances in the understanding of fault zone internal structure: a review. *Geological Society, London, Special Publications,* 299**,** 5-33.
Wiens, D. A. & Snider, N. O. 2001. Repeating deep earthquakes: evidence for fault reactivation at great depth. *Science,* 293**,** 1463-1466.
Williams, H. 1979. Appalachian orogen in Canada. *Canadian Journal of Earth Sciences,* 16**,** 792-807.

9. Appendix

1. **Microscopical descriptions**
2. **Fold map**
3. **Photo-stitch of the Orkanger Road cut**
4. **Orkanger Road Cut sketch (cross section)**

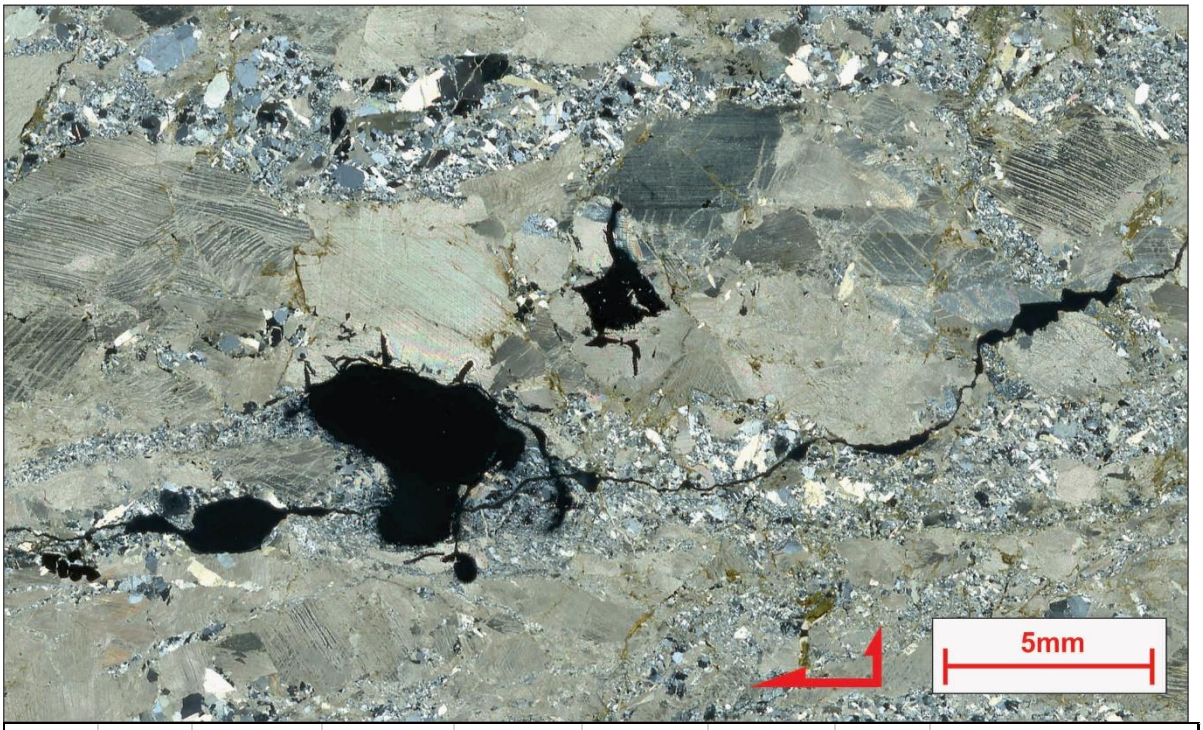

Sample:	18_3							
Macroscopic description:								
Colour:	Grey							
Minerals:	Quartz, feldspar, sulphides							
Grain size:	0,5-6mm							
Structure:	Cataclasite							
Microscopic description:								
Mineral content:		Ca: 75%	Plg: 10%	Qtz: 10%	Sphd: 3%	Ti: 1%	Chlt: 1%	
Texture:	Brittle fracture zones consisting of quartz, plagioclase and calcite going through porfyrblastic calcite. Odler plagioclse and calcite are fractured by extensional veins consisting of calcite and quartz. Thin section is divided into alternating sections of homogeneous domains (calcite) and heterogeneous domains (calcite, plagioclase and quartz). A late vein set filled with calcite cuts the alternation sections at an angle of 60 degrees.This vein set is consistent throughout the sample.							
Mineral description:								
Plagioclase:	Anhedral grains with 1. order grey interference colours and heavy sausseritization. Average grain size 0,3mm							
Quartz	Occurs as veinmaterial and matrix. SGR							
Calcite:	Kinked approx. 0,70mm porph kinked							
Sulphides:	Opaque, 0,32-1,3 mm sub-angular grains in calcite fracture veins which are later cut again by calcite filled veins. Also present as inclusions							
Chlorite:	Occuring in center of cataclastic zone with light green pleochroism. Dark blue intereference colors.							
Sphene	As inclusions in calcite crystals and along their grain boundaries							
Comment:	Riedel shears indicating sinstral sense of shear is found cutting through calcite and feldspar (may be later event?)							
Shear sense:	Sinistral							
Facies:	Greenschist							

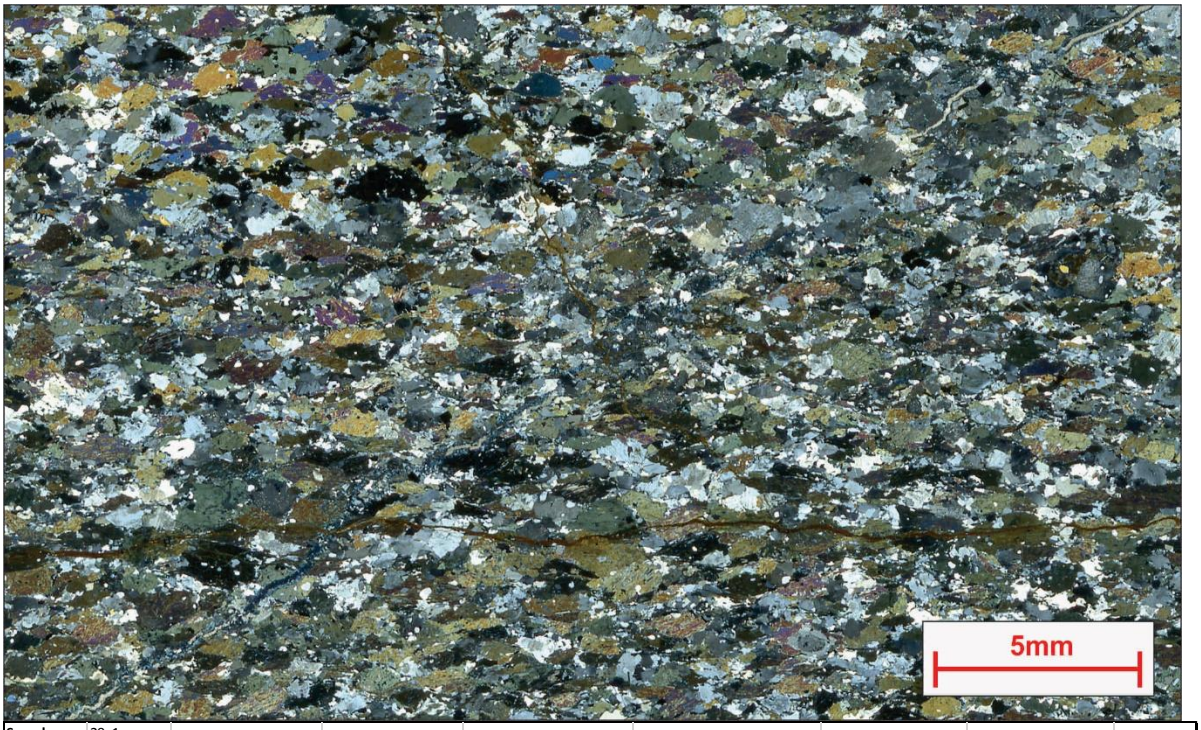

Sample:	20_1							
Macroscopic description:								
Colour:	Dark with bright spots							
Minerals:	Amphibole, feldspar, sulphides							
Grain size:	0,5-2mm							
Structure:	Amphibolite schist							
Microscopic description:								
Mineral content:		Hbl: 50%	Plg: 30%	Qtz: 10%	Cal: 5%	Chlt: 5%		
Texture:	Both calcite and chlorite is found in a vein in the lower right corner of the thin section. Chlorite is deposited in contact with the vein walls. Calcite makes up the center of the vein. Poikiloblastic hornblende with inlcusions of epidote (common alteration product of hornblende).							
Mineral description:								
Quartz	50/50 intragrain and intergrain, occur as inclusions in hornblende							
Hornblende	Green pleochroism with high 1. order blue and red. Chlorite inclusions are also found.							
Sulphide	Opaque anhedral to cubic 0,3mm-1mm, 50/50 intragrain and intergrain							
Plagioclase	Anhedral-subhedral deformation twinning and sausseritisation of old grains (altered into calcite). Sausseritization in lamellaes. Undulatory extinction.							
Calcite	Extreme birefringence occuring as vein material.							
Chlorite	Lower second order blue. Occurs as vein precipitae and alteration products along hornblende cleavage							
Epidote	Anhedral lower 3. order yellow and blue interference colours							
Zircon	Occurs as reaction halos in chlorite							
Comment:								
Shear sense:	none							
Facies:	Amphibolite							

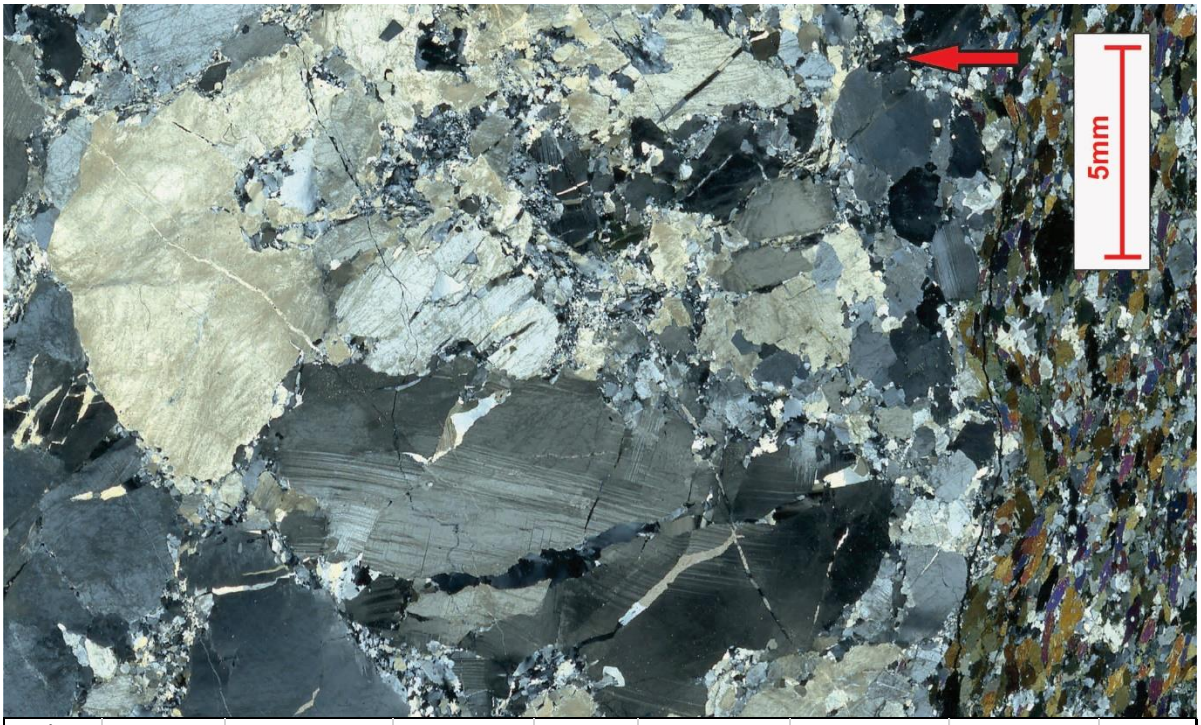

Sample:	30_1							
Macroscopic description:								
Colour:	Green and white							
Minerals:	Feldspar, quartz, amphibole, sulphides							
Grain size:	0,5-12mm							
Structure:	Pegmatite							
Microscopic description:								
Mineral content:		Plg: 75%	Hbl: 14%	Qtz: 8%	Sphd: 2%	Cal: 1%		
Texture:	Thin section is divided into two sections with the upper section consisting mostly of hornblende and lesser amounts of quartz and plagioclase. This section is juxtaposed by a massive section of plagioclase phenocrysts and quartz (pegmatite) making up 80% of the thin section.							
Mineral description:								
Quartz	Extensive GBM and SGR, undulatory extinction, 1. order grey and white							
Plagioclase	Anhedral grains with 1. order grey intereference colours showing deformation twins, polysynthetic twins, heavy sausseritization, undulatory extinction and deformation kinking. Grainsize ranging from 0,5-7mm							
Hornblende	Elongated 2. order interference colours with average grain size of 0,7mm							
Sulphides	Intergranular, anhedral opaque grains occuring only in amphibolite section of the thin section							
Calcite	Extremely fine grained with extreme birefringence.							
Chlorite	1. order brown interference colours, occuring in contact with hornblende							
Epidote	Anhedral, 3. order interference colour 1,6 mm							
Comment:								
Shear sense:	none							
Facies:	Amphibolite							

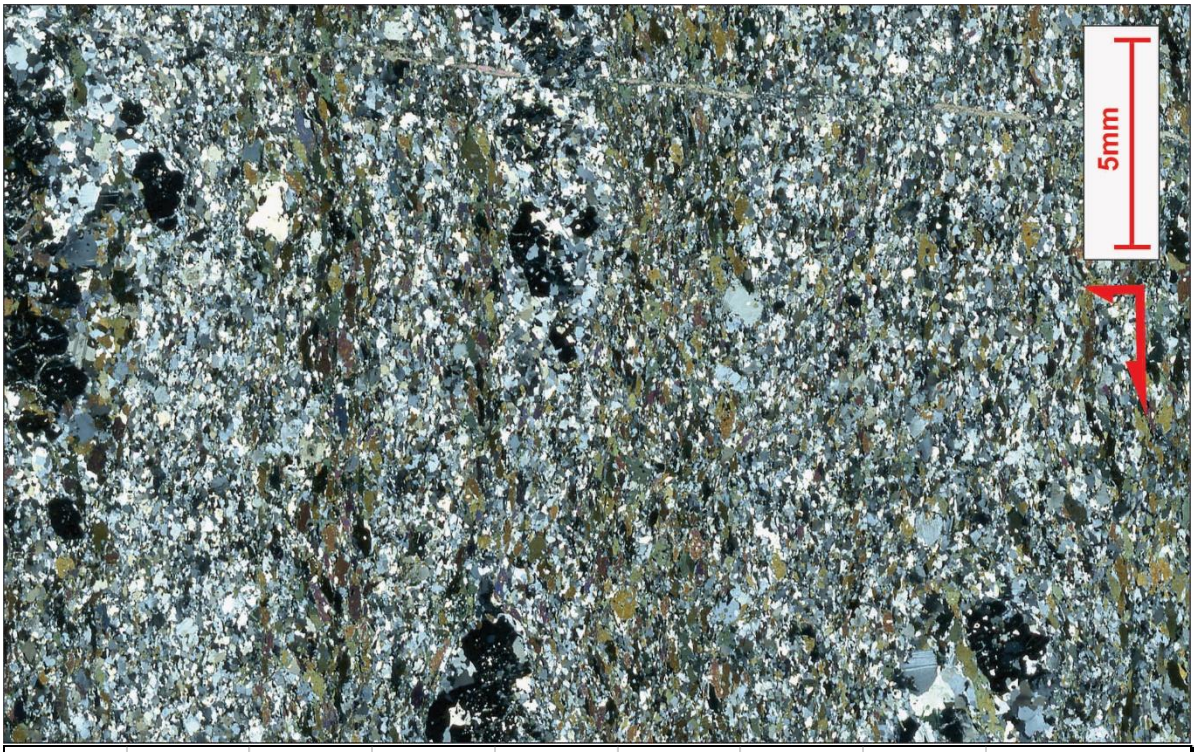

Sample:	101_1							
Macroscopic description:								
Colour:	Dark grey							
Minerals:	Amphibole, garnet, sulpdide, feldspar, quartz							
Grain size:	0,5-1,3mm							
Structure:	Amphibolite garnet schist							
Microscopic description:								
Mineral content:		Plg: 40%	Hbl: 37%	Qtz: 10%	Gt: 8%	Cal: 2%	Chlt: 2%	Sphd: 1%
Texture:	Porphyblasts of garnet occuring in chains in recrystallized quartz bands. These quartz bands are juxtaposed to poikiloblastic hornblende dominated bands. This sequence of minerals is seen throughout the thin section							
Mineral description:								
Quartz	Extensive polygonal grain boundaries with little of no undulatory extinction, heavily recrystallized.							
Hornblende	Elongated, subhedral crystals with many feldspar inclusions							
Calcite	Fine grained, occuring in veins cutting foliation sup-perpendicularly							
Plagioclase	Anhedral grains (size: 0,22-0,7mm, avg.: 0,22mm), partly altered w. perthite lamellaes. Also polysynthetic twins							
Sulphide	Opaque intergranular anhedral grains ranging from 0,022-0,22mm							
Garnet	Anhedral altered porphyroblasts with poikiloblastic growth of feldspar and chlorite in fractures.							
Chlorite	Grows along fractures inside garnets and in vein systems							
Comment:	Shearbands consisting of fragmented hornblene indicate dextral sense of shear, opposite of what was observed in the field. The occurence of chlorite in veins and around garnets indicate a reaction with an aqueous fluid. A later event is evident as sub-vertical veins consisting of calcite cuts through foliation. This is also reflected in hornblende crystals and garnets which are cut by fractures parallel to the larger veins filled with calcite.							
Shear sense:	Dextral?							
Facies:	High amphibolite							

Sample:	102_1	140901						
Macroscopic description:								
Colour:	Dark grey							
Minerals:	Amphibole, quartz, garnet, feldspar, sulphide							
Grain size:	0,5-2mm							
Structure:	Amphibolite garnet schist							
Microscopic description:								
Mineral content:		Hbl: 50%	Plg: 30%	Qtz: 13%	Slphd: 3%	Gt: 2%	Ep: 1%	Ti: 1%
Texture:	Plagioclase bands with poikilitic porphyroblasts of garnet making up a bookshelf structure in a fine grained matrix consisting of plagioclase, hornblende and quartz. Hornblende phenocrysts make up the							
Mineral description:								
Hornblende	Strong green pleochroism,							
Plagioclase	1. order interference colours, average grain size: 0,03mmm							
Quartz	Recrystallized quartz with little undulatory extinction							
Garnet	Isotropic anhedral poikiloblastic grains withh feldspar inclusions							
Sphene	Anhedral grains averaging 0,022mm with extreme birefringence occur mostly inside garnets and some hornblende crystals							
Epidote	Anhedral 3.order interference colours							
Sulphide	Anhedral grains averaging 0,022mm are disseminated intergranularly across the thin section							
Comment:	Sampled from within shera zone							
Shear sense:	Dextral							
Facies:	Amphibolite							

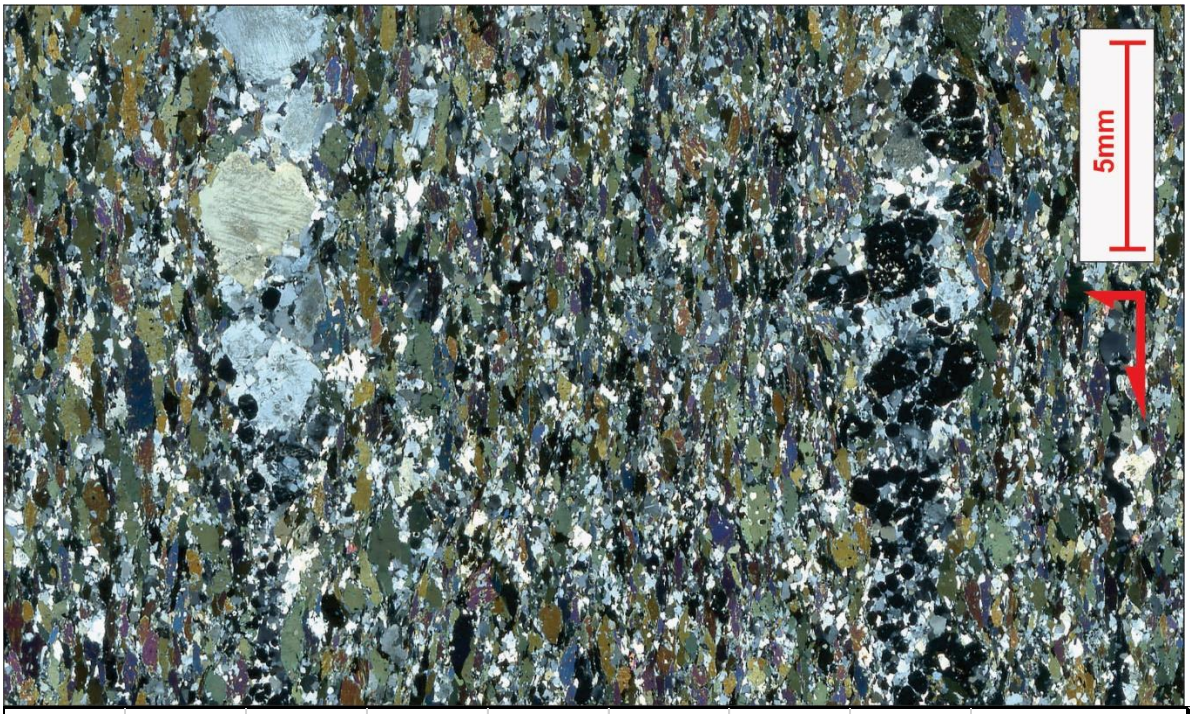

Sample:	102_2	666						
Macroscopic description:								
Colour:	Dark grey							
Minerals:	Amphibole, garnet, feldspar, quartz, sulphides							
Grain size:	0,5-3mm							
Structure:	Amphibolite garnet schist							
Microscopic description:								
Mineral content:		Hbl: 55%	Plg: 20%	Qtz: 14%	Gt: 7%	Sphd: 1%	Ep: 1%	Ti+Chlt: 2%
Texture:	A penetrating fracture set intersects the general foliation at 80 degrees to the foliation. Fractues can be traced through hornblende and feldspars.							
Mineral description:								
Quartz	1. order grey intereference colours, SGR, static annealing							
Hornblende	Green pleochroism, sub-hedral, elongated, high 1. order orange and purple.							
Garnet	Isotropic, euhdral partially revolved porphyroblasts with alteration and chlorite infillings. Occurs mainly in two different bands parallel to foliation making up garnet chains linked together							
Chlorite	1. order grey, anomalous navy blue.							
Plagioclase	Anhedral grains (0,11-3,1mm, avg.: 0,18) showing polysynthetic twins, and some deformation twins, sericitisation							
Sulphides	Mainly anhedral opaque grains (0,010-0,7mm) occuring mostly as hornblende inclusions							
Epidote	2. order yellow and blue, high relief							
Sphene	Anhedral grains with an average grainsize of 0,07mm with extreme birefringence occur as inclusions in plagioclase and hornblende							
Comment:	Hornblende wraps around 1-4mm large garnets. Altered garnets are filled with chlorite which indicates retrograde metamorphism. Boudinaged felspar clasts and garnet clasts are wrapped by hornblende crystals.							
Shear sense:	?							
Facies:	Upper amphibolite							

Sample:	103_1	140900						
Macroscopic description:								
Colour:	Grey							
Minerals:	Amphibole, feldspar, sulphides							
Grain size:	0,5-2mm							
Structure:	Amphibolite schist							
Microscopic description:								
Mineral content:		Hbl: 48%	Plg: 28%	Ep: 16%	Qtz: 5%	Slphd: 2%	Ti: 1%	
Texture:	Thin section is made up of four distinct sections, where the upper part consist of coarse grained hornblende, the middle part consist of a quartz and plagioclase band which is divided from the epiodte section by a second hornblende rich section.The lowermost section is dominated by epidote with inclusions. Epidote and hornblende are aligned parallel to foliation.							
Mineral description:								
Hornblende	Anhedral grains (0,022-1,4mm) with 1.order yellow and red interfernce colors.							
Plagioclase	Anhedral grains (0,22-0,9mm, avg.: 0,25mm) showing 1. order grey interference colours with some primary twins							
Epidote	Anhedral grains with 2. and 3.order yellow, red and green intereference colours. Some grains are total pseudomorphs of plagioclase. Others have inclusions of hornblende and plagioclase							
Sulphide	Opaque interranular grains showing							
Sphene	Sphenoidal grains with extreme birefringence ranging from 0,022-0,22mm occuring as intragrains in hornblende, pseudomorph epidote and as intergrains.							
Quartz	1.order grey with SGR							
Comment:								
Shear sense:	Pure shear?							
Facies:	Lower amphibolite							

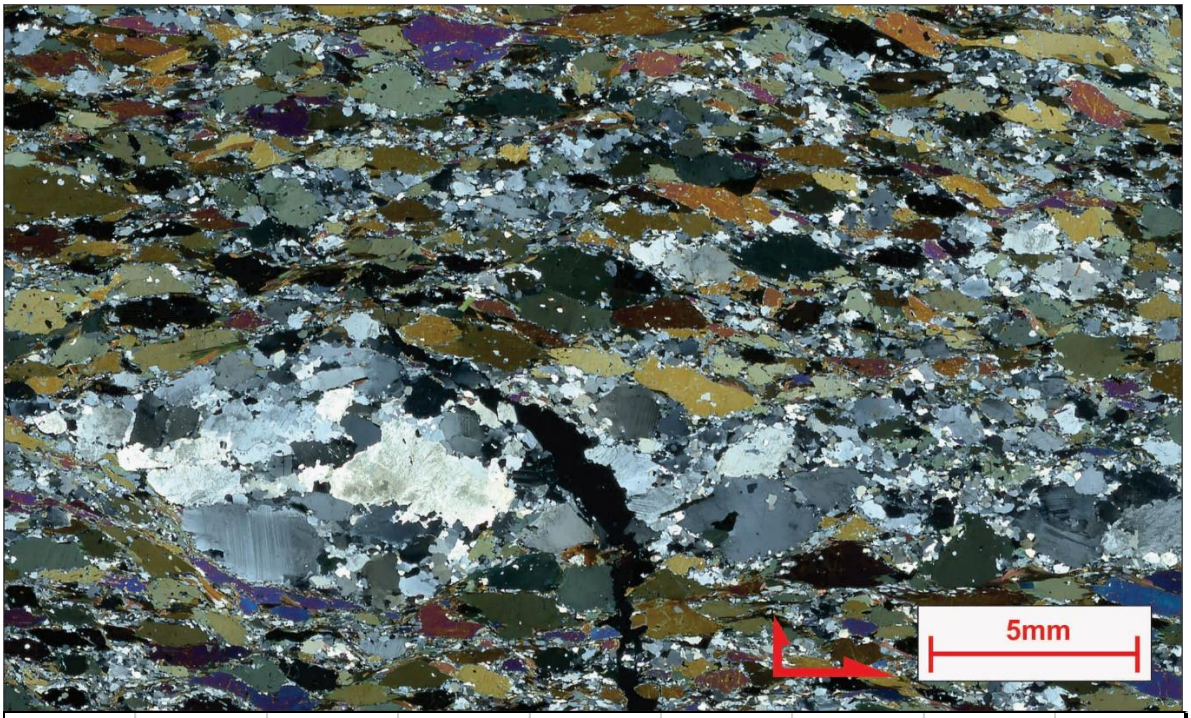

Sample:	169_1	667						
Macroscopic description:								
Colour:	Black and white							
Minerals:	Amphibole, feldspar, quartz, sulphides							
Grain size:	0,5-2mm							
Structure:	Boudinaged feldspars							
Microscopic description:								
Mineral content:		Plg: 45%	Hbl: 30%	Qtz: 12%	Bt: 10%	Ti: 1%	Sulphides: 2%	
Texture:	Biotite laths and hornblende crystals oriented parallel to foliation. Biotite replaces hornblende several places in the thin section. Sulphides and biotite seem to be present at the same places.							
Mineral description:								
Quartz	Quartz occurs in two banded zones where the largest zone is 10 mm wide with a grain size of 0,15mm.							
Hornblende	2. order green with angular elongated grains, dark green pleochroism							
Biotite	Elongated 1. order brown with reaction halos from zircon found in contact with hornblende							
Zircon	Grains occurring as inclusions inside biotite with grainsize 0,08 showing pleochroic halos							
Plagioclase	Primary twins, deformation twins pinching out. Grains up to2,2mm in diameter.							
Sulphide	Opaque anhedral-subhedral intergranular grains in contact with hornblende							
Sphene	Sphenoidal grains with average grainsize 0,11mm are oriented parallel to foliation							
Comment:	Above the feldspar clast, shearbands occuring as S-C structures indicate sinstral sense of shear							
Shear sense:	Sinistral		(top to N-NE extension)					
Facies:	Greenschist/lower Amphibolite							

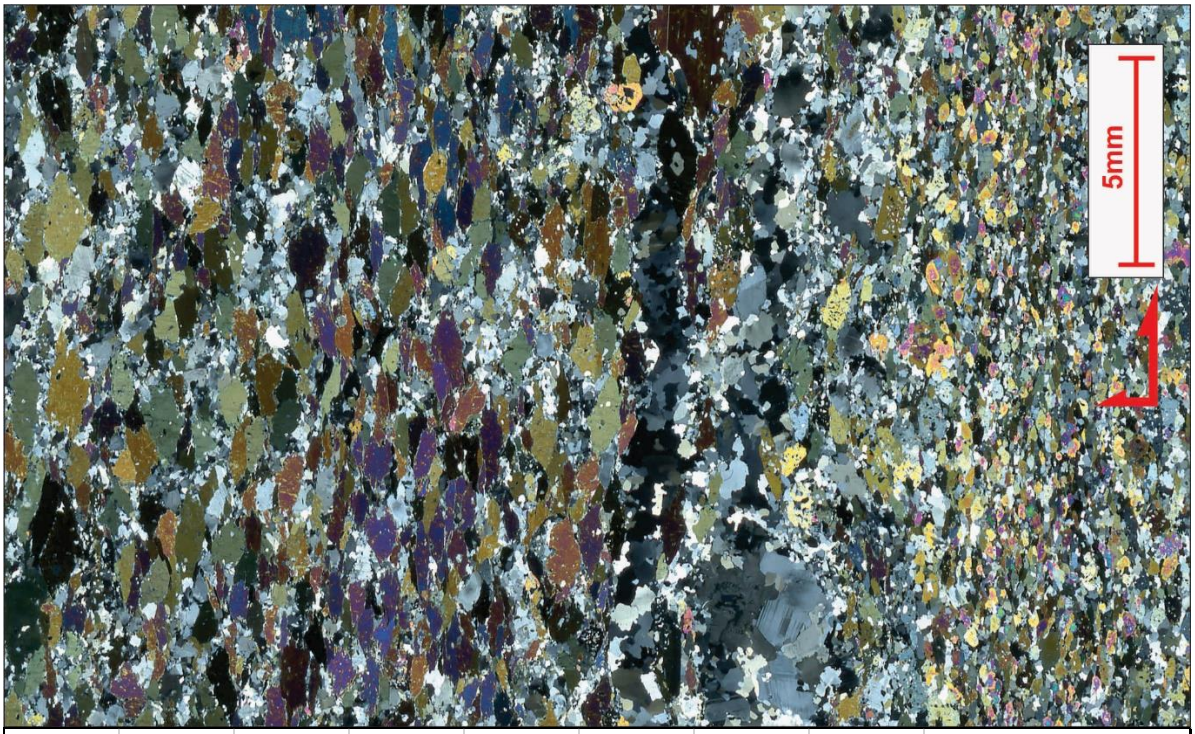

Sample:	169_2	668						
Macroscopic description:								
Colour:	Grey and white							
Minerals:	Amphibole, feldspar, quartz, sulphides							
Grain size:	0,5-3mm							
Structure:	Amphibolite gneiss							
Microscopic description:								
Mineral content:		Hbl: 35%	Ep: 25%	Qtz: 20%	Plg: 18%	Ti: 1%	Bt: 1%	
Texture:	Thin section is divided into two main parts marked by a 2,2 mm thick band of recrystallized quartz and plagioclase. The upper section made up of coarse grained plagioclase and hornblende. The lower part consists of medium grained epidote and plagioclase. Fracture set running perpendicular to foliation.							
Mineral description:								
Hornblende	Distinct deep green pleochroism with elongated grains of high 2.order yellow and pink colour. A fracture set runs perpendicular to the elongation throughout the whole thin section.							
Quartz	Little or no undulatory extinction. SGR, GBM indicate static recrystallization with polygonal grain boundaries.							
Epidote	Subhedral to anhedral 3. order yellow and pink grains ranging from 0,07-0,7mm in diameter, concentrated in bottom 15 mm of the thinsection. Nearly all grains contain plagioclase inclusions.							
Plagioclase	Anhedral 1. order grey grains with some primary twins and traces of sausseritization							
Biotite	Needle shaped with 1.order brown anhedral grains.							
Sphene	Largely euhedral monoclinic sphenoid crystals ocurring as inclusions in hornblende and as intergrains. Grainsize : 0,08 mm - 2,16 mm, crystals are strongly aligned with general foliation.							
Comment:	Hornblende grains show consistent dextral sense of shear							
Shear sense:	Dextral							
Facies:	lower amphibolite							

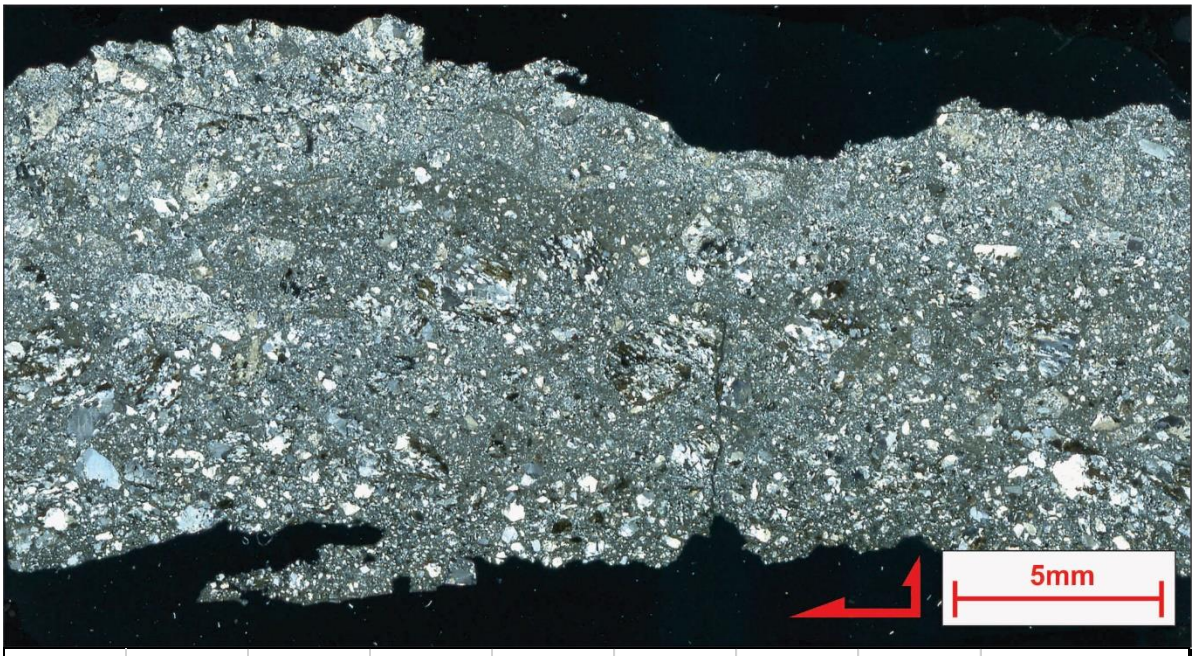

Sample:	172_1	669						
Macroscopic description:								
Colour:	Light grey							
Minerals:	Quartz, feldspar							
Grain size:	0,5-3mm							
Structure:	Cataclasite							
Microscopic description:								
Mineral content:		Plg: 55 %	Chlt: 35%	Hbl: 7%	Ti: 2%	Ca: 1%		
Texture:	Fine crushed fragments of quartz and plagioclase making up the matrix and larger quartz and feldspar clasts make up the mantle. Large 2,5mm plagioclase crystals show extensive recrystallization with sausseritization. Cataclastic clasts (d=0,7mm) consist of plagioclase, chlorite, and quartz and are angular indicating extensive grinding and presence of an aqueous fluid. The thin section show alternating layers of darker and brighter matrix which may represent the segregation of quartz and plagioclase from hornblende. Clast with GBM (picture) indicate that cataclasis postdates the recrystallization which probably was a part of peak metamorphosis.							
Mineral description:								
Quartz	Grain size from 0,016mm up to 0,48 mm. GBM and SGR (400-500 °C)							
Plagioclase	Sub-hedral crystals with 1.order grey int. colors.							
Chlorite	Light green pleochroism with 1. order brown int. colours, flaky 1,1mm grains in contact with feldspar							
Calcite	Anhedral, extreme birefringence with polysynthetic twins							
Sphene	Anhedral grains averaging 0,22mm with extreme birefringence occur inside large plagioclase crystals							
Comment:								
Shear sense:	?							
Facies:	Greenschist							

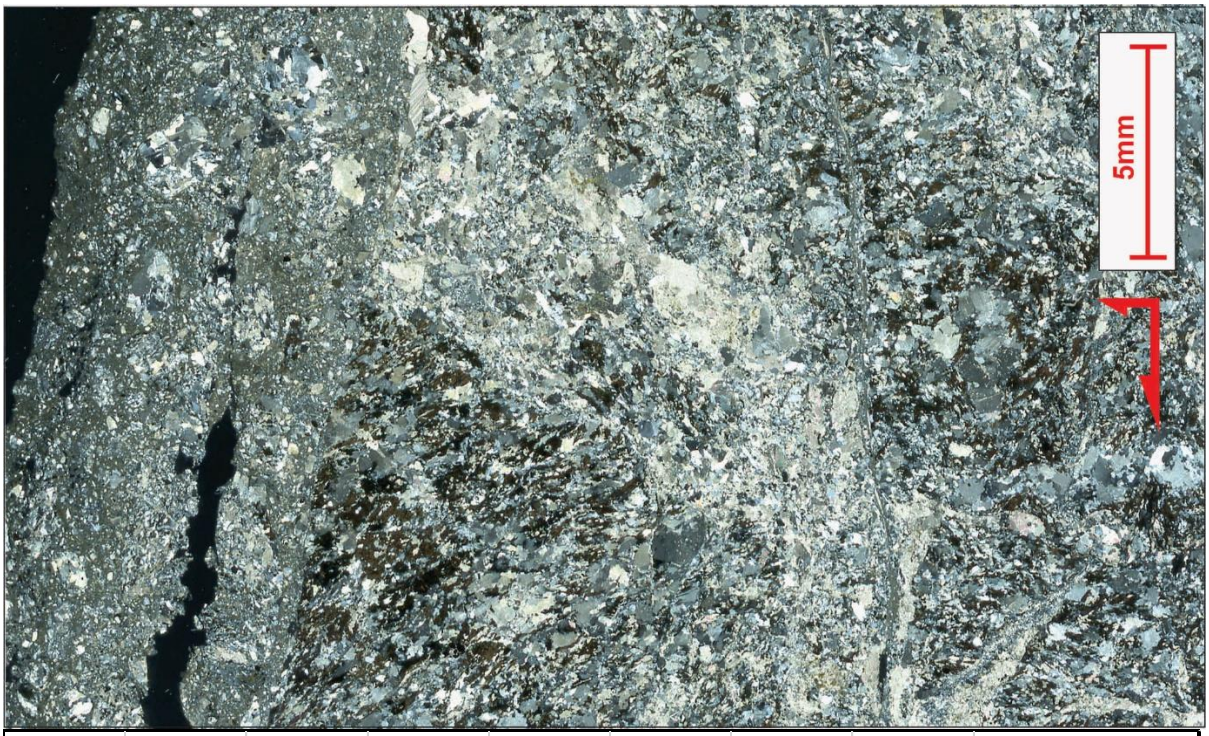

Sample:	173_1	670						
Macroscopic description:								
Colour:	Grey with white spots							
Minerals:	Feldspar, quartz, chlorite, amphibole							
Grain size:	0,5-1,5mm							
Structure:	Cataclasite							
Microscopic description:								
Mineral content:		Plg: 30%	Chlt: 28%	Cal: 32%	Qtz: 6%	Sphd: 3%		
Texture:	Plagioclase show a succession of gradually more cataclastially deformed plagioclase towards the fault slip plane. Aggregates of plagioclase are only present in the less intensely fractured zone and show some roundness.							
Mineral description:								
Calcite	Occuring as anhedral intergrains showing polysynthetic twinning, as vein material with extreme birefringence and as massive overprint.							
Chlorite	Lower 1.order brown oriented in accordance with shear sense in vicinity of fault zone. Occurs everywhere except in the main cataclastic zone.							
Plagioclase	1. order grey interefence colours with intense evidence of sausseritization and presence of undulatory extinction							
Quartz	Lower 1. order grey and white, SGR.							
Sulphides	Opaque, anhedral.							
Comment:	Chlorite is clearly rotated in the cataclastic fault center yielding a sinistral shear sense. The presence of chlorite together with sulphides and overprinting calcite suggest a massive influx of aqueous fluids. Presence of chlorite indicate two events of cataclasis, there are domains totally lacking chlorite consisting of quartz and calcite.							
Shear sense:	Sinistral							
Facies:	Greenschist							

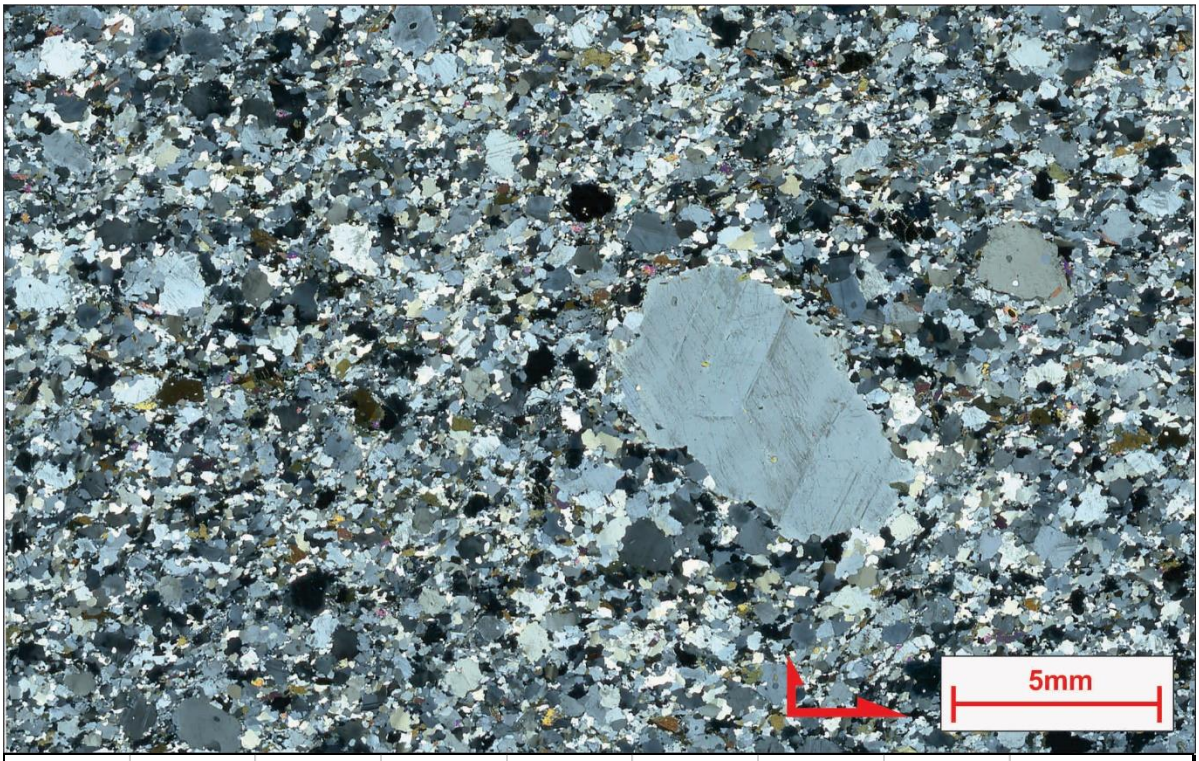

Sample:	194_1	671						
Macroscopic description:								
Colour:	Grey and white spots							
Minerals:	Feldspar, quartz, amphibole, garnet, biotite							
Grain size:	0,5-7mm							
Structure:	Amphibolite gneiss							
Microscopic description:								
Mineral content:		Plg: 70%	Qtz: 10%	Hbl: 8%	Bt: 5%	Gt: 3%	Chlt: 1%	
Texture:	Biotite make up the foliation of the thin section which consists almost entirely of feldspar.							
Mineral description:								
Plagioclase	Alteration of euhedral crystals with primary twins and deformation twins.							
Quartz	Anhedral grains with 1. order grey int. colours showing GBM and SGR							
Hornblende	Anhedral crystals with light green pleochroism.							
Biotite	Upper 3. order intereference colours							
Epidote	3. order yellow and green occuring as single anhedral grains and as subhedral inclusion crystals in plagioclase.							
Garnet	Anhedral skeletal porphyroblasts and fragments with grainsize ranging from 0,48mm-1,6mm							
Chlorite	Innfill in altered garnets							
Zircon	small inclusions of zircon in hornblende crystals							
Comment:	Very plagioclase-rich with almost no hornblende.							
Shear sense:	Dextral							
Facies:	High amphibolite							

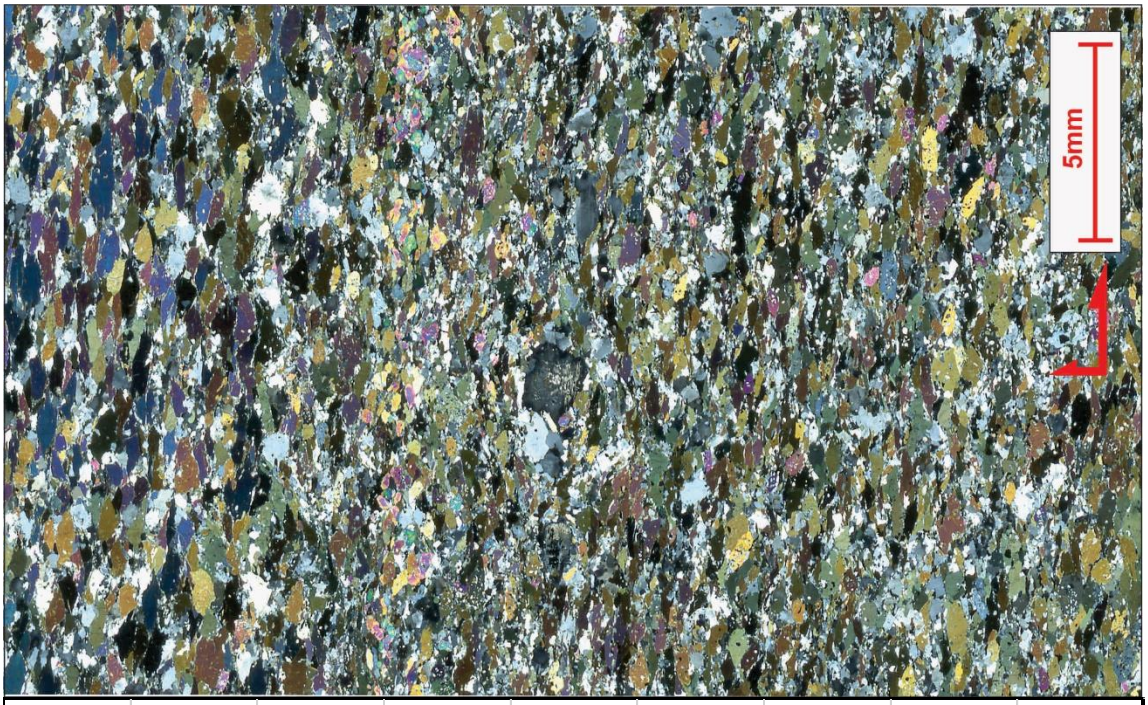

Sample:	210_1	672						
Macroscopic description:								
Colour:	Dark grey							
Minerals:	Amphibole, plagioclase, garnet, sulphide							
Grain size:	0,5-1,5mm							
Structure:	Amphibolite schist							
Microscopic description:								
Mineral content:		Hbl: 55%	Plg: 30%	Ep: 5%	Sulphides: 5%	Rest: 5%		
Texture:	Weak compositional banding with sigmoidal hornblende crystals. Shear bands occur due to aligned hornblende and biotite grians.							
Mineral description:								
Hornblende	2.order yellow, elongated grains							
Quartz	SGR							
Plagioclase	Primary twins in some grains. Low 1. order grey							
Epidote	High 2.order yellow and pink, euhedral to anhedral. Occurs also as inclusion in hornblende							
Sulphides	Opaque							
Calcite	Primary twins, extreme birefringence							
Sphene	Angular, extreme birefringence							
Allanite	(inclusion in an epidote, masked brown							
Biotite	Laths, 1. order brown							
Ilmenite	Opaque, inclusion in titanite							
Garnet	Isotropic with inclusions							
Comment:	Very well defined shear band structures and indicate clear sinistral sense of shear which makes the ductile fault a thrust.							
Shear sense:	Sinistral							
Facies:	Amphibolite							

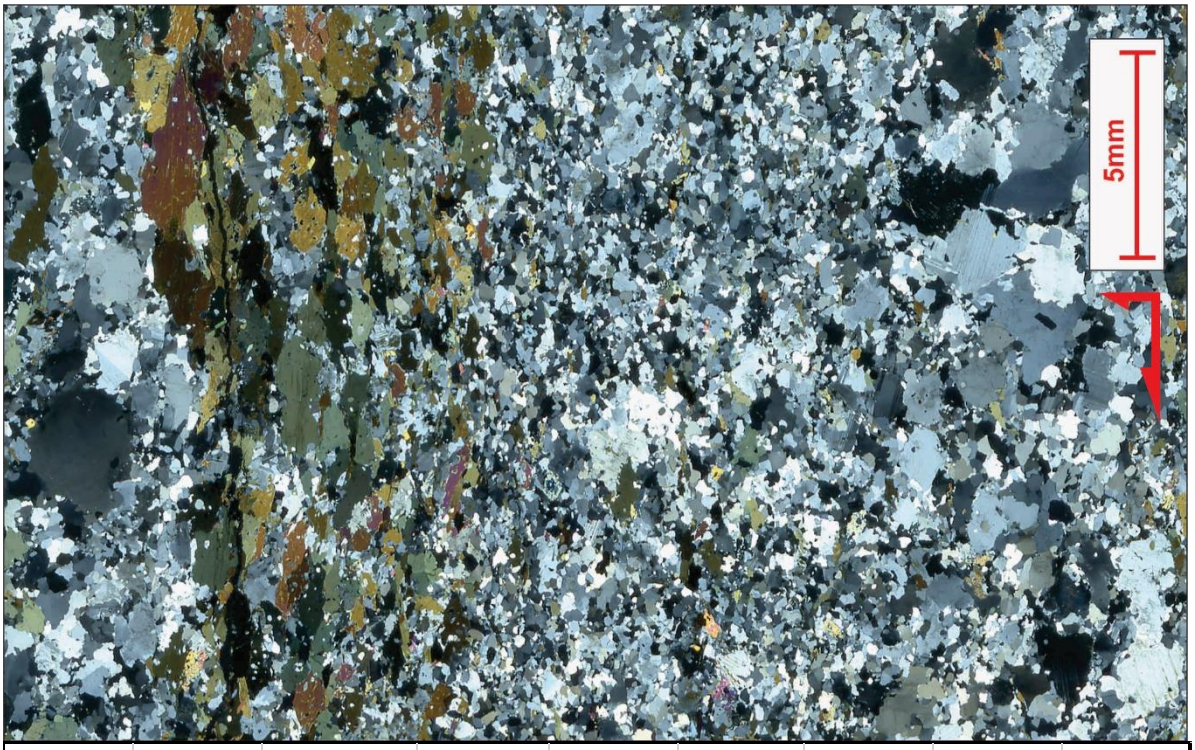

Sample:	220_1	673						
Macroscopic description:								
Colour:	Dark grey and white bands							
Minerals:	Amphibole, feldspar, quartz, sulphide							
Grain size:	0,5-4mm							
Structure:	Boudinaged pegmatite							
Microscopic description:								
Mineral content:		Plg: 65%	Qtz: 20	Hbl: 10%	Ti: 2%	Slphd: 2%	Bt: 1%	
Texture:	Compositional banding. Hornblende is restricted to thic a 9mm band running parallel to foliation. This band is surrounded by 0,48 mm anhedral crystals of plagioclase. This fine grained band of plagioclase is followed by a coarser d = 1,92mm plagioclase band.							
Mineral description:								
Quartz	SGR, inclusions and crystals							
Hornblende	Subhedral to anhedral 1. ord elongated lenses							
Microcline	Anhedral grey, crosshatched twinning							
Sulphides	Opaque euhedral grains, mostly anhedral, 80% of sulhpides are found in hornlende bands							
Plagioclase	Anhedral 1. order grey, prim Twinning							
Biotite	High 2. order brown int. colours							
Epidote	Anhedral skeletal shape, developed by alteration with grainsize 0,16 - 0,64 mm							
Sphene	Extreme birefringence anhedral to subhedral monoclinic sphenoids.							
Comment:	Very plagioclase rich sample							
Shear sense:	?							
Facies:	Greenschist/amphibolite							

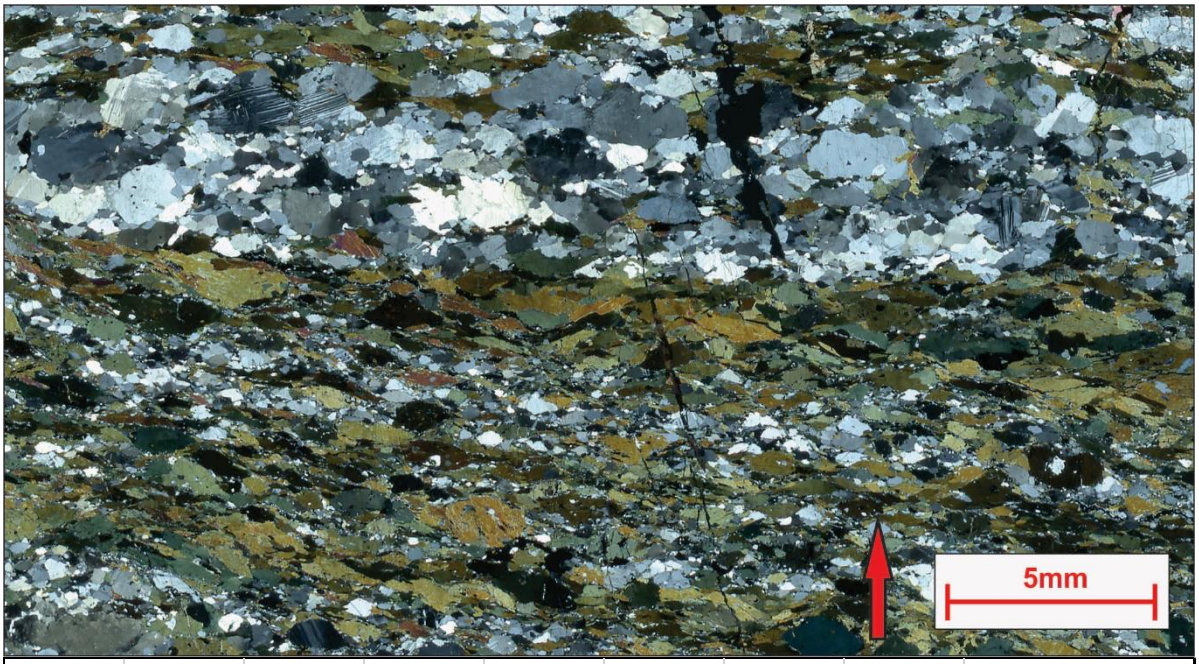

Sample:	228_1							
Macroscopic description:								
Colour:	Dark green and white							
Minerals:	Amphibolite, feldspars, quartz, sulphides							
Grain size:	0,5-3mm							
Structure:	Amphibolite schist							
Microscopic description:							Ti: 0,5%	Cal: 0,5%
Mineral content:		Qtz: 45%	Hbl: 30%	Plg: 15%	Sulphides: 5%	Ep: 2%	Chl: 2%	Bt: 2%
Texture:	Seriate rock with euhedral to anhedral crystals ranging from 0,16 - 2,3mm. Strong foliation consisting of alternating layers of quartz and hornblende crystals oriented parallel to each other.							
Mineral description:								
Plagioclase	Euhedral crystals with deformation twins, 1.order grey. Primary polysynthetic twins occur as well.							
Hornblende	Poikilitic sigmoidal crystals with biotite. Well developed amphibole cleavage							
Quartz	Anhedral crystals with deformation lamellaes and SGR							
Chlorite	Occurs as fibrous vein material							
Sulphides	0,016-0,96mm occuring mostly in fracure zones with quartz where they wrap around hornblende crystals but also as intergrowths.							
Epidote	0,08mm anhedral epidote crystals							
Biotite	Occuring as inclusions inside hornblende crystals and wrapping around phenocrysts og plagioclase and hornblende							
Sphene	Sub-hedral 0,08-0,16 to Euhedral crystals occuring as inclusions inside hornblende crystals							
Zircon	0,03mm anhedral crystal with alteration halo							
Calcite	Sub-hedral 0,32mm crystal observed as inclusion in alteration of hornblende							
Comment:	Very coarse grained plagioclase and hornblende crystals							
Shear sense:	Dextral							
Facies:	Upper greenschist							

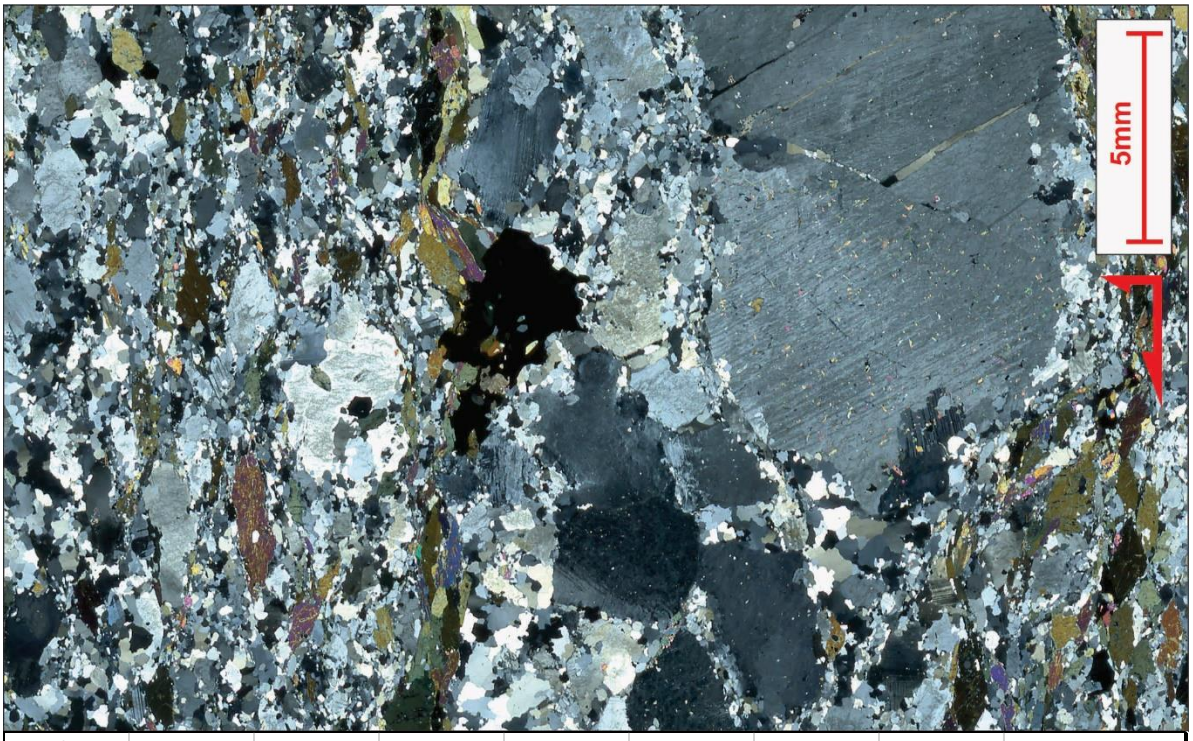

Sample:	229_1	675						
Macroscopic description:								
Colour:	Black and white bands							
Minerals:	Feldspar, amphibole, quartz, sulphide, garnet							
Grain size:	0,5-5mm							
Structure:	Amphibolite schist							
Microscopic description:								
Mineral content:		Plg: 50%	Hbl: 15%	Qtz: 30%	Ep: 3%	Sulph: 1%	Rest: 1%	
Texture:	Large plagioclase clasts enveloped by hornblende grains. Sinistral, quartz sigma clast in the middle of the upper part of the thin section with recrystallized quartz in upper left section and lower right section.							
Mineral description:								
Quartz	Anhedral crystals with undulation, BLG, SGR and lots of epidote inclusions.							
Amphibole	Anhedral grains with 1. order yellow and red, sigmoidal shapes showing sinstral sense of shear							
Epidote	Occurring as inlcusions (d inclusions							
Plagioclase	Anhedral to sub-hedral crystals ranging from 0,20mm up to15mm large grains which show perthite lamellaes. Large grain show lots of smal epidote crystals randomly distributed.							
Sulphides	Oapque, anhedral crystal measuring 2,4mm in diameter							
Biotite	Low 2. order blue, occuring in hornblene fractures							
Sphene	Anhedral grains with extreme birefringence and high relief, occuring as inlcusions inside hornblende crystals							
Chlorite	Alteration product from hornblende crystals							
Comment:	Several inclusions of epidote within the large feldspar clast							
Shear sense:	Sinstral							
Facies:	Greenschist/amphibolite							